44727

National Library of Canada
Canadian Theses Division
Ottawa, Canada
K1A 0N4

Bibliothèque nationale du Canada
Division des thèses canadiennes

PERMISSION TO MICROFILM — AUTORISATION DE MICROFILMER

• Please print or type — Écrire en lettres moulées ou dactylographier

Full Name of Author — Nom complet de l'auteur

Alaa Eldin Elwi

Date of Birth — Date de naissance	Country of Birth — Lieu de naissance
July, 27, 1950	Egypt

Permanent Address — Résidence fixe

24 Burnham Ave., ST. Albert, Alberta T8N 0A7

Title of Thesis — Titre de la thèse

Nonlinear Analysis of Axisymmetric Reinforced Concrete Structures

University — Université

University of Alberta

Degree for which thesis was presented — Grade pour lequel cette thèse fut présentée

Ph. D

Year this degree conferred — Année d'obtention de ce grade	Name of Supervisor — Nom du directeur de thèse
1980	Dr. D.W. Murray

Permission is hereby granted to the NATIONAL LIBRARY OF CANADA to microfilm this thesis and to lend or sell copies of the film.

The author reserves other publication rights, and neither the thesis nor extensive extracts from it may be printed or otherwise reproduced without the author's written permission.

L'autorisation est, par la présente, accordée à la BIBLIOTHÈQUE NATIONALE DU CANADA de microfilmer cette thèse et de prêter ou de vendre des exemplaires du film.

L'auteur se réserve les autres droits de publication; ni la thèse ni de longs extraits de celle-ci ne doivent être imprimés ou autrement reproduits sans l'autorisation écrite de l'auteur.

Date	Signature
April, 23, 1980	Alaa A. Elwi

NL-91 (4/77)

National Library of Canada
Collections Development Branch

Canadian Theses on
Microfiche Service

Bibliothèque nationale du Canada
Direction du développement des collections

Service des thèses canadiennes
sur microfiche

NOTICE

The quality of this microfiche is heavily dependent upon the quality of the original thesis submitted for microfilming. Every effort has been made to ensure the highest quality of reproduction possible.

If pages are missing, contact the university which granted the degree.

Some pages may have indistinct print especially if the original pages were typed with a poor typewriter ribbon or if the university sent us a poor photocopy.

Previously copyrighted materials (journal articles, published tests, etc.) are not filmed.

Reproduction in full or in part of this film is governed by the Canadian Copyright Act, R.S.C. 1970, c. C-30. Please read the authorization forms which accompany this thesis.

AVIS

La qualité de cette microfiche dépend grandement de la qualité de la thèse soumise au microfilmage. Nous avons tout fait pour assurer une qualité supérieure de reproduction.

S'il manque des pages, veuillez communiquer avec l'université qui a conféré le grade.

La qualité d'impression de certaines pages peut laisser à désirer, surtout si les pages originales ont été dactylographiées à l'aide d'un ruban usé ou si l'université nous a fait parvenir une photocopie de mauvaise qualité.

Les documents qui font déjà l'objet d'un droit d'auteur (articles de revue, examens publiés, etc.) ne sont pas microfilmés.

La reproduction, même partielle, de ce microfilm est soumise à la Loi canadienne sur le droit d'auteur, SRC 1970, c. C-30. Veuillez prendre connaissance des formules d'autorisation qui accompagnent cette thèse.

THIS DISSERTATION
HAS BEEN MICROFILMED
EXACTLY AS RECEIVED

LA THÈSE A ÉTÉ
MICROFILMÉE TELLE QUE
NOUS L'AVONS REÇUE

Ottawa, Canada
K1A 0N4

NL-339 (Rev. 8/80)

THE UNIVERSITY OF ALBERTA

Nonlinear Analysis of Axisymmetric Reinforced Concrete Structures

by

(C)

ALAA A. ELWI

A Thesis

Submitted to the Faculty of Graduate Studies and Research in Partial Fulfilment of the Requirements for the Degree of Doctor of Philosophy

DEPARTMENT OF CIVIL ENGINEERING

EDMONTON, ALBERTA

SPRING, 1980

THE UNIVERSITY OF ALBERTA

FACULTY OF GRADUATE STUDY AND RESEARCH

The undersigned certify that they have read, and recommend to the Faculty of Graduate Studies and Research for acceptance, a thesis entitled NONLINEAR ANALYSIS OF AXISYMMETRIC REINFORCED CONCRETE STRUCTURES submitted by ALAA A. ELWI in partial fulfilment of the requirements for the degree of Doctor of Philosophy in Civil Engineering.

D.W. Murray - ~~Supervisor~~

J.B. Haddow

T.M. Hrudey

J.G. MacGregor

J. Warwaruk

E.L. Wilson - External Examiner

DATE January 28th, 1980

ABSTRACT

A nonlinear elastic (hypoelastic) constitutive relation is proposed for analysis of plane and axisymmetric reinforced and/or prestressed concrete structures. The constitutive relation is based on the equivalent uniaxial strain concept. A now characterization of Poisson's ratio is introduced. Strain softening behavior is assumed in tension and post failure conditions are imposed on three dimensional ultimate strength and corresponding equivalent uniaxial strain surfaces. Special isoparametric finite elements are developed for representation of reinforcing bars and prestressing layers. The finite element model as well as the proposed constitutive relations are incorporated in a finite element program (FEPARCS5) for nonlinear analysis of axisymmetric or plane reinforced and/or prestressed concrete structures. Program FEPARCS5 is then used to analyze a finite element model of an axisymmetric prestressed concrete test structure resembling a secondary containment building under increasing internal pressure. The results of the analysis are then compared to the results of the test structure and a theoretical elastic plastic analysis of the same test structure.

ACKNOWLEDGEMENTS

The author wishes to express his deep gratitude to Dr. D.W. Murray, Professor of Civil Engineering, University of Alberta for his supervision, patience and support throughout the course of this study. Appreciation is also due to Dr. T. Hrudey, Professor of Civil Engineering, University of Alberta for his valuable comments and for reading and correcting the manuscript. The author also wishes to thank Dr. S.H. Simmonds and Dr. J.G. MacGregor, Professors of Civil Engineering, University of Alberta, for serving as members of the supervisory committee.

The author wishes to acknowledge the permission of Dr. S.H. Simmonds, Dr. J.G. MacGregor and Dr. D.W. Murray to use Figures 5.1, 5.2, 5.3, 6.1, 6.2, 6.3 and 6.4. Financial support and computer facilities were provided by the Izak Walton Killam Memorial Foundation, the Computing Services of the University of Alberta, the National Research Council of Canada, and the Atomic Energy Control Board of Canada.

The assistance of Mrs. Doreen Wyman who typed the manuscript is gratefully acknowledged.

Finally the author wishes to express his deep appreciation for his wife Azza Darwish without whose support and encouragement this work would not have been possible.

TABLE OF CONTENTS

	PAGE
CHAPTER 1 - INTRODUCTION	1
1.1 Background to the Problem	1
1.2 Scope and Objectives of Thesis	3
1.3 Organization of Thesis	3
CHAPTER 2 - CONSTITUTIVE THEORY	5
2.1 Introduction	5
2.2 Literature Review	6
2.3 The Proposed Material Model	12
2.3.1 Introduction	12
2.3.2 The Constitutive Equation	12
2.3.3 The Equivalent Uniaxial Strain Concept	14
2.3.4 The Equivalent Uniaxial Strain - Stress Relation	16
2.3.5 Young's Moduli and the Shear Modulus	19
2.3.6 Poisson's Ratio	20
2.3.7 The Ultimate Surfaces	22
2.3.8 Failure Modes	25
2.3.9 Verification of the Constitutive Relation	27
CHAPTER 3 - FINITE ELEMENT MODEL	40
3.1 Introduction	40
3.2 Fundamental Variational Formulation	41
3.3 Iso-parametric Element Formulation	47

PAGE

3.3.1 Solid Element Formulation 47

3.3.2 Formulation of A Meridional Reinforcing Isoparametric Element 50

3.3.3 Formulation of A Circumferential Reinforcing Isoparametric Element 53

3.4 Body Forces 54

3.4.1 Gravity Loads 54

3.4.2 Thermal Loads 55

3.4.3 Equilibrating Loads 58

3.5 Surface Tractions 59

3.6 Boundary Conditions 61

CHAPTER 4 - PROGRAM FEPARCS5 65

4.1 Introduction 65

4.2 General Description 65

4.3 Basic Solution Techniques 67

4.3.1 The Numerical Solution Strategy 67

4.3.2 The Subincrement Method 70

4.3.3 Implementation of the Constitutive Relation 71

4.4 Special Capabilities 74

4.4.1 Initial Stresses 74

4.4.2 Post Tensioning 75

4.5 Flow of Operations for Program FEPARCS5 76

PAGE

CHAPTER 5 - PRELIMINARY INVESTIGATION 82

5.1 Introduction 82

5.2 Wall Segment Test Description 83

5.3 FEPARCS5 Modelling of the Wall Segments 84

5.4 Comparison of FEPARCS5 Analysis with the BOSOR5 Theoretical Analysis and with the Experimental Results 84

5.5 The Stress Path 85

CHAPTER 6 - ANALYSIS OF A CONTAINMENT STRUCTURE 96

6.1 Introduction 96

6.2 Description of Test Structure and Procedure . . 96

6.3 Finite Element Model of Test Structure 98

6.3.1 General Description 98

6.3.2 Modelling of Dome Prestressing 99

6.3.3 Materials 100

6.3.4 Loads 101

6.4 Analysis of Test Structure 101

6.5 Comparison of Results with the Experimental Results and the BOSOR5 Theoretical Analysis . . 103

6.5.1 Displacements 103

6.5.2 Surface Strains 104

6.5.3 Cracking Sequence 106

6.6 Limit States for Containment Structures 108

CHAPTER 7 - SUMMARY AND CONCLUSIONS 136

PAGE

REFERENCES 139

APPENDIX A - PARAMETERS OF ULTIMATE SURFACE 144

APPENDIX B - ISOPARAMETRIC SHAPE FUNCTIONS 147

APPENDIX C - MODELLING OF DOME PRESTRESSING TENDONS 148

LIST OF TABLES

TABLE	DESCRIPTION	PAGE
2.1	KHR Material Parameters	29
2.2	SW Material Parameters	29
5.1	Wall Segment Material Parameters (Concrete) . .	87
5.2	Wall Segment Material Parameters (Steel). . . .	88
5.3	Limit State Loads on Wall Segments	89
6.1	Concrete Material Properties of Test Structure	110
6.2	Load Steps of FEPARCS5 Analysis of Finite Element Model of Test Structure	111
6.3	Pressures Corresponding to Limit States of the Finite Element Model	112

LIST OF FIGURES

FIGURES	DESCRIPTION	PAGE
2.1	Compressive Stress Equivalent Uniaxial Strain Relation	30
2.2	Tensile Stress Equivalent Uniaxial Strain Relation	30
2.3	Shear Stress Strain Relation	30
2.4	Mortar Cracks	31
2.5	Proposed Poisson Ratio - Equivalent Uniaxial Strain Relation	31
2.6	The Ultimate Strength Surface	32
2.7	Failure Conditions	33
2.8	Uniaxial Compression Comparison with KHR Data	34
2.9	Biaxial Compression (-1:-1) Comparison with KHR Data	34
2.10	Biaxial Compression (-1:-.32) Comparison with KHR Data	35
2.11	Compression Tension (-1:.204) Comparison with KHR Data	35
2.12	Rendulic Plane Comparison with Schickert Winkler Data	36
2.13	Triaxial Compression Comparison (-1:.5:.5 Stress Changes) with Schickert Winkler Data. .	37
2.14	Triaxial Compression Comparison (-1:0:1 Stress Changes) with Schickert Winkler Data. .	37
2.15	Triaxial Compression Comparison (.5:.5:-1 Stress Changes) with Schickert Winkler Data. .	38
2.16	Flow Chart for Following a Specified Stress Path	39
3.1	Element K	63
3.2	The Serendipity Finite Element Family	63

FIGURE	DESCRIPTION	PAGE
3.3	Normalized Coordinates	63
3.4	The Reinforcing Element	64
3.5	Surface Tractions	64
4.1	Iterative Schemes	79
4.2	Flow Chart of Problem Preparation Stage of FEPARCS5	80
4.3	Flow Chart of Solution Stage of FEPARCS5 . . .	81
5.1	Elevation of Wall Segment Specimen	90
5.2	Typical Section A-A through Wall Segment Specimen	91
5.3	Typical Section B-B through Wall Segment Specimen	91
5.4	Axisymmetric Modelling of Wall Segment Specimen	92
5.5	Finite Element Modelling of Wall Segment Specimen	92
5.6	Reinforcing and Circumferential Layers of Wall Segment Finite Element Model	92
5.7	Load Strain Comparison for Segment No. 1 . . .	93
5.8	Load Strain Comparison for Segment No. 3 . . .	94
5.9	Stress Path Comparison for Segment No. 3 . . .	95
6.1	Elevation of Test Structure	113
6.2	Prestressing and Rebars for the Dome of the Test Structure	114
6.3	Detail of Ring Beam of Test Structure	115
6.4	Detail of Cylinder Wall Base Connection of Test Structure	116
6.5	Finite Element Mesh of Test Structure	117
6.6	Boundary Condition Simulation for Finite Element Model of Test Structure	118

FIGURE	DESCRIPTION	PAGE
6.7	Detail of Finite Element Model of Ring Beam Area	119
6.8	Reinforcing and Prestressing Layers of Finite Element Model of Test Structure	120
6.9	Local Coordinate Directions of Finite Element Mesh	121
6.10	Stress Strain Curves of Reinforcing Bars	122
6.11	Stress Strain Curves of Prestressing Tendons	123
6.12	Comparison of Deflection Profiles at 120 psi	124
6.13	Comparison of Internal Pressure Versus Maximum Deflection of Wall and Dome	125
6.14	Comparison of Meridional Strains in Wall at 28 inches Above Base	126
6.15	Comparison of Circumferential Strains in Wall at 28 inches Above Base	127
6.16	Comparison of Meridional Strains in Wall at 65 inches Above Base	128
6.17	Comparison of Circumferential Strains in Wall at 65 inches Above Base	129
6.18	Comparison of Meridional Strains Near Top of Dome	130
6.19	Comparison of Circumferential Strains Near Top of Dome	131
6.20	Progress of Vertical Cracking	132
6.21	Progress of Horizontal Cracking	133
6.22	Profile of Strain in Meridional Prestressing Tendons	134
6.23	Profile of Strain in Circumferential Prestressing Tendons	135
C.1	Vector Representation of the Dome Prestressing Mesh	153
C.2	Meridional Contributions of the Dome Prestressing Mesh	154
C.3	Circumferential Contributions of the Dome Prestressing Mesh	155

LIST OF NOTATIONS

a	:	material constant
a_o, a_1, a_2	:	coefficients relating minor radius of failure surface to hydrostatic stress
A	:	area, an area per unit length, an area per unit width.
A_{ijkl}	:	compliance tensor
b_o, b_1, b_2	:	coefficients relating major radius of failure surface to hydrostatic stress
$[B]$	:	matrix of differential operators relating displacement field to strain field
B_{ij}	:	matrix coefficients of Eq. 2.15.
c	:	material constant
$\vec{C}$	:	unit vector along the circumferential direction
$[C]$	:	constitutive matrix
C_{ijkl}	:	constitutive tensor
$\vec{db}_1, \vec{db}_2$	:	elements of vectors forming sides of element area
d	:	denotes a differential element
dr_1, dr_2	:	radial or horizontal components of vectors $\vec{db}_1$ and $\vec{db}_2$
$[D]$	:	the inverse of $[C]$
$\frac{d()}{d()}$	:	denotes a differentiation of the numerator with respect to the denominator
E	:	Young's Modulus
E_{1b}, E_{2b}	:	effective Young's moduli in directions 1 and 2
f_1, f_2, f_3, f_4	:	functions
f_{cb}	:	biaxial compressive strength
f_{cu}	:	uniaxial compressive strength

f_{tu}, f_t : uniaxial tensile strength

$\underset{\sim}{F}$: a tensor functional of tensor arguments

$F_i, \langle F \rangle$: body forcefield in tensor or matrix field

F_s : spring force in a boundary element

F_t : element thermal force

G : denotes shear modulus

$[J], |J|$: Jacobian matrix and its determinant

J' : a transformation factor

K : bulk modulus of elasticity or, number of elements in a body

[K] : stiffness matrix

$[K_{be}]$: a boundary element stiffness matrix

ℓ : denotes length

m : a material constant

$\vec{M}$: a unit vector in the meridional direction

n : number of tendons in one mesh in dome

n_j : components of a vector normal to surface on which traction is applied, see Eq. 3.2.

[N] : matrix of interpolating functions

N : number of strain subincrements

$\vec{O}_\xi, \vec{O}_\mu$: unit normals to planes ξ and μ

p : material constant

$\vec{P}$: unit vector along position vector of the point of intersection of two tendons

$q_i, \langle q \rangle$: displacement field in tensor and matrix forms

Q : denotes equilibrating forces resulting from integration of stresses over volume.

$\vec{Q}_\xi, \vec{Q}_\mu$: vectors tangent to dome prestressing tendons

r : radius of the deviatoric trace of the failure surface, or horizontal coordinate, or radius

$\{r\}$: displacements or degrees of freedom of a structure

r_1, r_2 : minor and major radii of the deviatoric trace of the failure surface respectively

R : denotes loads, or radius of dome

S_{ij} : deviatoric stress tensor

S : denotes surface

S_q : surface on which displacements are prescribed

S_σ : surface on which tractions are prescribed

t : denotes a scalar thermal field

$T_i, \langle T \rangle$: surface traction field in tensor and matrix forms

$[Th]_s, [Th]_{mr}, [Th]_{cr}$: summations in the square brackets of Eqs. 3.53, 3.54a and 3.54b respectively.

u : displacement in the horizontal direction

$\underline{u}$: nodal horizontal displacement

v : displacement in the vertical direction

V : denotes volume

w : displacement along a boundary element

w^n, w^m : Gaussian integration weights

$w_{c\xi}, w_{c\mu}$: circumferential contributions of ξ, μ tendons

$w_{m\xi}, w_{m\mu}$: meridional contributions of ξ, μ tendons

w_{ma}, w_{ca} : tendon average meridional and circumferential contributions

w_{mi}, w_{ci} : meridional and circumferential contributions of tendon number i

x, y : orthogonal axes of the orthogonal dome prestressing tendon meshes

z : vertical coordinge

α : principal stress ratio or coefficient of thermal expansion, or an angle, or a factor

$\alpha_1, \alpha_2, \alpha_3$: parameters of descending branch of stress strain curve

α_c, α_t : ratios of biaxial compressive and uniaxial tensile strengths to uniaxial compressive strength

$\alpha_{ij}, \{\alpha\}$: thermal expansion tensor in tensor and matrix forms

α_i : coefficient of thermal expansion in direction i

β_1, β_2 : parameters of the descending branch of stress strain curve

β_ξ, β_μ : factors of Eqs. C.6a and C.6b

γ : specific weight, or factor of Eq. C.10

γ_{oc} : octahedral shear strain

γ_{12} : shear strain associated with planes 1 and 2

σ_{c12} : shear strain corresponding to ultimate shear strength on planes 1 and 2

δ : denotes a variation, or a factor in Eq. C.13

Δ : denotes an increment

ε : denotes strain

ε_c : equivalent uniaxial strain corresponding to ultimate strength

ε_i : strain in direction i

ε_{cu} : strain corresponding to uniaxial compressive strength

ε_o : normal octahedral strain

ε_u : equivalent uniaxial strain

ε_{ij}, $\langle\varepsilon\rangle$: strain in tensor and matrix forms

η : equivalent Poisson's ratio

θ : angle of similarity, or angle of inclination of a reinforcing layer to the horizontal axis

θ_ξ, θ_μ : angles that planes ξ and μ describe with the vertical axis

λ : a factor of Eq. 2.3

λ_r, λ_p : convergence tolerances for displacements and loads respectively

μ : nondimensional local coordinate

ν : denotes Poisson's ratio

ξ : nondimensional local coordinate of a finite element

ξ_1, ξ_2 : nondimensionalized mean normal stresses in compression

ξ_o : nondimensionalized mean normal stress in tension denoting the apex of the ultimate strength surface

π : an irrational number denoting the ratio of circumference of a circle to its diameter

π_p : potential energy

ρ_1, ρ_2 : nondimensionalized mean shear stresses at nondimensionalized mean normal stresses ξ_1 and ξ_2 respectively

σ : denotes stress

σ_a : mean normal stress

σ_c : ultimate strength

σ_i : normal stress in direction i

$\bar{\sigma}_a$: nondimensionalized mean normal stress

σ_{ij}, $\{\sigma\}$: stress tensor in index and matrix forms

τ	:	shear stress
ϕ	:	a function of Poisson's ratio, or shape functions
$(\ )_e$	:	denotes an element
$(\ )^m, (\ )^n$	:	denotes order of Guassian integration
$(\ )^o, (\ )_o$	:	denotes initial quantities
$(\ )_r$	:	denotes radial quantities
$(\ )_s$	:	denotes secant quantities
$(\ )^T$	:	denotes transpose
$(\ )^t, (\ )_t$	:	denotes thermal quantities
$(\ )_z$	:	denotes vertical direction
$(\ )_\xi, (\ )_\mu$	:	denotes quantities in directions ξ, μ
$\bar{(\ )}$	:	denotes prescribed quantities
$\underline{(\ )}$	:	denotes nodal quantities
$< >$	:	denotes row matrix
$\{ \}$	:	denotes column matrix
$[ ]$	:	denotes matrix
$\frac{\partial(\ )}{\partial(\ )}$	:	denotes partial differentiation of the numerator with respect to the denominator

CHAPTER ONE

INTRODUCTION

1.1 Background to the Problem

In the field of nuclear energy, extreme risks are associated with accident conditions such as overpressure, earthquake loads or catastrophic impact. Therefore, the ability to predict the entire response of a structure such as a secondary containment building or a primary containment vessel and to identify the conditions under which limit states occur in order to assess possible damage is highly desirable. This task calls for complicated nonlinear analyses which are generally expensive. Often economic constraints lead the analyst either to abandon or to oversimplify the problem. These considerations call for the development of more efficient and versatile solution procedures (Almroth, Stren and Brogan, 1979).

There are several aspects to the nonlinear analysis of such structural problems. Some of the major aspects are the constitutive modelling of the material, the finite element modelling of the structure and the loads, and the numerical solution technique of the nonlinear problem. In addition, it is important to realize that there is a strong interaction between these aspects (Bathe and Ramaswamy, 1979).

Since 1974 a research program has been underway at the University of Alberta, Edmonton sponsored by the Atomic Energy Control Board of Canada to investigate the effect of over-pressure

on Gentilly-2 type secondary containment structures which house CANDU nuclear reactors. An advanced elastic plastic constitutive relation for biaxial behavior of concrete has been developed (Epstein and Murray, 1978 and Murray, et al., 1978) and implemented by Murray, Chitunyanondh and Wong (1978) in a modification of the BOSOR5 code (Bushnell, 1973). Subsequently, a series of tests were conducted on reinforced and prestressed concrete wall segments under biaxial and uniaxial tension to assess the performance and parameters of the constitutive relation. In addition, a reinforced and prestressed test structure composed of a cylinder and a dome was built and tested under internal pressure. The test results have been compared to the modified BOSOR5 analysis of the same test structure in order to assess the capability of the program and the constitutive relation to predict the behavior of the test structure.

Although this thesis is not, formally, a part of that research program, the motivation behind the work reported herein, is to develop a parallel sophisticated capability founded upon alternative technology. A three dimensional constitutive relation is developed to take account of thick and thin shell action and an axisymmetric finite element thickshell model is used to accommodate it. Both are implemented in a nonlinear finite element program for analysis of axisymmetric reinforced and/or prestressed concrete structures.

1.2 Scope and Objectives of Thesis

The scope of this thesis is the nonlinear static analysis of three dimensional (axisymmetric) reinforced and/or prestressed structures. Displacements are small, rotations are negligible and strains are assumed to be infinitesimal. High temperature and creep effects are outside the scope of this work.

The objectives of the study can be listed as

1. To develop a three dimensional nonlinear elastic constitutive relation for concrete.
2. To formulate a finite element model capable of representing axisymmetric behavior of reinforced and/or prestressed concrete structures.
3. To develop a nonlinear finite element program for analysis of such structures.
4. To demonstrate the capabilities of this program through application to a complicated structure such as a prestressed concrete containment structure and to identify the limit states associated with over-pressure loading of this structure.

1.3 Organization of Thesis

Chapter Two contains a literature review of some of the existing constitutive relations for multiaxial behavior of concrete, and the development and description of a proposed nonlinear elastic constitutive relation for three dimensional (axisymmetric) behavior of concrete.

In Chapter Three a finite element model for incremental displacement analysis of axisymmetric reinforced and/or prestressed concrete structures is presented. The necessary incremental variational principles are discussed. Finite elements representing concrete, meridional reinforcing and circumferential reinforcing are formulated and the associated boundary conditions and the work equivalent loads are derived.

A finite element program (FEPARCS5) for nonlinear analysis of axisymmetric reinforced and/or prestressed concrete structures is described in Chapter Four. The solution techniques incorporated in the program, as well as special capabilities such as initial stress and post-tensioning simulation, are discussed and the flow of operations is presented.

A preliminary investigation of the capabilities of program FEPARCS5 is carried out in Chapter Five. Chapter Six contains an analysis, using program FEPARCS5, of a prestressed containment structure under internal pressure which was built and tested to failure, in the I.F. Morrison Structural Laboratory. The test structure and procedure are briefly described. The finite element model of the test structure is presented. The results of the analysis are compared with the test results as well as with the results of an elastic plastic analysis. Finally some of the limit states associated with the loading program are identified.

In Chapter Seven conclusions are drawn on the performance of the constitutive model and the capabilities of program FEPARCS5.

CHAPTER TWO

CONSTITUTIVE THEORY

2.1 Introduction

A multiaxial constitutive relationship is an essential component in any finite element nonlinear analysis of reinforced concrete structures. Unfortunately, the behavior of concrete under multiaxial states of stress is complex both in the strength and in the deformation domains. While information on uniaxial response of concrete is abundant, biaxial and triaxial responses are not yet fully understood. This situation is not improved by the scarcity of reliable data on which to base analytical models. There is a general lack of strain data particularly near and beyond peak strengths. Cracking and post-crushing behavior are major problems since a large part of the response to failure of a reinforced concrete structure must of necessity be traced after part or most of the structure have cracked and some concrete may have crushed.

The scope of analysis of concrete structures can range from linear small displacement infinitesimal strain analysis to large displacement finite strain analysis. Therefore, choice of constitutive relations suitable to the type of analysis enhances efficiency. However, the physical nonlinearity of concrete is always dominant. Approaches to the material model range from elastic-plastic to nonlinear elastic. One popular approach to modelling the behavior of concrete under multiaxial states of stress is to consider the material to be orthotropic nonlinear

elastic and to organize the constitutive model around some equivalent uniaxial relation. Since 1972 a number of studies have been published along that line; Liu, Nilson and Slate (1972), Coon and Evans (1972), Kupfer and Gerstle (1973), Romstadt, et al. (1974), Darwin and Pecknold (1974, 1977a and 1977b), Sarne (1974), Link (1976) and Bashur and Darwin (1978).

In this chapter a brief review of some of these models is presented and a nonlinear three dimensional (axisymmetric) constitutive relation for concrete is developed.

2.2 Literature Review

Truesdell (1955) defines hypoelastic materials as those for which the rate of stress is a function of the rate of deformation and the stress history. Argyris, et al. (1976) and Schnobrich (1977) classify the models referred to in Section 2.1 as hypoelastic. The following discussion is confined to this approach since the model proposed by the writer falls under the same classification. The underlying assumption of these models besides the definition of Truesdell is that the material is nonlinear elastic. Therefore, tangent or secant constitutive equations are used in the form of the generalized Hooke's Law. The problem then is to determine the variation of the moduli involved in a given form of Hooke's Law throughout the loading history. In the absence of time dependent effects and high temperatures, these moduli become functions of the level, type and ratios of the stresses and/or the strains.

Liu, Nilson and Slate (1972) have proposed a biaxial orthotropic model of concrete. In this model a stress-strain curve which takes into consideration Poisson's ratio and the ratio of principal stresses is defined as

$$\sigma_i = \varepsilon_i E_o / \{(1 - \nu\alpha)\,[1 + (E/E_{si}\,(1 - \nu\alpha) - 2)(\varepsilon_i/\varepsilon_{ci}) + (\varepsilon_i/\varepsilon_{ci})^2]\}\ ,\quad i = 1,2 \quad \text{(no sum)} \tag{2.1}$$

where, E_s is the secant modulus at peak strength, ε_c is the strain at peak strength and α is the principal stress ratio. The incremental constitutive equation is written as

$$\begin{Bmatrix} \Delta\sigma_1 \\ \Delta\sigma_2 \\ \Delta\tau_{12} \end{Bmatrix} = \begin{bmatrix} \lambda\, E_{1_b}/E_{2_b} & \lambda\nu & 0 \\ \lambda\nu & \lambda & 0 \\ 0 & 0 & (E_{1_b}\, E_{2_b})/(E_{1_b} + E_{2_b} + 2E_{2_b}\nu) \end{bmatrix} \begin{Bmatrix} \Delta\varepsilon_1 \\ \Delta\varepsilon_2 \\ \Delta\gamma_{12} \end{Bmatrix} \tag{2.2}$$

where,

$$\lambda = E_{1b}/(E_{1b}/E_{2b} - \nu^2) \tag{2.3}$$

and E_{1_b} and E_{2_b} are effective tangent moduli, derived by differentiation of Eq. 2.1 with respect to the strain ε_i. Eq. 2.1 is used in compression only, while in tension a straight line relation ending with a tension cut off criterion is used.

Kupfer and Gerstle (1973) have suggested a secant isotropic model for biaxial behavior of concrete in which the shear and bulk moduli, respectively G_s and K_s, are used as expressed in the equation.

$$\begin{Bmatrix} \sigma_1 \\ \sigma_2 \\ \tau_{12} \end{Bmatrix} = 4G_s/(3K_3 + 4G_s) \begin{bmatrix} (3K_s + G_s) & (3K_s - G_s)/2 & 0 \\ (3K_s - G_s)/2 & (3K_s + G_s) & 0 \\ 0 & 0 & (3K_s + 4G_s)/4 \end{bmatrix} \begin{Bmatrix} \varepsilon_1 \\ \varepsilon_2 \\ \gamma_{12} \end{Bmatrix} \quad (2.4)$$

Kupfer and Gerstle suggest relationships for the shear and bulk moduli as functions of the octahedral shear strain as

$$G_s = G_o(1 - a\,(\tau_{oc}/f_{cu})^m) \quad (2.5a)$$

$$K_s = K_o(G_s/G_o)\,\exp\,(c\gamma_{oc}^p) \quad (2.5b)$$

where G_o and K_o are the initial shear and bulk moduli respectively, τ_{oc} and γ_{oc} are the octahedral shear stress and strain, f_{cu} is the uniaxial compressive strength and a, m, c and p are constants. These authors have used the failure surface proposed by Kupfer, Hilsdorf and Rüsch (1969) as a biaxial failure criterion. This type of analysis agrees well with test data in the compression zone but is not successful in other zones (Darwin and Pecknold, 1977b and Kupfer and Gerstle, 1973).

Cedolin, Crutzen and Poli (1976 and 1977) have suggested an extension of the same concept to three dimensional cases. However, the bulk modulus in this case is assumed to be a function of the normal octahedral strain ε_o. Their recommended expressions are

$$G_s = G_o\,(.81\,(2^{-\gamma_{oc}/.002}) - 2\gamma_{oc} + .9) \quad (2.6a)$$

$$K_s = K_o\,(.85\,(2.5^{-\varepsilon_o/.0014}) + .15) \quad (2.6b)$$

While Argyris, et al. (1974) admit that there may be a relation between the deviatoric and hydrostatic moduli, they state that the assumption of isotropy is limiting under general conditions such as nonproportional load paths and cyclic loading.

Romstadt, et al. (1974) has defined a strain space which is divided into several progressive damage zones. As the material strains from one damage zone to another, Young's modulus and Poisson's ratios assume different values. The variation of Young's modulus takes into account the previous history of damage. Although this concept is very interesting, it has not been pursued by other investigators.

Link (1976 and 1977) has developed a number of functions to describe Young's moduli and Poisson's ratios to be used in a two dimensional orthotropic material model. These functions employ the level and ratio of principal stresses as independent variables. The functions are extremely complicated and have not been extended to three dimensional behavior.

Geistfeldt (1977a and 1977b) has suggested a hyperelastic approach to obtain the required elastic moduli for an isotropic biaxial behavior of concrete. Geistfeldt (1977b) suggests that limited extension to three dimensions can be achieved.

Darwin and Pecknold (1974, 1977a and 1977b) have developed the concept of equivalent uniaxial strains for orthotropic biaxial behavior of concrete. The incremental constitutive relation is of the form

$$\begin{Bmatrix} \Delta\sigma_1 \\ \Delta\sigma_2 \\ \Delta\tau_{12} \end{Bmatrix} = 1/(1-\nu^2) \begin{bmatrix} E_1 & \nu\sqrt{E_1E_2} & 0 \\ \nu\sqrt{E_1E_2} & E_2 & 0 \\ 0 & 0 & G_{12}(1-\nu^2) \end{bmatrix} \begin{Bmatrix} \Delta\varepsilon_1 \\ \Delta\varepsilon_2 \\ \Delta\gamma_{12} \end{Bmatrix} \tag{2.7}$$

The equivalent uniaxial strain increment is defined as

$$\Delta\varepsilon_{ui} = \Delta\sigma_i/E_i \quad \text{(no sum)} \quad , \quad i = 1,2 \tag{2.8}$$

Eqs. 2.7 and 2.8 are defined in the principal axes of orthotropy which are assumed to lie along the axes of principal stresses. The accumulation of the increments of equivalent uniaxial strains yields the total equivalent uniaxial strains which generally do not form a second order tensor and, therefore, are not transformable.

$$\varepsilon_{ui} = \Sigma\Delta\sigma_i/E_i \quad \text{(no sum)} \quad , \quad i = 1,2 \text{ (over loadpath)} \tag{2.9}$$

Darwin and Pecknold have chosen the uniaxial compressive stress strain relation of Saenz (1964) to act as an instantaneous stress equivalent uniaxial strain relation in compression. A straight line relation ending in a cut off has been used in tension. The parameters of peak strength appearing in the relation are obtained from a modified form of the Kupfer, Hilsdorf and Rüsch failure envelope (1969).

It is noted that most investigators have used a tension cutoff criterion. The proponents of the gradual softening approach in tension claim that cracking (when treated in a smearing fashion) cannot occur over every point in a region where stiffness is represented by an integral. Therefore, the material must retain a

a certain measure of stiffness represented by a descending branch (Scanlon and Murray, 1974, and 1972, Murray, et al., 1978 and Elwi and Murray, 1979). The descending branch in tension is observed in indeterminate tests, e.g. Evans and Marathe (1968), and its characteristics must be functions of the steel ratio in real structures.

The above has been a brief discussion of some of the proposed models for the behavior of concrete under multiaxial states of stress, and has been confined to hypoelastic proposals. Many other contributions of equal importance have been published. Coon and Evans (1972) have introduced a true hypoelastic approach; Murray (1979) has developed octahedral based tangential stiffness matrices; Sarne (1974) has extended the hypoelastic approach to three dimensions; Ottosen and Andersen (1975 and 1977) have proposed yet different models; Ottosen (1979) has recently proposed a secant based constitutive relation which tackled the post failure behavior. On the other hand, elastic plastic models have been used and are still being developed. Among these are the Chen and Chen (1975) three dimensional elastic plastic model, the investigation by Mroz (1972) of nonassociated flow rules, the three parameter elastic plastic biaxial constitutive theory suggested by Epstein and Murray (1978) and the further developments by Murray, et al. (1978). In a separate category the endochronic theory developed by Bazant and coworkers (1975 and 1976) must be mentioned.

2.3 The Proposed Material Model

2.3.1 Introduction

A constitutive relationship based on a hypoelastic orthotropic approach is proposed to model the behavior of a three dimensional (axisymmetric) concrete continuum. The model assumes small displacements, infinitesimal strains and negligible rotations. No rate, temperature or creep effects are provided for. It is defined in the form of an incremental stress-strain constitutive equation in which the material parameters are obtained from stress-equivalent uniaxial strain relationships. The model draws heavily on the earlier work of Darwin and Pecknold (1974, 1977a and 1977b), of Saenz (1964) and of Willam and Warnke (1975). In the following, the constitutive matrix, the stress equivalent uniaxial strain relation, the constitutive or material parameters and the ultimate strength and corresponding equivalent uniaxial strain criteria, incorporated into the model, are discussed.

2.3.2 The Constitutive Equation

The proposed constitutive relation is intended for use in the analysis of axisymmetric structures. Therefore, the constitutive matrix is 4 x 4. When orthotropy is assumed, the number of independent variables in the constitutive matrix is restricted to ten. When the relation is referred to the principal axes of orthotropy it can be written in the form of an incremental Hooke's Law as follows

$$\begin{Bmatrix} d\varepsilon_1 \\ d\varepsilon_2 \\ d\varepsilon_3 \\ d\gamma_{12} \end{Bmatrix} = \begin{bmatrix} 1/E_1 & -\nu_{12}/E_2 & -\nu_{13}/E_3 & 0 \\ -\nu_{21}/E_1 & 1/E_2 & -\nu_{23}/E_3 & 0 \\ -\nu_{31}/E_1 & -\nu_{32}/E_2 & 1/E_3 & 0 \\ 0 & 0 & 0 & 1/G_{12} \end{bmatrix} \begin{Bmatrix} d\sigma_1 \\ d\sigma_2 \\ d\sigma_3 \\ d\tau_{12} \end{Bmatrix} \tag{2.10}$$

It will be assumed that the constitutive matrix will remain symmetric throughout the analysis. This symmetry gives rise to the following relations

$$\nu_{12} E_1 = \nu_{21} E_2 \tag{2.11a}$$

$$\nu_{13} E_1 = \nu_{31} E_3 \tag{2.11b}$$

$$\nu_{23} E_2 = \nu_{32} E_3 \tag{2.11c}$$

substituting Eqs. 2.11 into Eq. 2.10 and rearranging, the following symmetric form of Eq. 2.10 can be obtained,

$$\begin{Bmatrix} d\varepsilon_1 \\ d\varepsilon_2 \\ d\varepsilon_3 \\ d\gamma_{12} \end{Bmatrix} = \begin{bmatrix} 1/E_1 & -\eta_{12}/\sqrt{E_1E_2} & -\eta_{31}/\sqrt{E_1E_3} & 0 \\ & 1/E_2 & -\eta_{23}/\sqrt{E_2E_3} & 0 \\ & \text{Sym.} & 1/E_3 & 0 \\ & & & 1/G_{12} \end{bmatrix} \begin{Bmatrix} d\sigma_1 \\ d\sigma_2 \\ d\sigma_3 \\ d\tau_{12} \end{Bmatrix} \tag{2.12}$$

which when inverted yields

$$\begin{Bmatrix} d\sigma_1 \\ d\sigma_2 \\ d\sigma_3 \\ d\tau_{12} \end{Bmatrix} = 1/\phi \begin{bmatrix} E_1(1-\eta_{23}^2) & \sqrt{E_1E_2}\,(\eta_{31}\eta_{23}+\eta_{12}) & \sqrt{E_1E_3}\,(\eta_{12}\eta_{23}+\eta_{31}) & 0 \\ & E_2(1-\eta_{31}^2) & \sqrt{E_2E_3}\,(\eta_{12}\eta_{31}+\eta_{23}) & 0 \\ & \text{Sym.} & E_3(1-\eta_{12}^2) & 0 \\ & & & G_{12}\phi \end{bmatrix} \begin{Bmatrix} d\varepsilon_1 \\ d\varepsilon_1 \\ d\varepsilon_3 \\ d\gamma_{12} \end{Bmatrix} \tag{2.13}$$

where

$$\eta_{12}^2 = \nu_{12}\,\nu_{21} \tag{2.14a}$$

$$\eta_{23}^2 = \nu_{23}\,\nu_{32} \tag{2.14b}$$

$$\eta_{31}^2 = \nu_{13}\,\nu_{31} \tag{2.14c}$$

$$\phi = (1 - \eta_{21}^2 - \eta_{23}^2 - \eta_{31}^2 - 2\eta_{12}\eta_{23}\eta_{31}) \tag{2.14d}$$

Eqs. 2.13 and 2.14 are the basis of the constitutive relation. The symmetry assumed above is by no means trivial and will be enlarged upon later.

2.3.3 The Equivalent Uniaxial Strain Concept

Having defined the form of the incremental constitutive equation it remains to determine the variation of the tangential hypoelastic moduli. For this purpose, the concept of equivalent uniaxial strains which has been developed by Darwin and Pecknold (1974, 1977a, 1977b) is used with slight modifications. This concept is briefly described as follows.

Let Eq. 2.13 be written as

$$\begin{Bmatrix} d\sigma_1 \\ d\sigma_2 \\ d\sigma_3 \\ d\tau_{12} \end{Bmatrix} = \begin{bmatrix} E_1B_{11} & E_1B_{12} & E_1B_{13} & 0 \\ E_2B_{21} & E_2B_{22} & E_2B_{23} & 0 \\ E_3B_{31} & E_3B_{32} & E_3B_{33} & 0 \\ 0 & 0 & 0 & G_{12} \end{bmatrix} \begin{Bmatrix} d\varepsilon_1 \\ d\varepsilon_2 \\ d\varepsilon_3 \\ d\gamma_{12} \end{Bmatrix} \tag{2.15}$$

in which the coefficients B_{ij} are defined by identifying the matrix terms of Eq. 2.15 with the corresponding terms of Eq. 2.13. Carrying out the multiplications of Eq. 2.15 yields

$$d\sigma_1 = E_1 (B_{11}d\varepsilon_1 + B_{12}d\varepsilon_2 + B_{13}d\varepsilon_3) \quad (2.16a)$$

$$d\sigma_2 = E_2 (B_{21}d\varepsilon_1 + B_{22}d\varepsilon_2 + B_{23}d\varepsilon_3) \quad (2.16b)$$

$$d\sigma_3 = E_3 (B_{31}d\varepsilon_1 + B_{32}d\varepsilon_2 + B_{33}d\varepsilon_3) \quad (2.16c)$$

$$d\tau_{12} = G_{12}\, d\gamma_{12} \quad (2.16d)$$

Eqs. 2.16 is written in matrix form as follows

$$\begin{Bmatrix} d\sigma_1 \\ d\sigma_2 \\ d\sigma_3 \\ d\tau_{12} \end{Bmatrix} = \begin{bmatrix} E_1 & 0 & 0 & 0 \\ 0 & E_2 & 0 & 0 \\ 0 & 0 & E_3 & 0 \\ 0 & 0 & 0 & G_{12} \end{bmatrix} \begin{Bmatrix} d\varepsilon_{1u} \\ d\varepsilon_{2u} \\ d\varepsilon_{3u} \\ d\gamma_{12} \end{Bmatrix} \quad (2.17)$$

where $< d\varepsilon_u >$ is defined as the equivalent uniaxial strain increment and is written in terms of the actual strain increment as

$$d\varepsilon_{ui} = \sum_{j=1}^{3} B_{ij}\, d\varepsilon_j \quad , \quad i = 1,3 \quad (2.18)$$

The equivalent uniaxial strain increment can be evaluated from Eq. 2.17 in the simple form

$$d\varepsilon_{ui} = d\sigma_i/E_i \quad \text{(no sum)} \quad , \quad i = 1,3 \quad (2.19)$$

and the total equivalent uniaxial strain may be determined by integrating Eq. 2.19 over the load path

$$\varepsilon_{ui} = \int_{\text{(over load path)}} d\sigma_i/E_i \quad \text{(no sum)} \quad , \quad i = 1,3 \quad (2.20)$$

Eqs. 2.16 are defined in the principal axes of orthotropy. Darwin and Pecknold assumed that the principal axes of orthotropy

follow the principal axes of stresses. However, in axisymmetric shell structures the meridional and circumferential stress directions predominate. Therefore, the proposed model assumes that the principal axes of orthotropy at a point are fixed in the local meridional, circumferential and normal directions. The equivalent uniaxial strains will be treated in the same manner as real strains and will be transformed using the usual coordinate transformation methods. A physical interpretation for the equivalent uniaxial strains and the diagonal matrix of Eq. 2.17 is attempted in the following. The increment equivalent uniaxial strain of Eq. 2.19 is the increment of the strain in direction i that the material would exhibit if subjected to a stress increment $d\sigma_i$ while all other stress increment contributions are equal to zero. In other words, the matrix of Eq. 2.17 is the constitutive matrix of a fictitious material with zero Poisson's ratios.

2.3.4 The Equivalent Uniaxial Strain-Stress Relation

In the hypoelastic theory developed by Truesdell (1955) the stress strain relation follows from the incremental constitutive equations. In the material model proposed herein it is assumed that the total stresses are functions of the current equivalent uniaxial strains.

For the purposes of this work, the uniaxial compressive stress strain relationship of Saenz (1964) is generalized in a

manner similar to that proposed by Darwin and Pecknold (1974, 1977a and 1977b) and used to describe compressive as well as tensile responses on the ascending part of the stress-equivalent uniaxial strain curve. Writing Saenz's relationship in terms of the equivalent uniaxial strain yields

$$\sigma_i = E_{oi}\varepsilon_{ui}/[1 + (R_E - 2)\ (\varepsilon_{ui}/\varepsilon_{ci}) + (\varepsilon_{ui}/\varepsilon_{ci})^2] \qquad (2.21)$$

where

$$R_E = E_{oi}/E_{si} \quad \text{(no sum)} \qquad (2.22a)$$

$$E_{is} = \sigma_{ci}/\varepsilon_{ci} \quad \text{(no sum)} \qquad (2.22b)$$

The type of curve described by Eq. 2.21 is illustrated in Fig. 2.1 on which the variables of Eqs. 2.21 and 2.22b are shown. More specifically, E_{oi} is the initial modulus of elasticity in direction i and σ_{ci} and ε_{ci} are the maximum stress associated with direction i and the corresponding equivalent uniaxial strain respectively.

The descending branch of Eq. 2.21 is too steep for lightly reinforced concrete in tension. Therefore, in this study a bilinear descending branch is adopted, as follows (no sum)

$$\sigma_i = \sigma_{ci}\ (1 - \alpha_1\ (\varepsilon_{ui}/\varepsilon_{ci} - 1)) \quad 1 < \varepsilon_{ui}/\varepsilon_{ci} \leq \beta \qquad (2.23a)$$

$$\sigma_i = \sigma_{ci}\ \alpha_2\ (\beta_2 - \varepsilon_{ui}/\varepsilon_{ci}) \quad \beta_1 < \varepsilon_{ui}/\varepsilon_{ci} \leq \beta_2 \qquad (2.23b)$$

$$\sigma_i = 0 \quad \beta_2 < \varepsilon_{ui}/\varepsilon_{ci} \qquad (2.23c)$$

where α_1, α_2, β_1 and β_2 are shown on Fig. 2.2.

In compression, Eq. 2.21 is retained up to $\varepsilon_{ui} = 2\varepsilon_{ci}$ at which point it is assumed that concrete crushes. The complete curves for compression and tension are shown on Figs. 2.1 and 2.2 respectively.

Eq. 2.16d shows that the shear strain can be accumulated directly. For the purposes of this study the Saenz relation was adopted for shear and is written as

$$\tau_{12} = G_{o12}\gamma_{12}/[1 - (R_G - 2)(\gamma_{12}/\gamma_{c12}) + (\gamma_{12}\ \gamma_{c12})^2] \quad (2.24)$$

where

$$R_G = G_{s12}/G_{o12} \quad (2.25a)$$

$$G_{s12} = \tau_{c12}/\gamma_{c12} \quad (2.25b)$$

and G_{o12} is the initial shear modulus, and τ_{c12} and γ_{c12} are the maximum shear stress and the corresponding shear strain respectively. Eq. 2.24 is adopted up to the peak of the shear curve. For the descending branch of the shear response a straight line is used as follows

$$\tau_{12} = \tau_{c12}\ (1 - \alpha_3\ (\gamma_{12}/\gamma_{c12} - 1)) \quad 1 < \tau_{12}/\tau_{c12} \quad (2.26)$$

where α_3 is a constant. The shear stress strain curve is shown in Fig. 2.3. In this study shear deformations are expected to be low in the particular coordinate system chosen. Therefore, the difference between Eq. 2.24 and the equations of Kupfer and Gerstle (1973) or Cedolin, et al. (1976 and 1977) is expected to be of no importance and the point is not further pursued.

2.3.3 Young's Moduli and the Shear Modulus

Eq. 2.21 serves to define the incremental elastic moduli of Eq. 2.17, for by Eq. 2.19

$$E_i = d\sigma_i/d\varepsilon_{ui} \qquad \text{(no sum)} \tag{2.27}$$

Differentiating Eq. 2.21 with respect to ε_{iu} yields

$$E_i = E_{oi}(1 - (\varepsilon_{ui}/\varepsilon_{ci})^2/[1 - (R_\varepsilon - 2)(\varepsilon_{ui}/\varepsilon_{ci}) + (\varepsilon_{ui}/\varepsilon_{ci})^2]^2 \qquad \text{(no sum)} \tag{2.28}$$

which defines Young's moduli.

The incremental shear modulus G_{12} can be obtained from Eq. 2.24 using similar reasoning as

$$G_{12} = G_{o_{12}}(1 - (\gamma_{12}/\gamma_{c12})^2)/[1 - (R_G - 2)(\gamma_{12}/\gamma_{c12}) + (\gamma_{12}/\gamma_{c12})^2]^2 \tag{2.29}$$

Eqs. 2.28 and 2.29 are confined to the ascending branches of the respective responses, except in compression where Eqs. 2.28 is still used for the descending branch. In tension and shear however, the required moduli are assumed to be

$$E_i = -\alpha_1 E_{si} \qquad 1 < \varepsilon_{ui}/\varepsilon_{ci} < \beta_1 \tag{2.30a}$$

$$E_i = -\alpha_2 E_{si} \qquad \beta_1 < \varepsilon_{ui}/\varepsilon_{ci} < \beta_2 \tag{2.30b}$$

$$G_{12} = -\alpha_3 G_{s12} \qquad 1 < \gamma_{12}/\gamma_{c12} \tag{2.30c}$$

The choice of α_1, α_2, β_1, β_2 and α_3 depends on the amount of steel in the neighbourhood of the point under consideration. In

order that a tangential stiffness approach be successful, it is recommended that the overall uniaxial stiffness of a region including steel be required to be positive definite (Chitnuyanondh, et al., 1979).

2.3.6 Poisson's Ratio

Prior to implementing the incremental stress strain relationship it is necessary to determine the values of Poisson's ratios appearing in Eq. 2.13. It is assumed herein that a strain dependent Poisson's ratio may be applied to each equivalent uniaxial strain, that is, three independent Poisson's ratios are postulated in the form

$$\nu_i = \nu_o \, f\,(\varepsilon_{ui}/\varepsilon_{ci}) \qquad \text{(no sum)} \qquad (2.31)$$

in which ν_o is the initial Poisson's ratio. Eqs. 2.14a to 2.14c may now be written as

$$\eta_{12}^2 = \nu_1 \, \nu_2 \qquad (2.32a)$$

$$\eta_{23}^2 = \nu_2 \, \nu_3 \qquad (2.32b)$$

$$\eta_{31}^2 = \nu_3 \, \nu_1 \qquad (2.32c)$$

In compression, the function $f(\varepsilon_{ui}/\varepsilon_{ci})$ appearing in Eq. 2.31 has been determined from the uniaxial compression data of Kupfer, Hilsdorf and Rüsch (1969) by a least squares fit of a cubic polynomial. This results in the approximation

$$\nu = \nu_o(1.0000 + 1.3763\ (\varepsilon/\varepsilon_{cu}) - 5.3600\ (\varepsilon/\varepsilon_{cu})^2 + 8.5860\ (\varepsilon/\varepsilon_{cu})^3) \qquad (2.33)$$

in which ε is the strain in the direction of loading and ε_{cu} is the strain at ultimate strength. Substituting ε_{ui} and ε_{ci} for ε and ε_{cu} respectively, Eq. 2.33 assumes the form of Eq. 2.31.

Micro-cracks exist in concrete along the aggregate mortar interfaces even at the virgin state (Hsu, et al., 1963). At 30% of ultimate strength these cracks increase in number, width, and length. At approximately 75% of ultimate strength these cracks penetrate the mortar between pieces of aggregate forming a continuous pattern appropriate to the stress condition. Although Hsu, et al. (1978) studied concrete in compression, the same behavior may be expected in tension but developing more rapidly than in compression. Consider a block of concrete under tension in direction i with a pattern of internal cracks as shown in Fig. 2.4. Let the block be subjected to tension or compression in any direction perpendicular to direction i. The contraction or expansion in direction i due to the applied stresses in a perpendicular direction will be absorbed, in part, by filling or increasing the volume of cracks. In other words the total Poisson's ratio effect on the block will be diminished. Once the material has reached its ultimate strength in tension in direction i, these cracks may become wide enough to inhibit interaction between direction i and the normal plane, except for the shear provided by aggregate interlock, etc. Therefore, it has been assumed that Poisson's ratio in tension is constant up to the appearance of mortar cracks. It is further assumed that a definite pattern of mortar cracks in tension starts to appear at 50% of the ultimate tensile strength. At this point it is assumed that Poisson's ratio starts to degrade becoming zero at ultimate tensile strength.

This is expressed as follows, (see Figures 2.5a and 2.5b)

$$\nu_i = \nu_o \qquad 0 < \varepsilon_{ui}/\varepsilon_{ci} \leq 0.5 \qquad (2.34a)$$

$$\nu_i = 2\nu_o(1 - \varepsilon_{ui}/\varepsilon_{ci}) \qquad 0.5 < \varepsilon_{ui}/\varepsilon_{ci} \leq 1.0 \qquad (2.34b)$$

$$\nu_i = 0.0 \qquad 1.0 < \varepsilon_{ui}/\varepsilon_{ci} \qquad (2.34c)$$

At this point it should be noted that the variable ϕ appearing in Eq. 2.13 should always be non negative. A limiting value of 0.5 has therefore been placed on the values of ν_i in compression. This value corresponds to a limit of zero incremental volume change. Kotsovos and Newman (1977) have noted that the point at which this limit is reached corresponds to the onset of unstable micro-crack propagation. This is the process that causes the dilatation phenomena observed in concrete upon approaching the ultimate strength under uniaxial and biaxial compression. Therefore, it can be argued that the dilatation has no meaningful constitutive significance. Moreover, no dilatation is observed under triaxial compression (Schickert and Winkler, 1977). Rather, the material appears to flow which supports a limit of 0.5 on Poisson's ratio in compression.

2.3.7 The Ultimate Surfaces

The evaluation of the hypoelastic moduli described in Section 2.3.5 and 2.3.6 requires the specification of the parameters appearing on the right hand side of Eqs. 2.21 to 2.34, i.e. σ_{ci} and ε_{ci}. Since these parameters vary with the changing stress configuration as well as the loading history, the evaluation can be done by specifying a surface in stress space to define the three values

of σ_{ci} and a surface in the equivalent uniaxial strain space to define the three values of ε_{ci} that correspond to the σ_{ci}'s.

A surface in stress space that defines the ultimate strengths σ_{ci} for any ratio of stresses is called a "failure surface". This name is somewhat misleading in case of a material with strain softening behavior. It is proposed to call such a surface an "ultimate strength surface" (Elwi and Murray, 1979). The five parameter surface proposed by Willam and Warnke (1975) and illustrated in Fig. 2.6a is used in this work to define the ultimate strength surface as well as the corresponding equivalent uniaxial strain surface. The characteristics of this surface are reviewed briefly in the following.

Let the mean (average) normal stress be defined as

$$\sigma_a = \sigma_{ii}/3 \tag{2.35}$$

and let the mean (average) shear stress be defined as

$$\tau_a = \sqrt{s_{ij}\, s_{ij}/5} \tag{2.36}$$

where s_{ij} is the deviatoric stress tensor which is written as

$$s_{ij} = \sigma_{ij} - \sigma_{kk}\, \delta_{ij}/3 \tag{2.37}$$

Dividing by the uniaxial compressive strength f_{cu}, the variables σ_a and τ_a are nondimensionalized such that

$$\bar{\sigma}_a = \sigma_a/f_{cu} \tag{2.38a}$$

$$\bar{\tau}_a = \tau_a/f_{cu} \tag{2.38b}$$

The surface under consideration is assumed to intersect the deviatoric plane (σ_a = constant) in three symmetric elliptical segments forming a closed convex and continuous curve. This trace is shown in Fig. 2.6b on a triaxial plot, with the axes representing the main deviatoric stresses σ_i'. The elliptic trace may be mathematically described as

$$\bar{\tau}_a = r(\theta, \bar{\sigma}_a) \tag{2.39}$$

where θ is called the angle of similarity and is expressed in terms of the principal stresses as (Willam and Warnke, 1975)

$$\cos\theta = (\sigma_1 + \sigma_2 - 2\sigma_3)/\{\sqrt{2}[(\sigma_1 - \sigma_2)^2 + (\sigma_2 - \sigma_3)^2 + (\sigma_3 - \sigma_1)^2]^{1/2}\} \tag{2.40}$$

For $\sigma_1 \geq \sigma_2 \geq \sigma_3$, then $0 \leq \theta \leq 60°$, as may be seen in Fig. 2.6b. The function r in Eq. 2.39 is defined as (Willam and Warnke, 1975)

$$r = \frac{2r_2 r_1^2 \cos\theta + r_2(2r_1 - r_2)(4r_{12}\cos^2\theta + 5r_1^2 - 4r_1 r_2)^{1/2}}{4r_{12}\cos^2\theta + (r_2 - 2r_1)^2} \tag{2.41}$$

in which

$$r_{12} = r_2^2 - r_1^2 \tag{2.42}$$

The variables r_2 and r_1 are respectively the maximum ($\theta = 60°$) and minimum ($\theta = 0°$) radii of the deviatoric trace of the surface. These variables are assumed to be parabolic functions of the hydrostatic stress and are expressed as (Willam and Warnke, 1975)

$$r_1 = a_o + a_1 \bar{\sigma}_a + a_2 \bar{\sigma}_a^2 \tag{2.43a}$$

$$r_2 = b_o + b_1 \bar{\sigma}_a + b_2 \bar{\sigma}_a^2 \tag{2.43b}$$

Plotted on the so called "rendulic plane", the functions r_1 and r_2 are illustrated in Fig. 2.6c. The values of the coefficients a_o to b_2 in Eqs. 2.43 are chosen such that the variables r_1 and r_2 pass through a set of control points, as illustrated in Fig. 2.6c. Appendix A describes how these coefficients are evaluated. The surface proposed by Willam and Wanke (1975) is now completely defined and serves to evaluate the three σ_{ci}'s required in Sections 2.3.4 and 2.3.5.

However, Eqs. 2.21 to 2.34 also require the evaluation of the equivalent uniaxial strains ε_{ci} associated with σ_{ci}. For this purpose it is postulated that there is a surface in equivalent uniaxial strain space which has the same form as the stress surface described above. Therefore, the strain quantities ε_a and γ_a are defined to correspond with σ_a and τ_a respectively by replacing σ_1, σ_2, σ_3 in Eqs. 2.35 to 2.43 by the principal components of the equivalent uniaxial strain tensor. The analogous nondimensionalization of Eqs. 2.38 is carried out with ε_{cu}, the strain corresponding to uniaxial compressive strength, replacing f_{cu}. Analogous quantities for the strain control points follow directly and Eqs. 2.40 to 2.43 together with the equations of Appendix A can be used.

2.3.8 Failure Modes

The usage of the ultimate surfaces as implemented by Darwin and Pecknold assumes that instantaneously, the loading is proportional. Thus, joining the origin and the current stress point with a straight line and extending the straight line to intersect the surface the required ultimate point can be obtained. This

procedure has been found to be quite adequate in triaxial and biaxial compression, (Elwi and Murray, 1979). However, in other situations it becomes inadequate since it is conceivable that a point under tension may crack normal to the direction of loading, but can still support increasing stress in the other two directions in tension or compression, (Chitnuyanondh, et al., 1979). Therefore, the failure mode must be taken into consideration.

For the purpose of imposing failure modes on the evaluation of the parameters, σ_{ci} and ε_{ci}, a number of conditions are stipulated as follows:

(i) Compression-Compression-Compression:

In this case the parameters are obtained from the ultimate surfaces described in Section 2.3.7.

(ii) Compression-Compression-Tension:

In this case the tensile components are obtained from the ultimate surfaces. The compression components if greater than f_{cu} in case of stresses or greater than ε_{cu} in case of equivalent uniaxial strains may be taken equal to f_{cu} or ε_{cu} as the case may be. The term "greater than" in the last sentence is meant in the algebraic sense.

(iii) Tension-Tension-Compression:

In this case, the larger tensile components are obtained from the ultimate surfaces. The smaller tensile components may be taken as f_{tu} or ε_{tu} as the case may be. The compressive components may be taken as f_{cu} or ε_{cu} as the case may be.

(iv) Tension-Tension-Tension:

In this case all components may be taken as f_{tu} or ε_{tu} as

the case may be.

The stress paths that may produce conditions (ii) to (iv) are illustrated in Figures 2.7a to 2.7c.

2.3.9 Verification of the Constitutive Relation

In order for the constitutive relation proposed in this chapter to have validity, it should be able to predict strains associated with test results in the literature. The available experimental studies are associated with a predefined stress path. In this type of application stress increments are applied and it is required to find the associated strain increments. A flow chart for this type of application, which requires iteration, is shown in Fig. 2.16.

A comparison of predicted strains with selected sets of measurements by Kupfer, Hilsdorf and Rüsch (1969), hereinafter refered to as the KHR data, in a series of biaxial tests is shown in Figs. 2.8 to 2.11, inclusive. The parameters that have been used to model this material are given in Table 2.1. Fig. 2.8 shows the uniaxial compression comparison, and Fig. 2.9 shows the biaxial compression comparison. Since the peak stresses and corresponding strains are control points on the associated ultimate surfaces, exact correlation is obtained at these points. Fig. 2.10 shows the comparison for biaxial compression in the ratio of -1:-52. Since the chosen ultimate strength surface does not predict the same strength as the KHR failure surface there is a discrepancy of approximately 8% in this instance. A comparison of typical response in tension-compression is shown in Fig. 2.11.

The above comparisons are those of the three dimensional theory with plane stress tests. A comparison of the theory with some of the three dimensional tests of Schickert and Winkler (1977), hereinafter refered to as the SW data, has also been carried out. First, the parameters of Eqs. 2.43 have been evaluated for the control points and are shown in Table 2.2. The correspondence of these equations on the rendulic plane with the SW data is shown in Fig. 2.12. The values of r_1 and r_2 are seen to agree suitably with this data set. The SW tests were carried out by loading along a hydrostatic stress path with deviatoric stress equal to zero, and then incrementing the three principal stresses in such a way that the hydrostatic stress remained constant while the deviatoric stress varied. Fig. 2.13 illustrates results for deviatoric stress path along line 0 - A of Fig. 2.6b ($\theta = 60°$). Fig. 2.14 illustrates results for a deviatoric stress path along line 0 - C of Fig. 2.6b ($\theta = 30°$). Fig. 2.15 illustrates results for a deviatoric stress path along line 0 - B of Fig. 2.6b ($\theta = 0°$). It can be seen that the model reasonably simulates the SW data along each of these non-trivial stress paths.

Ultimate Strength Surface Parameters		Equivalent Uniaxial Strain Surface Parameters		Elastic Moduli	
f_{cu}^*	-4650.0	ε_{cu}	-0.00215	E_{01}^*	$4.7 * 10^6$
α_c	1.15	α_c	1.7512	E_{02}^*	$4.7 * 10^6$
α_t	0.091	α_t	0.046	E_{03}^*	0
ξ_1	13.50	ξ_1	50.0	G_{012}^*	$2.1 * 10^6$
ρ_1	0.0	ρ_1	0.0	ν_{01}	0.195
ξ_2	4.0	ξ_2	4.3	ν_{02}	0
ρ_2	0.0	ρ_2	0.0	ν_{03}	0

Table 2.1 KHR Material Model Parameters
(* in psi)

Ultimate Strength Surface Parameters		Equivalent Uniaxial Strain Surface Parameters		Initial Elastic Moduli	
f_{cu}^*	-4435.0	ε_{cu}	-0.00283	E_{01}^*	$3.8 * 10^6$
α_c	1.21	α_c	1.3	E_{02}^*	$3.8 * 10^6$
α_t	0.1	α_t	0.0461	E_{03}^*	$3.8 * 10^6$
ξ_1	13.50	ξ_1	22.5	G_{012}^*	$1.6 * 10^6$
ρ_1	0.0	ρ_1	0.0	ν_{01}	0.18
ξ_1	3.75	ξ_2	27.5	ν_{02}	0.18
ρ_2	0.0	ρ_2	0.0	ν_{03}	0.18

Table 2.2 Schickert-Winkler Material Mode Parameters

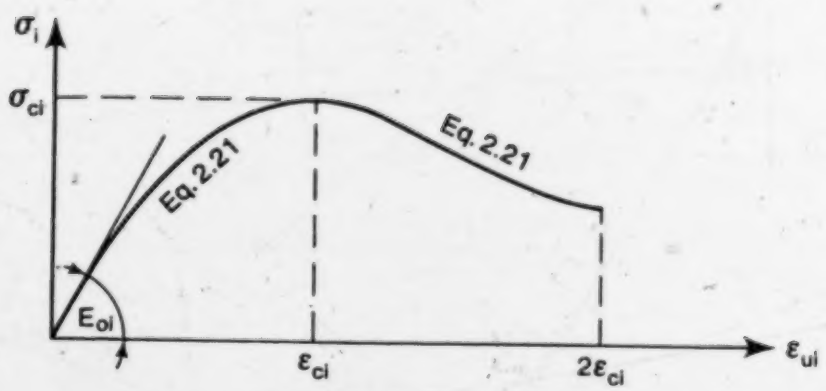

Fig. 2.1 Compressive Stress Equivalent Uniaxial Strain Relation

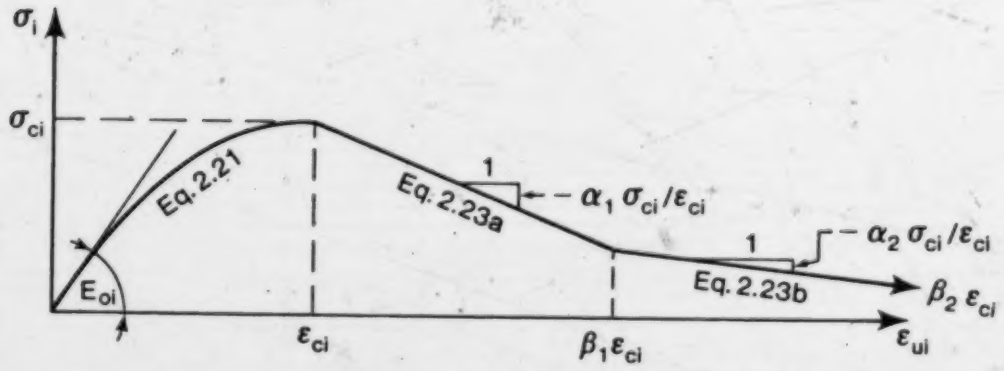

Fig. 2.2 Tensile Stress Equivalent Uniaxial Strain Relation

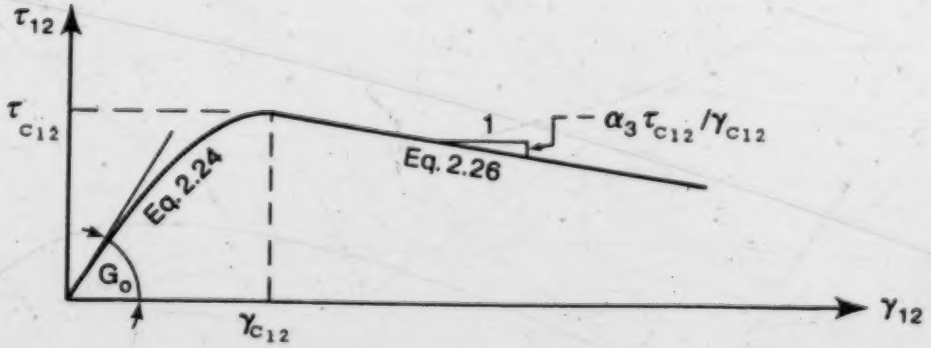

Fig. 2.3 Shear Stress Strain Relation

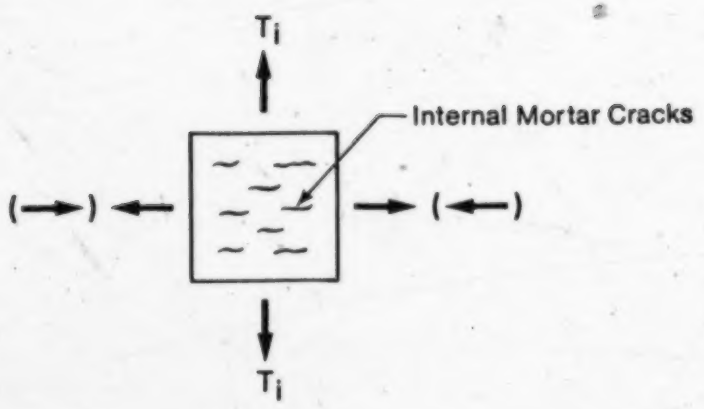

Fig. 2.4 Mortar Cracks

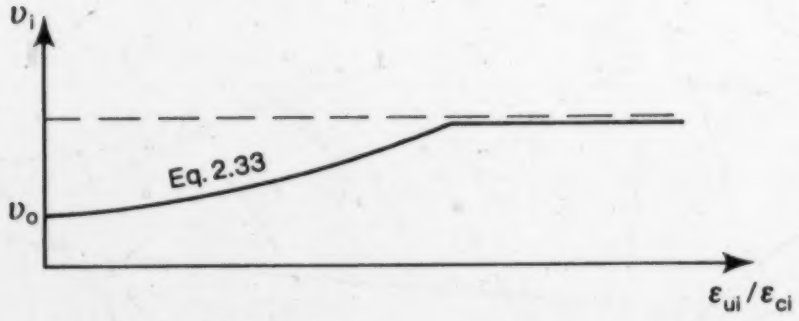

(a) Compression

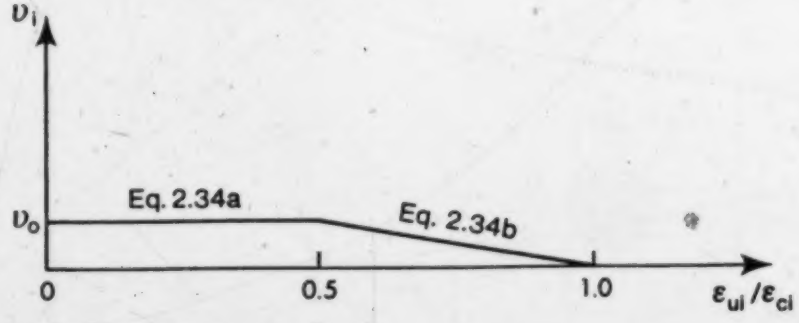

(b) Tension

Fig. 2.5 Proposed Poisson's Ratio-Equivalent Uniaxial Strain Relation

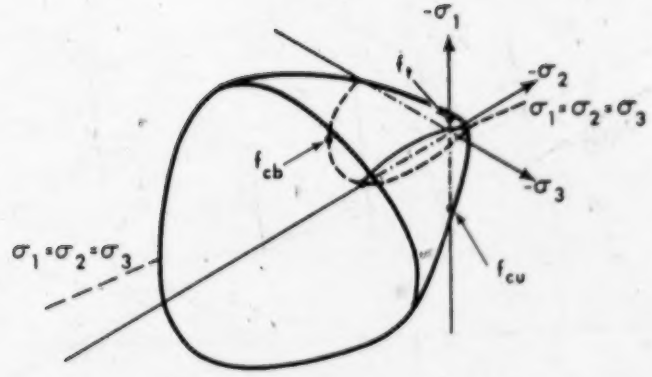

(a) General View of Argyris Failure Surface

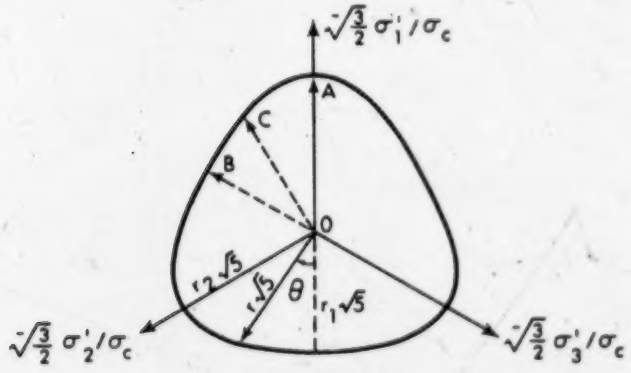

(b) A Deviatoric View of Argyris Surface

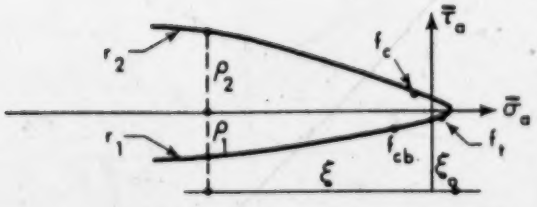

Point	$\bar{\sigma}_a$	$\bar{\tau}_a$
f_c	-1/3	$\sqrt{2/15}$
f_t	$\alpha_t/3$	$\alpha_t\sqrt{2/15}$
f_{cb}	$-2\alpha_c/3$	$\alpha_c\sqrt{2/15}$

(c) The Rendulic View of Argyris Surface

Fig. 2.6 The Ultimate Strength Surface

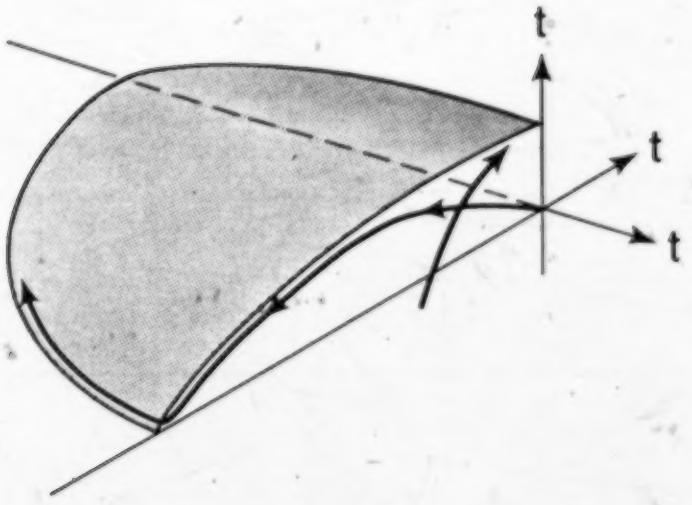

(a) Compression-Compression-Tension

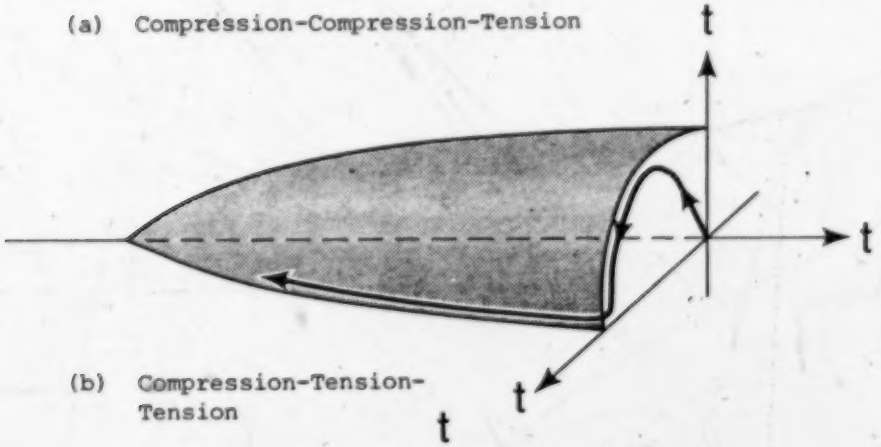

(b) Compression-Tension-Tension

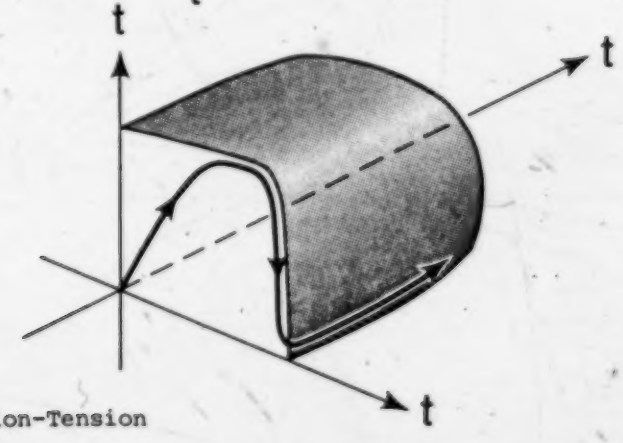

(c) Tension-Tension-Tension

Fig. 2.7 Failure Conditions

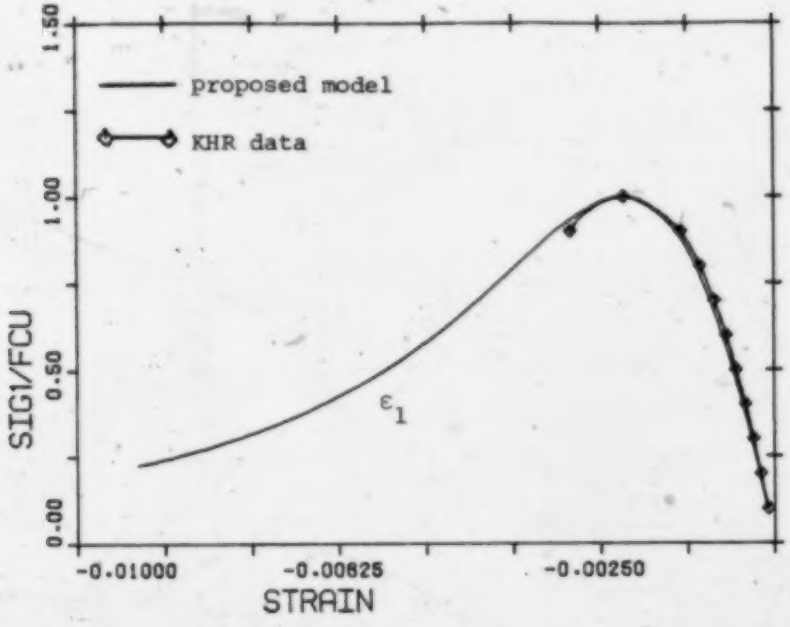

Fig. 2.8 Uniaxial Compression Comparison with KHR Data

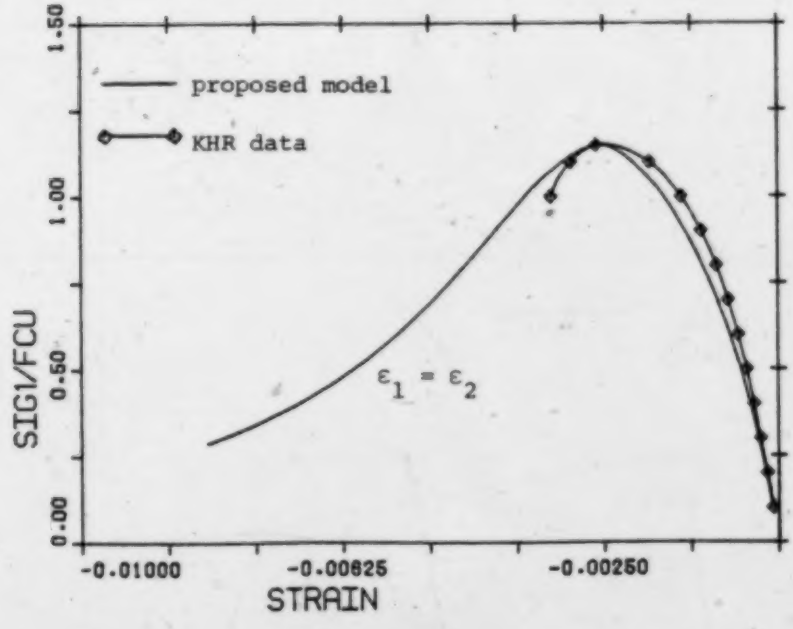

Fig. 2.9 Biaxial Compression (-1:-1) Comparison with KHR Data

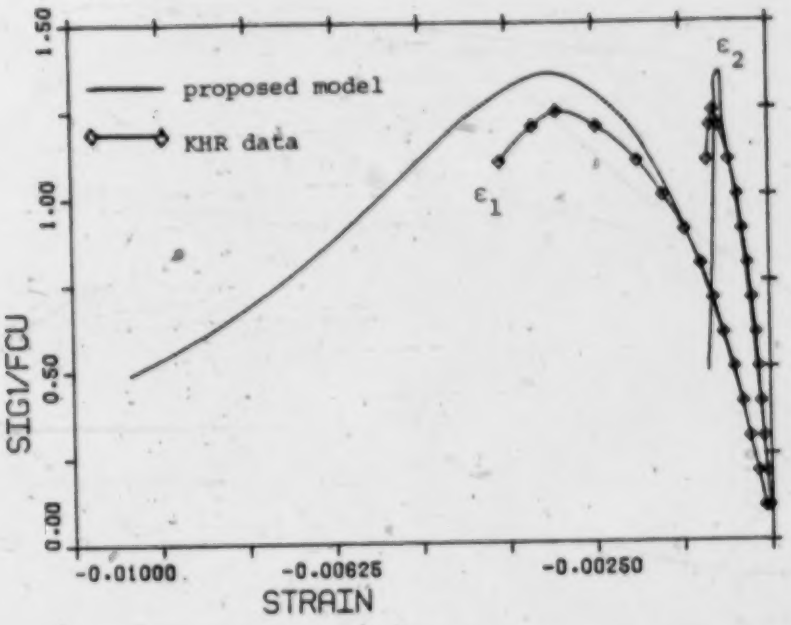

Fig. 2.10 Biaxial Compression (-1:-.52) Comparison with KHR Data

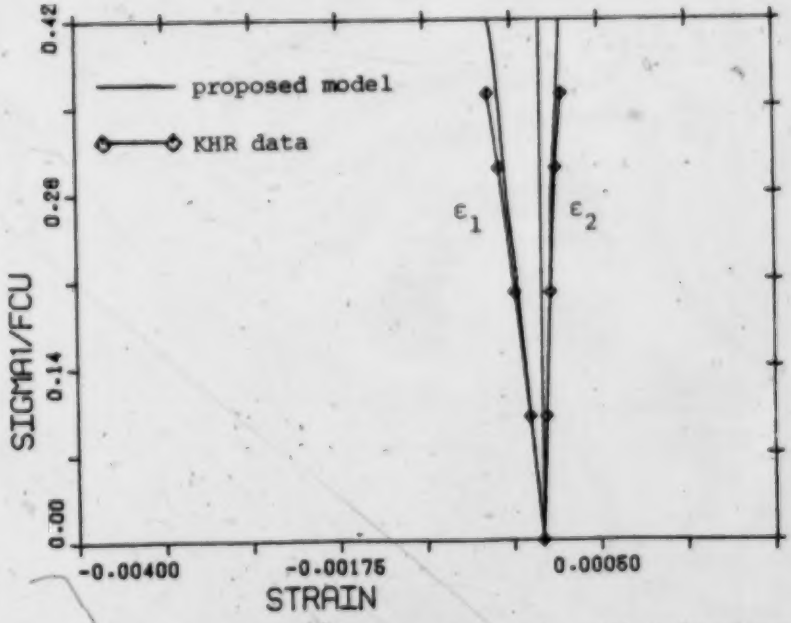

Fig. 2.11 Compression Tension (-1:.204) Comparison with KHR Data

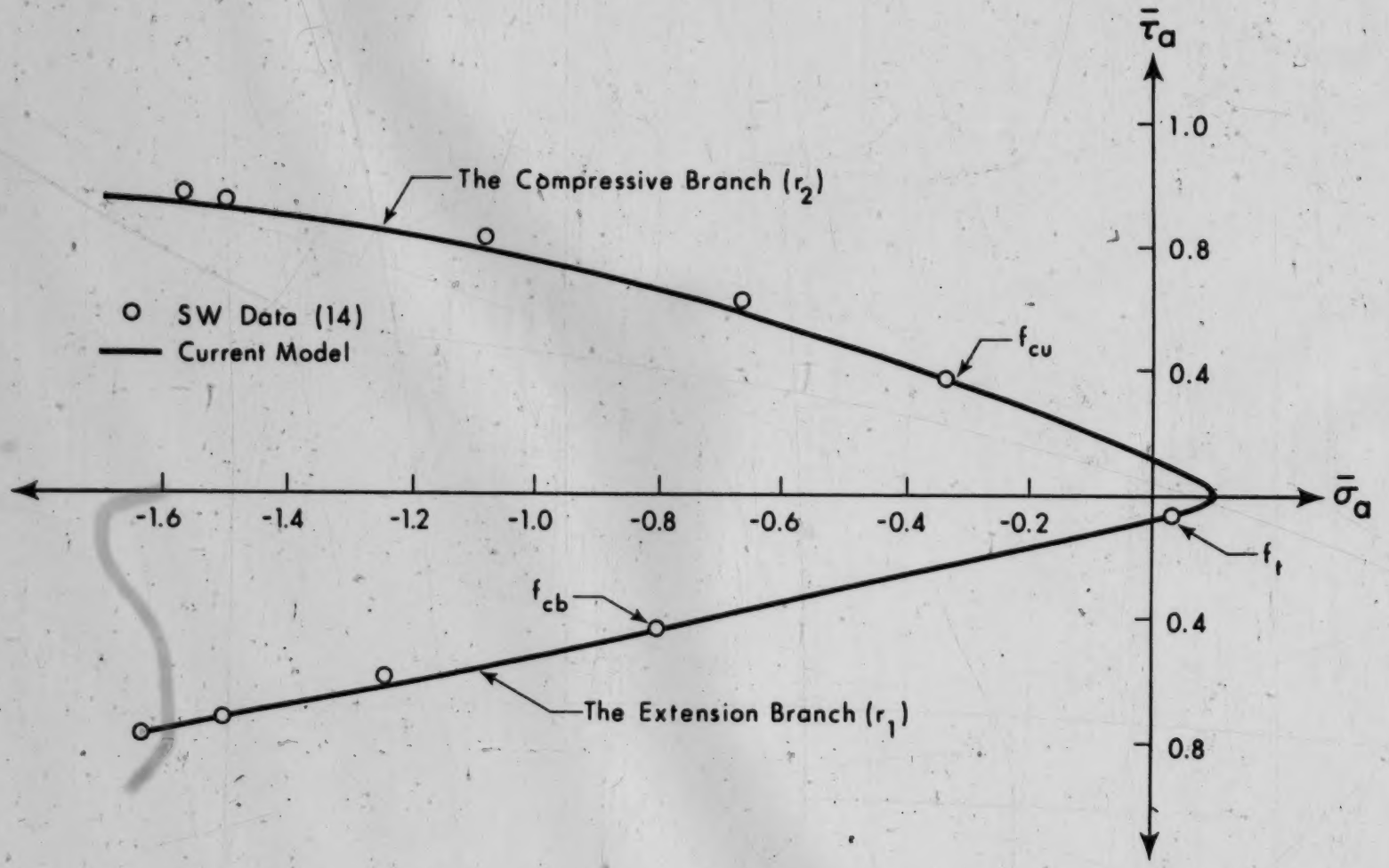

Fig. 2.12 Rendulic Plane Comparison with Schickert Winkler Data

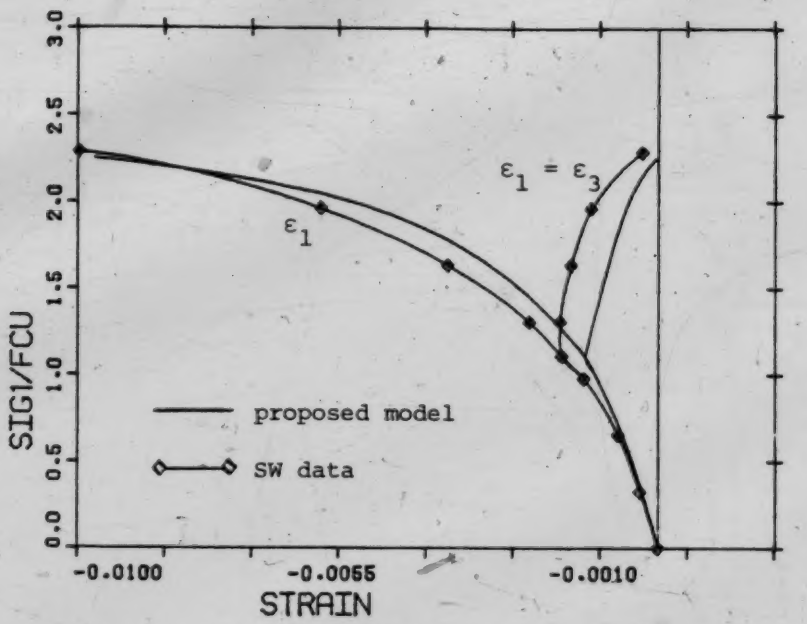

Fig. 2.13 Triaxial Compression Comparison (-1:.5:.5 stress changes) with Schickert and Winkler Data

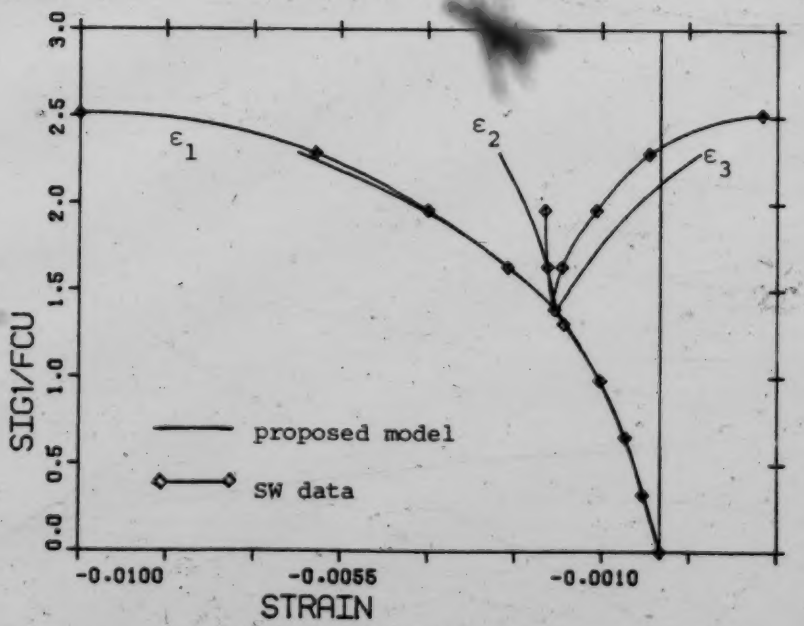

Fig. 2.14 Triaxial Compression Comparison (-1:0:1 stress changes) with Schickert and Winkler Data

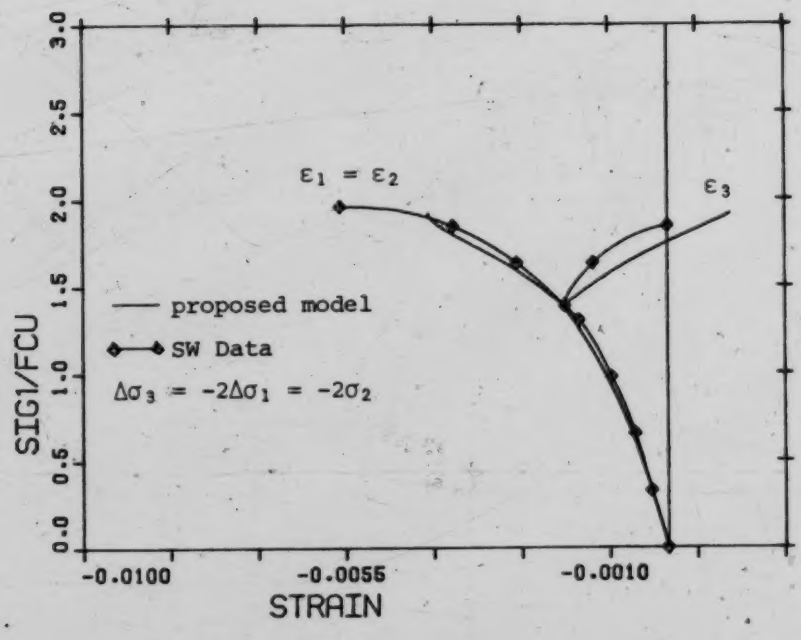

Fig. 2.15 Triaxial Compression Comparison (.5:.5:-1 stress changes) with Schickert Winkler Data

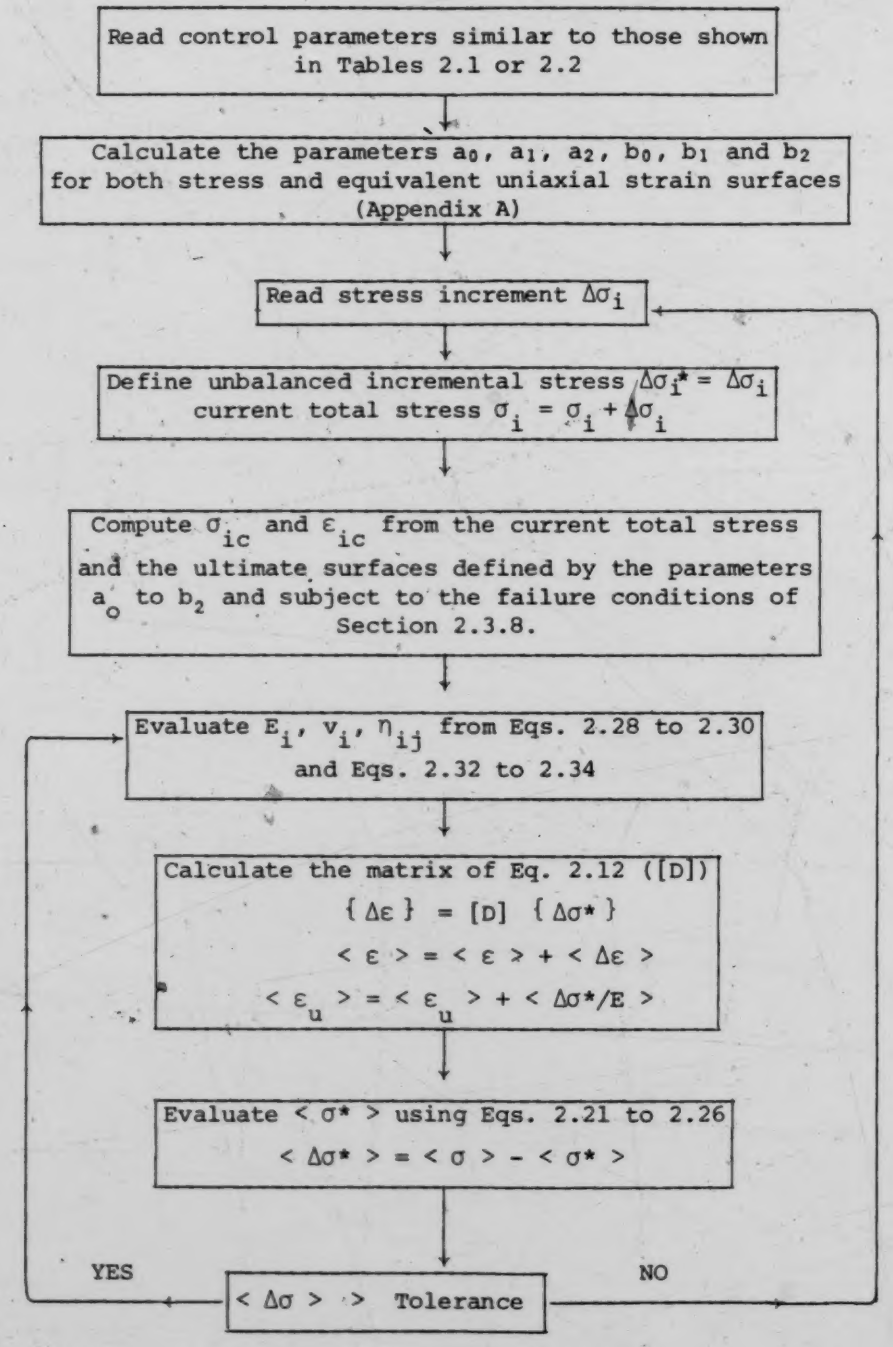

Fig. 2.16 Flow Chart for a Specified Stress Path

CHAPTER THREE

FINITE ELEMENT MODEL

3.1 Introduction

As described in Chapter One, it is the purpose of this study to develop a sophisticated tool for the analysis of reinforced concrete structures, for axisymmetric and planar problems, under static short term loads and small displacement fields. The rectangular serendipity family of finite elements (Zienkiewicz, 1971) has been chosen as the basis of program FEPARCS5. (FEPARCS is an acronym for 'Finite Element Program for the Analysis of Reinforced Concrete Structures'.) These elements can be converted easily from plane stress to axisymmetric state or vice versa without changing the frame of reference or the description of the strain field (Zienkiewicz, 1971). The main difference between axisymmetric and planar problems is in the description of material properties and the addition of circumferential strains (in case of axisymmetric formulation).

Three types of elements were developed; the solid element; a meridional reinforcing element and a circumferential reinforcing element. The meridional reinforcing element represents the reinforcing bars or prestressing tendons acting in z - r plane. The z-axis is the vertical axis of symmetry and the r-axis is horizontal radial axis. The circumferential reinforcing element represents the circumferential reinforcing bars or prestressing tendons. These elements are empty solid elements except for layers of reinforcing or prestressing. Strain compatibility between the steel and the

concrete is preserved by using the same shape functions and order of integration for all elements, (Buyucozturk, 1977).

A variational approach was used to derive the element stiffness matrices as well as different types of element loads such as gravity, thermal, and psuedo loads and surface tractions. In this chapter an incremental variational principle is reviewed, the element stiffness matrices are formulated, the loads resulting from body forces and surface tractions are derived and the boundary conditions are described.

3.2 Fundamental Variational Formulation

Before attempting to formulate the various element property matrices and vectors, it is necessary to establish the functional relationships governing the problem. The variational approach provides a powerful formulation technique for finite element theory. In this section the necessary variational principles are presented in incremental form based on small displacement fields.

Let the body shown in Fig. 3.1 be divided into "K" number of elements. Let V_e be the volume of an element and let S_{qe} and $S_{\sigma e}$ be those portions of the element surface on which the displacement and stresses are prescribed respectively. The superscript $(\ )^0$ indicates initial quantities at the beginning of a load step, and the prefix $\Delta(\ )$ denotes incremental quantities. Prescribed quantities will be denoted by $(\bar{\ })$. The incremental field equations can be written as

$$\sigma^0_{ij,j} + \Delta\sigma_{ij,j} + \bar{F}_i{}^0 + \Delta\bar{F}_i = 0 \qquad (3.1a)$$

$$\Delta\varepsilon_{ij} = \frac{1}{2}\,(q^0_{i,j} + q^0_{j,i}) + \frac{1}{2}\,(\Delta q_{i,j} + \Delta q_{j,i}) - \varepsilon^0_{ij} \qquad (3.1b)$$

$$\Delta\sigma_{ij} = C_{ijk\ell}\,\Delta\varepsilon_{k\ell} \qquad (3.1c)$$

Eqs. 3.1a to 3.1c are, respectively, the equilibrium equation, the strain displacement relation and the instantaneous stress increment strain increment relation. The symbols σ, ε, F, q and C denote respectively the stress tensor, the strain tensor, the body force per unit volume vector, the displacement field and the constitutive tensor (Pian, 1976).

The mechanical boundary conditions on $S_{\sigma e}$ are defined as (Pian, 1976)

$$\bar{T}_i{}^0 = \sigma^0_{ij}\,n_j \qquad (3.2a)$$

$$\Delta\bar{T}_i = \Delta\sigma_{ij}\,n_j \qquad (3.2b)$$

in which T denotes surface tractions and n denotes a unit vector normal to the surface. The displacement boundary conditions on S_{qe} are written as (Pian, 1976)

$$q_i{}^0 + \Delta q_i = \bar{q}_i{}^0 + \Delta\bar{q}_i \qquad (3.3)$$

Writing the first variation of Eqs. 3.1b and 3.3 and noting that initial and prescribed quantities do not vary, the following conditions are obtained.

$$\delta\,\Delta\varepsilon_{ij} = \frac{1}{2}\,(\delta\,\Delta q_{i,j} + \delta\,\Delta q_{j,i}) \quad (\text{on } V_e) \qquad (3.4a)$$

$$\delta \Delta q_i = 0 \qquad (S_{qe}) \qquad (3.4b)$$

Let the structure be forced through a virtual displacement field $\delta \Delta q$ subject to the condition stated in Eq. 3.4b. The virtual work δU of the internal forces and the virtual work δW of the external forces are expressed as

$$\delta U = \sum_K \left\{ \int_{V_e} (\sigma^0_{ij} + \Delta\sigma_{ij}) \; \delta\Delta\varepsilon_{ij} \; dV \right\} \qquad (3.5a)$$

$$\delta W = \sum_K \left\{ \int_{V_e} (\bar{F}_i^0 + \Delta \bar{F}_i) \; \delta\Delta q_i \; dV + \int_{S_e} (\bar{T}_i^0 + \Delta \bar{T}_i) \; \delta\Delta q_i \; dS \right\} \qquad (3.5b)$$

Substituting Eqs. 3.2 into the second term of Eq. 3.5b, applying the divergence theorm to the same term and using Eqs. 3.1a, 3.4a and 3.4b it can be proven that the virtual work of internal forces equals the virtual work of external forces subject to the conditions stated in Eqs. 3.4 which is called the "principle of virtual work" and can be written as

$$\sum_K \left\{ \int_{V_e} [(\sigma^0_{ij} + \Delta\sigma_{ij}) \; \delta\Delta\varepsilon_{ij} - (\bar{F}_i^0 + \Delta\bar{F}_i) \; \delta\Delta q_i] \; dV \right.$$

$$\left. - \int_{S_e} (\bar{T}_i^0 + \Delta\bar{T}_i) \; \delta\Delta q_i \; dS \right\} = 0 \qquad (3.6)$$

If the initial state is in equilibrium, then the virtual work associated with it must vanish. In this case Eq. 3.6 reduces to the form

$$\sum_K \left\{ \int_{V_e} [\Delta\sigma_{ij} \; \delta\Delta\varepsilon_{ij} - \Delta\bar{F}_i \; \delta\Delta q_i] dV - \int_{S_e} \Delta\bar{T}_i \; \delta\Delta q_i \; dS \right\} = 0 \qquad (3.7)$$

which is the incremental form of the principle of virtual work (Horrigmoe and Bregan, 1976).

The potential energy π_p associated with an increment of displacement Δq is defined as (Pian, 1976)

$$\pi_p(\Delta q) = \sum_K \left\{ \int_{V_e} [\sigma^0_{ij}\, \Delta\varepsilon_{ij} + \frac{1}{2}\, \Delta\varepsilon_{ij} C_{ijk\ell} \Delta\varepsilon_{k\ell} - (\bar{F}^0_i + \Delta\bar{F}_i)\Delta q_i]\, dV \right.$$

$$\left. - \int_{S_e} (\bar{T}^0_i + \Delta\bar{T}^0_i)\, \Delta q_i\, dS \right\} \tag{3.8}$$

Carrying out the first variation on Eq. 3.8 the right hand side becomes identical to the left hand side of Eq. 3.6. This means that the potential energy is stationary subject to the conditions stated in Eqs. 3.4. It is understood here that the material is linear elastic in the incremental region. In addition it can be proven that if the strain energy denoted by $(\frac{1}{2}\, \Delta\varepsilon_{ij}\, C_{ijk\ell}\, \Delta\varepsilon_{k\ell})$ is positive definite, then the stationary value of the potential energy is a local minimum (Fung, 1965). These two principles can be mathematically stated as

$$\delta\pi_p = 0 \tag{3.9a}$$

$$\pi_p(\Delta q + \delta\Delta q) - \pi_p(\Delta q) \geq 0 \tag{3.9b}$$

Having presented the incremental variational principles it becomes possible to formulate the set of equations necessary to solve the problem. Eq. 3.8 is written in matrix form as

$$\pi_p = \sum_K \{ \int_{V_e} [<\sigma>^0 \{\Delta\varepsilon\} - <\bar{F}>^0 \{\Delta q\}] dV - \int_{S_e} <\bar{T}^0> \{\Delta q\}\, dS$$

$$+ \int_{V_e} [\tfrac{1}{2} <\Delta\varepsilon> [C] \{\Delta\varepsilon\} - <\Delta\bar{F}> \{\Delta q\}] dV$$

$$- \int_{S_e} <\Delta\bar{T}> \{\Delta q\}\, dS\} \qquad (3.10)$$

Using interpolating functions, the displacement and strain fields can be described in terms of the nodal displacements as

$$\{\Delta q\} = [N] \{\Delta \underline{q}\} \qquad (3.11a)$$

$$\{\Delta\varepsilon\} = [B] \{\Delta \underline{q}\} \qquad (3.11b)$$

where [N] is the matrix of interpolating functions, [B] is a differential operators matrix and $\{\Delta \underline{q}\}$ are the nodal displacements. Substituting Eqs. 3.11 into Eq. 3.10, the latter assumes the form

$$\pi_p = \sum_K \{ \int_{V_e} [<\sigma^0> [B] \{\Delta \underline{q}\} - <\bar{F}^0> [N] \{\Delta \underline{q}\}] dV - \int <\bar{T}^0> [N] \{\Delta \underline{q}\}\, dS$$

$$+ \int_{V_e} [\tfrac{1}{2} <\Delta \underline{q}> [B]^T [C] [B] \{\Delta \underline{q}\} - <\Delta\bar{F}> [N] \{\Delta \underline{q}\}]\, dV$$

$$- \int_{S_e} <\Delta\bar{T}> [N] \{\Delta \underline{q}\}\, dS\} \qquad (3.12)$$

The summation over the elements making up the continuum under consideration can be carried out over the individual terms of Eq. 3.12 yielding

$$\pi_p = \frac{1}{2} \sum_K <\Delta q> [K_e] \{\Delta q\} - \sum_K <\Delta q> \{\Delta \bar{F}_e\}$$

$$- \sum_K <\Delta q> \{\Delta \bar{T}_e\} + <\Delta q> \{\Delta Q_e\} \qquad (3.13)$$

where

$$[K_e] = \int_{V_e} [B]^T [C][B] \, dV \qquad (3.14a)$$

$$\{\Delta \bar{F}_e\} = \int_{V_e} [N]^T \{\Delta \bar{F}\} \, dV \qquad (3.14b)$$

$$\{\Delta \bar{T}_e\} = \int_{S_e} [N]^T \{\Delta \bar{T}\} \, dS \qquad (3.14c)$$

$$\{\Delta Q_e\} = \int_{V_e} [B]^T \{\sigma^0\} - [N]^T \{\bar{F}^0\}] \, dV - \int_{S_e} [N]^T \{\bar{T}^0\} \, dS \qquad (3.14d)$$

The terms $[K_e]$, $<\Delta \bar{F}_e>$ and $<\Delta \bar{T}_e>$ represent, respectively, the element stiffness matrix, the increment of body forces and the increment of surface tractions. The term $<\Delta Q_e>$ should vanish if the initial state is in equilibrium and may represent the unbalanced forces otherwise. The principle of Eq. 3.9a can be applied to Eq. 3.13 subject to the conditions stated in Eqs. 3.4, recognizing the arbitrary nature of $<\delta \Delta q>$, yielding

$$\sum_K [K_e] \{\Delta q\} - \sum_K \{\Delta \bar{F}_e\} - \sum_K \{\Delta \bar{T}_e\} + \sum_K \{\Delta Q_e\} = 0 \qquad (3.15)$$

It must be noted that the summations of Eq. 3.15 are carried out in the direct stiffness sense and can be summarized as

$$[K]\{\Delta r\} - \{\Delta R\} + \{\Delta Q\} = 0 \qquad (3.16)$$

where [K] is the structure stiffness matrix, $<\Delta r>$ is the increment of nodal displacements, $<\Delta R>$ is the increment of prescribed loads and $<\Delta Q>$ is the unbalanced load at the end of the previous load step. Eq. 3.16 together with the condition of Eq. 3.4b make up a nonsingular system of equations which can be solved for the increment of displacement $<\Delta r>$.

3.3 Isoparametric Element Formulations

3.3.1 Solid Element Formulation

The formulation of a finite element depends on the unique description of unknown functions within the element in terms of parameters associated with the values of the functions at the nodes, (Zienkiewicz, et al., 1970). These parameters are based on what are called "shape functions". The shape functions depend on the spatial description of the element and must satisfy two conditions:

a) Continuity of the function and derivatives up to the order required by the variational formulation which is one order less than the maximum order of differentiation appearing in the functional (continuity of class C^0 is required in this study).

b) The ability to represent a constant field of the unknown function over the entire volume of the element.

Condition (a) can be satisfied if the number of nodes on a boundary is sufficient to determine uniquely the variation of the function along the boundary and if only the interboundary nodes between two adjacent elements influence the value of the unknown function on

this boundary. In this study only linear, quadratic and cubic rectangular isoparametric elements of the serendipity family are used (see Fig. 3.2). The shape functions for these elements are given in Appendix B.

Since the elements used are isoparametric elements, the same shape functions can be used to interpolate geometry as well as displacements as follows

$$< r\ z > = < \phi > [\ \underline{r}\ \underline{z}\ ] \tag{3.17a}$$

$$< u\ v > = < \phi > [\ \underline{u}\ \underline{v}\ ] \tag{3.17b}$$

where r and z are horizontal radius and vertical coordinate respectively (axisymmetric formulation), u and v are the horizontal and vertical displacements respectively, the symbol (_) denotes nodal values and $< \phi >$ is the set of shape functions.

A differential element of volume dV representing a radian sector in any axisymmetric continuum can be written as

$$dV = rdA$$

where dA is an element of area and is defined as the magnitude of the cross product of the two vectors $\vec{db}_1$ and $\vec{db}_2$ making up the sides of the element of area as shown in Fig. 3.3b. Writing the cross product in terms of the r and z components, Eq. 3.18 assumes the form

$$dV = r \begin{vmatrix} dr_1 & dz_1 \\ dr_2 & dz_2 \end{vmatrix} \tag{3.19}$$

The components dr and dz can be written in terms of the normalized coordinates ξ and μ (see Fig. 3.3a) as

$$< dr\ dz > = < d\xi\ d\mu > [\,J\,] \tag{3.20a}$$

$$[\,J\,] = \begin{bmatrix} \frac{\partial r}{\partial \xi} & \frac{\partial z}{\partial \xi} \\ \frac{\partial r}{\partial \mu} & \frac{\partial z}{\partial \mu} \end{bmatrix} \tag{3.20b}$$

where [J] is the Jacobian matrix. This matrix is expressed in terms of the shape function derivatives as

$$[\,J\,] = \begin{vmatrix} < \frac{\partial \phi}{\partial \xi} > \\ < \frac{\partial \phi}{\partial \mu} > \end{vmatrix} [\,\underline{r}\ \ \underline{z}\,] \tag{3.21}$$

Since dA is arbitrary it can be chosen such that $\vec{db}_1$ corresponds to $< d\xi\ o >$ and db_2 corresponds to $< o\ d\mu >$. Thus Eq. 3.19 can be written as

$$dV = r\,|\,J\,|\,d\xi d\mu \tag{3.22}$$

where the symbol (| |) denotes a determinant.

The purpose of this section is to evaluate the integral of Eq. 3.14a. Assuming that the constitutive matrix [C] is known and that the element of volume can be represented by the right hand side of Eq. 3.22, it remains to evaluate the matrix [B] in terms of the shape functions and derivatives. Let the strains of Eq. 3.11b be expressed for axisymmetric strain fields as (Zienkiewicz, 1971).

$$\begin{Bmatrix} \Delta\varepsilon_r \\ \Delta\varepsilon_z \\ \Delta\varepsilon_\theta \\ \Delta\gamma_{rz} \end{Bmatrix} = \begin{bmatrix} < \partial\phi/\partial r > & 0 \\ 0 & < \partial\phi/\partial r > \\ < \phi/r > & 0 \\ < \partial\phi/\partial z > & < \partial\phi/\partial r > \end{bmatrix} \begin{Bmatrix} \{\Delta \underline{u}\} \\ \{\Delta \underline{v}\} \end{Bmatrix} \tag{3.23}$$

The derivatives appearing in Eq. 3.23 may be evaluated as

$$\begin{bmatrix} <\partial\phi/\partial r> \\ <\partial\phi/\partial z> \end{bmatrix} = [J]^{-1} \begin{bmatrix} <\partial\phi/\partial\xi> \\ <\partial\phi/\partial\mu> \end{bmatrix} \tag{3.24}$$

Since the matrix $[J]^{-1}$ has polynomials in the denominator it becomes impractical to try to integrate Eq. 3.14a in closed form. Therefore, integrations are evaluated numerically. For the purposes of this study, Gaussian integration was selected as a viable scheme. Thus Eq. 3.14a may now be written as

$$[K_e] = \sum_{i=1}^{n} \sum_{j=1}^{m} [B(\xi_i,\mu_j)]^T [C][B(\xi_i,\mu_i)] w_i^n w_j^m |J| r \tag{3.25}$$

where n and m are the order of Gaussian integration in directions ξ and μ respectively, and w_i^n and w_j^m are the weights associated with each point in directions ξ and μ respectively.

3.3.2 Formulation of the Meridional Reinforcing Isoparametric Element

In order to model the meridional reinforcing and prestressing layers within a solid element, a compatible element can be described such that the integration is carried out only along the required layers. An element which can accommodate layers along the μ or ξ directions is formulated in this section, see Fig. 3.4a.

Let the potential energy of the element be written as

$$\pi_p(\Delta\varepsilon) = \int_{V_e} (\sigma^0\Delta\varepsilon + \frac{1}{2}\Delta\sigma\Delta\varepsilon)\, dV \tag{3.26}$$

where the strain and the stress are defined only along the layer under consideration. The element of volume dV is written in terms

of the element of length along the layer $d\ell$, the area of the layer per unit width A and the radius (axisymmetric formulation) as

$$dV = rAd\ell \tag{3.27}$$

The strain increment is expressed in terms of the global strain and the orientation of the layer as

$$\Delta\varepsilon = \Delta\varepsilon_r \cos^2\theta + \Delta\varepsilon_z \sin^2\theta + \gamma_{rz} \sin\theta\cos\theta \tag{3.28}$$

where,

$$\cos\theta = \frac{dr}{d\ell} \tag{3.29a}$$

$$\sin\theta = \frac{dz}{d\ell} \tag{3.29b}$$

Using the definition of the strain increment stated in Eq. 3.1b neglecting initial strains and using Eqs. 3.29, Eq. 3.28 may be written as

$$\Delta\varepsilon = \frac{\partial\Delta u}{\partial r}\frac{dr}{d\ell}\frac{dr}{d\ell} + \frac{\partial\Delta v}{\partial z}\frac{dz}{d\ell}\frac{dz}{d\ell} + \frac{\partial\Delta u}{\partial z}\frac{dr}{d\ell}\frac{dz}{d\ell} + \frac{\partial\Delta v}{\partial r}\frac{dr}{d\ell}\frac{dz}{d\ell} \tag{3.30}$$

Eq. 3.30 can be rearranged such that

$$\Delta\varepsilon = \frac{d\Delta u}{d\ell}\frac{dr}{d\ell} + \frac{d\Delta v}{d\ell}\frac{dz}{d\ell} \tag{3.31}$$

Let the layer under consideration be in the μ direction. The element of length $d\ell$ and the direction cosines are expressed in terms of the normalized coordinates as

$$d\ell = J' d\mu \tag{3.32a}$$

$$\cos\theta = \frac{\partial r}{\partial \mu} / J' \tag{3.32b}$$

$$\sin\theta = \frac{\partial z}{\partial \mu} / J' \tag{3.32c}$$

where J is a transformation factor which can be derived using Eqs. 3.20 and is written as

$$J' = \left((\partial r/\partial \mu)^2 + (\partial z/\partial \mu)^2 \right)^{1/2} \tag{3.33}$$

Eq. 3.31 can now be stated as

$$\Delta\varepsilon = \frac{d\Delta u}{d\mu}\frac{d\mu}{d\ell}\frac{dr}{d\mu}\frac{d\mu}{d\ell} + \frac{d\Delta v}{d\mu}\frac{d\mu}{d\ell}\frac{dz}{d\mu}\frac{d\mu}{d\ell} \tag{3.34}$$

Using the definitions of Eqs. 3.32, Eq. 3.34 can be simplified as

$$\Delta\varepsilon = \left(\frac{d\Delta u}{d\mu}\cos\theta + \frac{d\Delta v}{d\mu}\sin\theta \right) / J' \tag{3.35}$$

The increment of stress appearing in Eq. 3.26 can be stated in terms of the increment of strain $\Delta\varepsilon$ and the current elastic modulus E as

$$\Delta\sigma = E\,\Delta\varepsilon \tag{3.36}$$

Substituting for $\Delta\sigma$ and dV in Eq. 3.26 using Eqs. 3.27 and 3.36 yields

$$\pi p = \int_V \left[\sigma^o\,\Delta\varepsilon + \frac{1}{2}\Delta\varepsilon\, E\, \Delta\varepsilon \right] r A d\ell \tag{3.37}$$

The second term of Eq. 3.37 yields the element stiffness matrix as

$$[K_e] = \Sigma \left\{ \begin{bmatrix} \{\phi_{,\mu}\} & 0 \\ 0 & \{\phi_{,\mu}\} \end{bmatrix} \begin{Bmatrix} \cos\theta \\ \sin\theta \end{Bmatrix} E < \cos\theta \ \sin\theta > \begin{bmatrix} < \phi_{,\mu} > & 0 \\ 0 & < \phi_{\mu} > \end{bmatrix} \right.$$

$$\left. \frac{Ar}{J'} w_i^m \right\} \tag{3.38}$$

where w^m is the Gaussian weight and m is a suffix denoting the order of Gaussian integration. When the layer is along the ξ direction, ξ is substituted for μ in all the pertinent equations of this section.

3.3.3 Formulation of A Circumferential Reinforcing Isoparametric Element

Hoop reinforcing and prestressing layers can be modelled in the same manner as the meridional layers described in Section 3.3.2. Again, an element which can accomodate circumferential layers parallel to the μ and ξ coordinates has been formulated. In this case the potential energy of the element is defined as stated in Eq. 3.26. The element of volume is defined as

$$dV = rAd\ell \tag{3.39}$$

where A is the area of the layer under consideration and $d\ell$ is an element of length parallel to the direction of the layer. The strain however is defined as

$$\Delta\epsilon = \Delta u/r \tag{3.40}$$

Let the layer under consideration be in the μ direction. The element of length $d\ell$ is defined in terms of the normalized coordinate μ as

$$d\ell = J'd\mu \tag{3.41}$$

where J is the transformation factor defined by Eq. 3.33. For this element, the stiffness matrix is obtained from Eq. 3.37 by substituting the right hand side of Eq. 3.36 for the increment of stress and Eq. 3.40 for the strain increment as

$$[K_e] = \sum_i \{ \begin{Bmatrix} \{\phi\} \\ \{o\} \end{Bmatrix} E < < \phi > < o > > A \frac{J'}{r} w_i^m \} \qquad (3.42)$$

where w_i^m's are the Gaussian weights and m denotes the Gaussian order of integration.

3.4 Body Forces

The body forces that arise in this study are gravity loads and equilibrating loads. The latter are equivalent to the internal forces in the structure. Although this type of load is not applied to the structure its evaluation is required to check equilibrium and to evaluate the unbalance between the applied loads and the state of stress in the structure. In this section gravity loads and equilibrating loads as well as thermal loads arising from possible thermal fields are formulated on a work equivalent basis.

3.4.1 Gravity Loads

In this study gravity loads are assigned to the negative z direction and are calculated for the solid element alone. Let ΔF be an increment of gravity load per unit volume. The virtual work done by this load in going through the virtual displacement $\delta\Delta q$, which is compatible with the condition stated in Eq. 3.4b, is the second term on the right hand side of Eq. 3.7 and can be isolated as

$$\delta(\Delta F) = - \int_{V_R} \gamma \delta \Delta v \, dV \qquad (3.43)$$

where γ is the specific weight of the solid element material. In matrix form Eq. 3.43 can be written as

$$< \delta\Delta\underline{u}\ \delta\Delta\underline{v} > \{\Delta \bar{F}_e\} = - < \delta\Delta\underline{u}\ \delta\Delta\underline{v} > \int_{V_e} \gamma \begin{Bmatrix} o \\ \{\phi\} \end{Bmatrix} dV \qquad (3.44)$$

Substituting for the element of volume dV in Eq. 3.44 by the right hand side of Eq. 3.22 and carrying out the integration numerically, the work equivalent gravity loads $< \Delta \bar{F}_e >$ are expressed as

$$\{\Delta \bar{F}_e\} = - \gamma \sum_{i=1}^{n} \sum_{j=1}^{n} \begin{Bmatrix} o \\ \phi\ (\xi_i, \mu_j) \end{Bmatrix} Jr\ w_i^n\ w_j^m \qquad (3.45)$$

where J, r, w, n and m have been defined in Section 3.3.1.

3.4.2 Thermal Loads

Thermal loads arise when deformation due to the presence of a temperature distribution is partially or fully constrained by the presence of a gradient, external indeterminate restraints, variations in material thermal properties or internal indeterminacy. Let the increment of strain arising in a body, where one or more of the above described situations exist, be written as

$$\Delta \varepsilon_{ij} = A_{ijk\ell}\ \Delta\sigma_{k\ell} + \Delta\varepsilon_{ij}{}^{t} \qquad (3.46)$$

where $A_{ijk\ell}$ is the compliance tensor associated with $C_{ijk\ell}$ defined in Chapter Two and $\Delta\varepsilon_{ij}{}^{t}$ is the increment of strain occuring due to thermal change alone and is defined as

$$\Delta \varepsilon_{ij}{}^{t} = \alpha_{ij}\ \Delta t \qquad (3.47)$$

where Δt is the increment of temperature and α_{ij} is the thermal expansion tensor. It must be noted that in an orthotropic material shear stresses in the orthotropic directions do not occur due to

thermal changes. In the principal axes of orthotropy α_{ij} is defined as

$$\alpha_{ii} = \alpha_i \qquad \text{(no sum)} \qquad (3.48a)$$

$$\alpha_{ij} = 0 \qquad (i \neq j) \qquad (3.48b)$$

where α_i is the thermal expansion coefficient in direction i. Inverting and rearranging Eq. 3.46 the increment of stress due to the increment of temperature can be written as

$$\Delta\sigma_{ij} = C_{ijk\ell} \, (\Delta\varepsilon_{k\ell} - \alpha_{k\ell} \, \Delta t) \qquad (3.49)$$

Ignoring external work, Eq. 3.7 is reduced to the form

$$\sum_K \{ \int_{V_e} (\Delta \varepsilon_{k\ell} - \alpha_{k\ell} \, \Delta t) \, C_{ijk\ell} \, \delta \, \Delta \, \varepsilon_{ij} \, dV \} = 0 \qquad (3.50)$$

The first term of equation 3.50 gives rise to the element stiffness matrix. The second term gives rise to the thermal loads. Using Eq. 3.4a and Eq. 3.11b, the second term of Eq. 3.50 is stated in matrix form as

$$\{\Delta F_t\} = \sum_K \{ \int_{V_e} [B]^T [c] \{\alpha\} \, \Delta t \, dV \} \qquad (3.51)$$

The increment of temperature Δt is expressed in terms of the nodal values and shape functions as

$$\Delta t = \langle \phi \rangle \{ \Delta \underline{t} \} \qquad (3.52)$$

Using Eq. 3.52 and numerical integration, Eq. 3.51 can be written as

$$\{\Delta F_t\} = \sum_K \left[\sum_{i=1}^{n} \sum_{j=1}^{m} [B(\xi_i,\mu_j)]^T [C]\{\alpha\}\langle\phi(\xi_i,\mu_j)\rangle r J w_i^n w_j^m \right] \{\Delta \underline{t}\} \tag{3.53}$$

The foregoing formulation has been for a solid element. Similar formulations can be carried out for the meridional and the circumferential reinforcing elements described in Sections 3.3.2 and 3.3.3 resulting respectively, in

$$\{\Delta F_t\} = \sum_K \left[\sum_{i=1}^{n} \begin{bmatrix} \{\phi\} & 0 \\ 0 & \{\phi\} \end{bmatrix} \begin{Bmatrix} \sin\theta \\ \cos\theta \end{Bmatrix} \langle\phi\rangle \alpha A r E w_i^n \right] \{\Delta \underline{t}\} \tag{3.54a}$$

$$\{\Delta F_t\} = \sum_K \left[\sum_{i=1}^{n} \begin{Bmatrix} \{\phi\} \\ \{o\} \end{Bmatrix} \langle\langle\phi\rangle\langle o\rangle\rangle E \alpha r A J w_i^n \right] \{\Delta \underline{t}\} \tag{3.54b}$$

where the appropriate definitions of Sections 3.3.2 and 3.3.3 apply.

The summations enclosed in square brackets in Eqs. 3.53, 3.54a and 3.54b are carried out for a particular solid element and all the meridional and circumferential reinforcing layers within, summed up and then multiplied once by the element nodal temperatures. In this manner, efficiency of calculations is increased. Eqs. 3.53 and 3.54 are summarized in one equation as

$$\{\Delta F_t\} = \sum_K \{ \left[[Th]_s + [Th]_{mr} + [Th]_{cr} \right] \{\Delta \underline{t}\} \} \tag{3.55}$$

where $[Th]_s$, $[Th]_{mr}$ and $[Th]_{cr}$ and the summations enclosed in square brackets in Eqs. 3.53, 3.54a and 3.54b respectively.

3.4.3 Equilibrating Loads

Equilibrating loads are fictitious loads that are work equivalent to the state of stress in a structure. The estimation of these loads is necessary to check equilibrium and to calculate the unbalanced loads in case equilibrium is not satisfied. The equilibrating loads associated with an element constitute the first integral on the right hand side of Eq. 3.14d. Thus, for a solid element, using Gaussian integration and the definition of the element of volume in Eq. 3.22, the equilibrating loads are evaluated as

$$\{Q_e\} = \sum_{i=1}^{n}\sum_{j=1}^{m} [B(\xi_i,\mu_i)]^T \{\sigma\}^o \, r \, J \, w_i^n \, w_j^m \qquad (3.56)$$

The equilibrating loads associated with a meridional reinforcing element with layers running in the μ and ξ directions can be evaluated respectively as

$$\{Q_e\} = \sum_{j=1}^{m} \begin{bmatrix} \{\phi,_{\mu_j}\}\{o\} \\ \{o\}\{\phi,_{\mu_j}\} \end{bmatrix} \begin{Bmatrix} \sin\theta \\ \cos\theta \end{Bmatrix} \sigma \, r \, A \, w_j^m \qquad (3.57a)$$

$$\{Q_e\} = \sum_{j=1}^{n} \begin{bmatrix} \{\phi,_{\xi_i}\}\{o\} \\ \{o\}\{\phi,_{\xi_i}\} \end{bmatrix} \begin{Bmatrix} \cos\theta \\ \sin\theta \end{Bmatrix} \sigma \, r \, A \, w_i^n \qquad (3.57b)$$

For a circumferential reinforcing element the equilibrating loads are written as

$$\{Q_e\} = \sum_{i=1}^{m} \begin{Bmatrix} \{\phi\} \\ \{o\} \end{Bmatrix} A \, J \, w_i^m \, \sigma \qquad (3.58)$$

3.5 Surface Tractions

Program FEPARCS5 accepts surface tractions in the form of nodal pressure intensities which may be normal or tangential to an element surface. An element surface is defined as a group of adjacent nodes forming one side of an element. The normal pressure component is positive when prescribed along the right hand normal to an element surface. The tangential pressure component is positive when it describes 90° counterclockwise angle with right hand normal to the element surface, see Fig. 3.5a. The right hand normal to an element surface points to the right when the nodes which define the element surface are traversed in the order they are specified.

The third integral on the left hand side of Eq. 3.7 represents the virtual work done by surface tractions when acting through a virtual displacement field which satisfies the condition stated by Eq. 34b. This statement is mathematically expressed as

$$< \delta \underline{\Delta q} > \{ \Delta \underline{T} \} = \sum_{K} \int_{S_K} < \delta \Delta q > \{ \Delta p \} \, dS \qquad (3.59)$$

where $< \Delta p >$ is the pressure field, $< \delta \Delta q >$ is the virtual displacement field and $< \Delta T >$ is the nodal force vector equivalent to the pressure field. The pressure field is defined in terms of vertical and horizontal components, or alternatively in terms of the normal and tangential components as shown in Fig. 3.5b as follows

$$< \Delta p > = < \Delta p_r \quad \Delta p_z > \qquad (3.60)$$

$$\{\Delta p\} = \begin{bmatrix} \sin\alpha & -\cos\alpha \\ \cos\alpha & \sin\alpha \end{bmatrix} \begin{Bmatrix} \Delta p_n \\ \Delta p_t \end{Bmatrix} \tag{3.61}$$

where α is the angle which the right hand normal to the surface describes with the vertical axis as shown in Fig. 3.5c, and is defined mathematically as

$$\sin\alpha = dz/d\ell \tag{3.62a}$$

$$\cos\alpha = dr/d\ell \tag{3.62b}$$

where $d\ell$ is an element of length along the surface. In terms Δ of a normalized coordinate, e.g. μ, $d\ell$ can be written as

$$d\ell = J' d\mu \tag{3.63}$$

where J' is a transformation factor defined as

$$J = \sqrt{(\frac{\partial r}{\partial \mu})^2 + (\frac{\partial z}{\partial \mu})^2} \tag{3.64}$$

The element of surface dS appearingin Eq. 3.59 is defined for a one radian sector as

$$dS = r\, d\ell \tag{3.65}$$

Using Eqs. 3.65, 3.63 and 3.61, the surface tractions are expressed in terms of shape functions and normal and tangential components as

$$\{\Delta \underline{T}\} = \sum_K \int_{-1}^{1} \begin{bmatrix} \{\phi\} & \{o\} \\ \{o\} & \{\phi\} \end{bmatrix} \begin{bmatrix} \sin\alpha & -\cos\alpha \\ \cos\alpha & \sin\alpha \end{bmatrix} \begin{Bmatrix} \Delta p_n \\ \Delta p_t \end{Bmatrix} r J' d\mu \tag{3.66}$$

Using numerical integration and writing the pressure components in terms of nodal pressure intensities, Eqs. 3.66 can be written as

$$\{\Delta \underline{T}\} = \sum_{K}\sum_{i}\left[\begin{bmatrix}\{\phi\} & o\\ o & \{\phi\}\end{bmatrix}\begin{bmatrix}\sin\alpha & -\cos\alpha\\ \cos\alpha & \sin\alpha\end{bmatrix}\begin{bmatrix}<\phi> & o\\ o & <\phi>\end{bmatrix} r J w_i^m\right]\begin{Bmatrix}\{\Delta p_n\}\\ \{\Delta p_t\}\end{Bmatrix} \tag{3.67}$$

If the conditions of compatibility between elements described in Section 3.3.1 are satisfied, the same shape functions defined in Appendix B can be used.

3.6 Boundary Conditions

Boundary conditions in program FEPARCS5 are applied in the form of linear springs of very high stiffness compared to the stiffness of the structure under consideration. These springs can have any orientation in the plane r - z. Let the virtual work associated with a boundary element be written as

$$\delta U = \delta w\, F_s \tag{3.68}$$

where δw is the virtual displacement and F_s is the force in the spring. Since the spring is linear F_s is written as

$$F_s = wkr/\ell \tag{3.69}$$

for a one radian sector where k is the spring stiffness and ℓ is the length and r is the radius of the point at which the boundary element is attached. If the spring is inclined $\theta°$ to the vertical axis, the displacement w is written in terms of the horizontal and vertical components as

$$w = u \sin\theta + v \cos\theta \tag{3.70}$$

Substituting the right hand sides of Eqs. 3.70 and 3.69 into Eq. 3.68 the latter is written in matrix form as

$$\delta U = \langle \delta u \ \delta v \rangle \begin{Bmatrix} \sin\theta \\ \cos\theta \end{Bmatrix} \langle \sin\theta \ \cos\theta \rangle \, K_r \begin{Bmatrix} u \\ v \end{Bmatrix} \tag{3.71}$$

The contribution to the variation of the total internal virtual work of the structure due to the boundary element is therefore

$$\delta U = \langle \delta u \ \delta v \rangle [K_{be}] \begin{Bmatrix} u \\ v \end{Bmatrix} \tag{3.72}$$

where $[K_{be}]$ is the stiffness matrix of the boundary element and is written as

$$[K_{be}] = \begin{bmatrix} \sin^2\theta & \cos\theta \sin\theta \\ \cos\theta \sin\theta & \cos^2\theta \end{bmatrix} K_r \tag{3.73}$$

This stiffness matrix is added to the appropriate stiffness coefficents of the point (node) at which the boundary element is attached.

The reactions are calculated by multiplying $[K_{be}]$ by the actual displacements obtained at any stage in the solution. The reactions are necessary in the equilibrium check. They are added to the equilibrating loads obtained in section 3.4.3 as a method of applying the condition stated by Eq. 3.4b to virtual displacement field.

Fig. 3.1 Element K

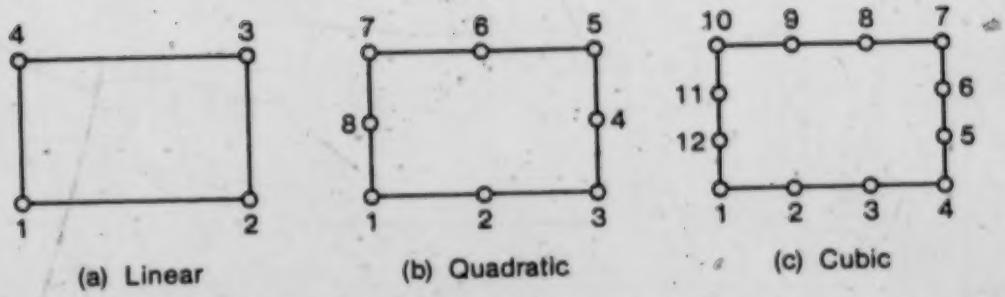

Fig. 3.2 The Serendipity Finite Element Family

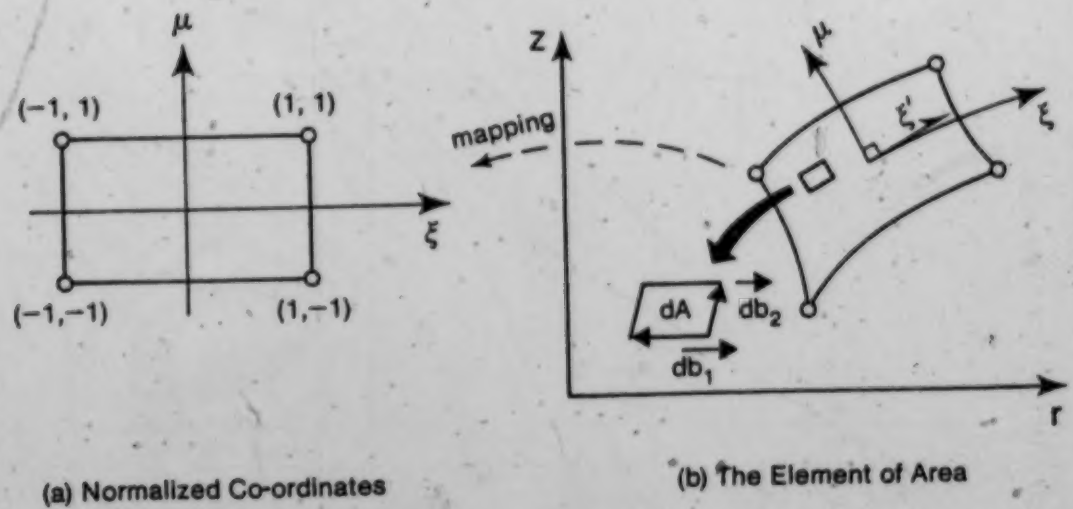

Fig. 3.3 Normalized Coordinates

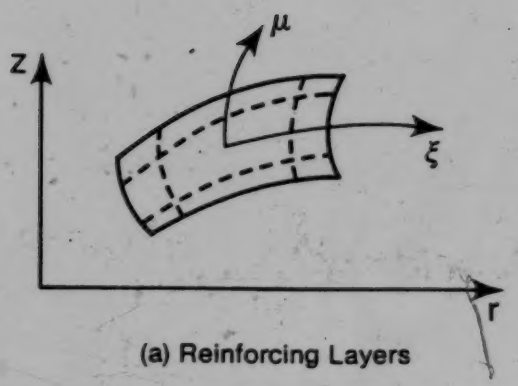

(a) Reinforcing Layers

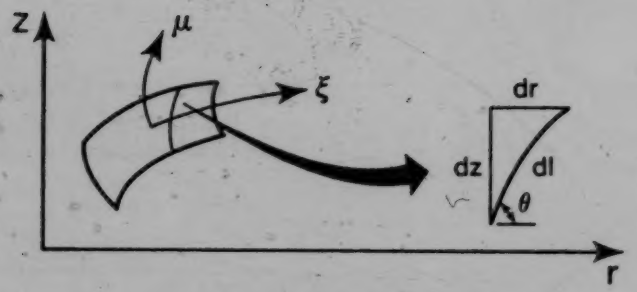

(b) The Element of Length

Fig. 3.4 The Reinforcing Element

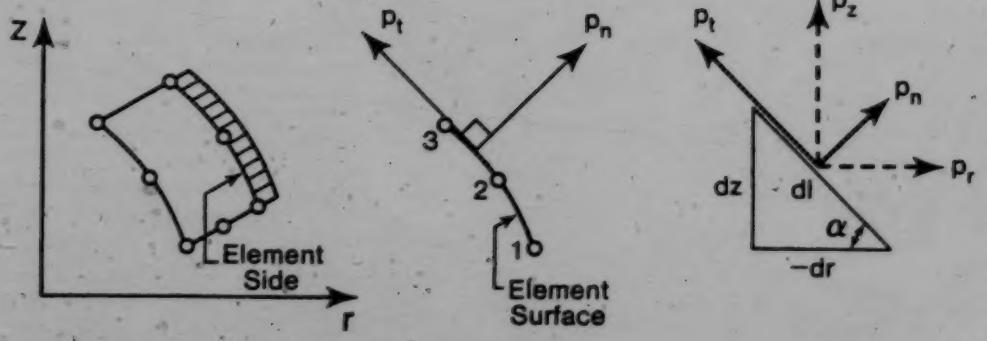

(a) Surface Tractions (b) Element Surface (c) Components

Fig. 3.5 Surface Tractions

CHAPTER FOUR

PROGRAM FEPARCS5

4.1 Introduction

Program FEPARCS5 is a finite element code for analysis of axisymmetric or plane, reinforced and/or prestressed concrete structure. In this program it is assumed that displacements are small, rotations are negligible and strains are infinitesimal. Although the program can handle linear problems, it is designed for problems with nonlinear material response.

In this chapter a general description of the program is presented, the basic solution techniques are discussed and the flow of operations for the program is briefly described.

4.2 General Description

Program FEPARCS5 is based on the finite element model formulated in Chapter Three. The program can handle combinations of linear, quadratic or cubic isoparametric elements. The solid element formulated in Section 3.3.1 represents the concrete continua. The meridional reinforcing layers and prestressing tendons are represented by the meridional element described in Section 3.3.2. Finally the element formulated in Section 3.3.3 represents the circumferential reinforcing layers and prestressing tendons.

The constitutive relation proposed in Chapter Two for three dimensional (axisymmetric) nonlinear elastic behavior of concrete is

implemented in program FEPARCS5 as the material model for concrete. A simple one dimensional elastic plastic constitutive relation is adopted for the reinforcing layers and prestressing tendons.

The program can handle five types of loads. Each type is stored in a separate load vector. These load vectors can be combined using load factors specified by the user for each load step to form a load increment vector. Dead loads can be a combination of gravity loads, hydrostatic pressures, and concentrated nodal loads. A separate vector for live concentrated nodal loads is provided. A load vector is provided for thermal loads. Normal and tangential surface pressures are handled by two separate load vectors. Besides those types of loads, program FEPARCS5 can simulate post tensioning using a specially prescribed thermal distribution. This procedure is described in detail in Section 4.4.1.

The input to the program is composed of control parameters, material properties, nodal geometry, boundary conditions, solid element information and topology, reinforcing and prestressing layer information, concentrated nodal loads, normal and tangential surface pressure nodal intensity distributions, hydrostatic pressure nodal intensity distribution and a thermal distribution. The specification of each load combination is done separately for each load step.

The output is composed of nodal displacements and increments of displacements in the global coordinates, local coordinate stress components (in the μ and ξ^1 directions of Fig. 3.3) for solid elements and stresses and strains of the reinforcing layers and prestressing tendons.

The program uses numerical integration for the evaluation of the different element relations as well as the loads wherever possible. A number of Gaussian integration rules have been provided ranging from one point rule for a linear displacement four node element to a three by seven two dimensional rule for higher order elements.

The program can use a tangential stiffness approach to the solution or alternatively the initial load method. Both these methods will be described in Section 4.3.1. The equation solving is done by a skyline equation solving in-core package (see Elwi, 1977 and Wilson and Bathe, 1975). Dynamic dimensioning is implemented through a data managing package described by Elwi (1977). Element shape functions and derivatives evaluated at the integration points as well as all integration point information such as stresses, strains, and material properties are stored on sequential files. In this manner the size of storage required by the program is kept to a minimum.

4.3 Basic Solution Techniques

4.3.1 The Numerical Solution Strategy

In Chapter Two a three dimensional constitutive relation for concrete was proposed. This relation can be summarized as

$$d\underset{\sim}{\sigma} = \underset{\sim}{F}\left(d\underset{\sim}{\varepsilon}, \int d\underset{\sim}{\sigma}\right) \qquad (4.1)$$

in which F represents a functional relationship, (Elwi and Murray, 1979). Eq. 4.1 implies that the stress increment is dependent on the previous stress history. In Chapter Three a finite element

model was formulated for axisymmetric reinforced concrete structures. This model is a displacement model. Therefore, it satisfies kinematic compatibility everywhere and it approximately satisfies equilibrium only on a global level. The incremental variational formulation included in Section 3.2 leads to the following set of equations.

$$[K]\{\Delta r\} = \{\Delta R\} - \{\Delta Q\} \qquad (4.2)$$

which is identical to Eq. 3.16. This equation is considered a piecewise linearization of the nonlinear structural response.

Since $\{\Delta R\}$ appearing in Eq. 4.2 is of finite predetermined magnitude, the result of solving the set of equations is an increment of displacement. The increment of displacement yields an increment of strain which through the constitutive matrix yields an increment of stress. The difference between the applied loads and the equilibrating loads, equivalent to the stress state which satisfies the constitutive law, is called the unbalanced load. One way to arrive at the state of stress which is kinematically compatible and at the same time satisfies equilibrium, is to eliminate the unbalanced load through an iterative scheme. Iterative schemes of the Newtonian type can be divided into two main categories. These are the tangential stiffness method (Argyris, et al., 1974) which is sometimes known as the Newton Raphson Method (Zienkiewicz, 1971) and the initial load method (Argyris, et al., 1974) which is sometimes known as the modified Newton Raphson method (Zienkiewicz, 1971).

In the tangential stiffness method, a new stiffness matrix is evaluated at the beginning of each load increment, based on the

current material properties. This method is powerful and comes near to simulating the actual load process. The main disadvantage of this method appears when strain softening behavior is exhibited. In this case, the tangential stiffness matrix may lose its positive definite character or at least become ill conditioned. In this study, however, it has been assumed that the amount of steel reinforcing and prestressing tendons is enough to retain the positive definiteness of the problem. In addition, the stiffness matrix may become nonsymmetric when nonhomogeneous materials are present or where nonassociated flow rules are used (Argyris, et al., 1974). In this case, the computational effort associated with re-evaluating the stiffness matrix may become prohibitive.

In the initial load method a positive definite stiffness matrix (usually the initial stiffness matrix) is retained and the softening is simulated by altering the unbalanced load vector (Argyris, et al., 1974). Although this method avoids some of the problems associated with the tangential stiffness method, a much larger number of iterations may be required to satisfy equilibrium particularly when approaching the ultimate load.

The two methods described above can be illustrated schematically as shown in Figures 4.1a and 4.1b. Many improvements can be introduced for both methods. For example, over-relaxation may be used to improve the convergence rate of the initial load method. Under-relaxation and numerical damping can be used to enlarge the convergence domain of the tangential stiffness method (Almroth, Stren and Brogan, 1979 and Fellipa, 1974 and 1976). Re-evaluation of the stiffness matrix every few iterates within a load step can be carried out in association with the tangential stiffness method.

In program FEPARCS5 both the tangential stiffness approach with the capability of re-evaluating the stiffness matrix every few iterates and the initial load approach have been implemented. Provisions have been made for a relaxation factor. Convergence of the iterative scheme is based on both the displacements and the loads. The test for convergence is carried out as follows

$$\frac{||\Delta r^i||}{||r||} \leq \lambda_r \tag{4.3a}$$

$$\frac{||\Delta Q^i||}{||R||} \leq \lambda_R \tag{4.3b}$$

where λ_r and λ_R are the user specified tolerances on the displacements and loads respectively, Δr^i is the increment of displacement vector obtained in the i^{th} iteration, r is the current displacement vector, ΔQ^i is the unbalanced load at the end of the i^{th} iteration and R is the total load vector. The symbol || || denotes the Eucleadian norm.

4.3.2 The Subincrement Method

The piecewise linearization process described in Section 4.3.1 requires that the load increment be reasonably small. When the constitutive law is path dependent the resulting strain increments may still be large enough to cause drift of the solution, particularly when strain softening behavior is exhibited. The ultimate strength parameters defined in Section 2.3.4 lie on the intersection of a stress path with the ultimate surfaces described in Section 2.3.7. Complicated ultimate surfaces may yield false parameters or roots

outside the defined range when a stress point, which does not yet satisfy the constitutive relation, falls outside the surface.

The subincrement method avoids these problems by dividing the strain increments into a number of smaller subincrements. In this manner, the stress point is changed gradually allowing close simulation of the behavior and the constitutive law remains stable even when the first derivative of the stress strain curve is not linear. Many investigators have used this method successfully such as Stricklin, Haisler and von Reissmann (1971), Bushnell (1973) and Murray, et al. (1978).

While the subincrement method ensures convergence to the right answer, it is expensive because the material handling routines consume a substantial portion of the execution time in nonlinear programs. Therefore, choosing the size of the subincrements must be done carefully. Murray, et al. (1978) have used a scheme based on the size of the strain increment as compared to the strain range. In FEPARCS5, however, the number of subincrements is set by the user for each load step. Thus, the economy of the solution is closely controlled.

4.3.3 Implementation of the Constitutive Relation

The implementation of the constitutive relation proposed in Chapter Two is divided into two main parts. In the first part the ultimate surfaces proposed in Section 2.3.7 are prepared by evaluating the constants of Eqs. 2.43a and 2.43b defined in Appendix A. This part is carried out in the problem preparation phase of FEPARCS5.

The second part of the implementation of the constitutive relation is related to active usage during the solution phase. In this part, the increments of strain are evaluated, the equivalent uniaxial strains are updated and the corresponding material properties and stresses are calculated at all integration points. Rather than using the increments of displacement resulting from the solution of Eq. 4.2 in each iterate, the increments are added to form a total increment of displacement vector starting at the beginning of each load step. This vector is then used to trace the variation of the stress point from the last converged position. In this manner drift of the solution is minimized. In the following the mechanics of this phase will be described in detailed steps.

1. The strain increment is calculated using the shape functions and derivatives as

$$\{ \Delta\varepsilon \} = [B]\{ \Delta q \} \tag{4.4}$$

2. The strain subincrement is calculated as

$$< \Delta\varepsilon >_s = < \Delta\varepsilon > / N \tag{4.5}$$

where N is the number of subincrements.

3. The strain subincrement is then transformed into the integration point local coordinates (chosen in Section 2.3.3 as the fixed orthotropy axes) as

$$< \Delta\varepsilon >_\ell \; : \; < \Delta\varepsilon >_s \rightarrow \text{local coordinate system} \tag{4.6}$$

The program then loops over the number of subincrements to perform the next steps.

4. The local stresses are updated as

$$\{\sigma\}_{\ell}^{i+1} = \{\sigma\}_{\ell}^{i} + [C]\{\Delta\varepsilon\}_{\ell} \tag{4.7}$$

where "i" indicates the number of subincrement which varies from "o" to "N-1" with "o" denoting the state of stress at the end of the previous load increment.

5. The equivalent uniaxial strains are updated as

$$<\varepsilon_u>^{i+1} = <\varepsilon_u>^{i} + <(\sigma_{\ell}^{i+1} - \sigma_{\ell}^{i})/E^{i}> \tag{4.8}$$

6. The strength and deformation parameters are calculated for the stress point $<\sigma_{\ell}>^{i+1}$ and the ultimate surfaces

$$<\sigma_c>_{\ell}^{i+1} : <\sigma>_{\ell}^{i+1} \rightarrow \text{stress ultimate surface} \tag{4.9a}$$

$$<\varepsilon_c>_{\ell}^{i+1} : <\varepsilon_u>_{\ell}^{i+1} \rightarrow \text{strain ultimate surface} \tag{4.9b}$$

7. The stress point is now updated using the stress equivalent uniaxial strain curves described in Section 2.3.4, the material properties are updated using the functions described in Sections 2.3.5 and 2.3.6 and the constitutive matrix is updated using the form described in Section 2.3.2 as

$$<\sigma_{\ell}>^{i+1} = <f_1(\varepsilon_u, \varepsilon_c, \sigma_c, E_o)> \tag{4.10a}$$

$$<E>^{i+1} = <f_2(\varepsilon_u, \varepsilon_c, \sigma_c, E_o)> \tag{4.10b}$$

$$<\nu>^{i+1} = <f_3(\varepsilon_u, \varepsilon_c, \nu_o)> \tag{4.10c}$$

$$[C] = [f_4(<E>^{i+1}, <\nu>^{i+1})] \qquad (4.10d)$$

in which f denotes functions.

8. At the end of the loop over the subincrements the program transforms the local stresses into the global coordinate system and obtains principal stresses.

The eight steps described above are repeated at each integration point for all elements. It must be noted that the constitutive matrix has been formed and stored in the local coordinate system. Therefore, when formulating the stiffness matrix of the structure care must be taken to transform the constitutive matrix into the global coordinate system.

Initial strains caused by temperature, if present, must be removed from the strain increment calculated in step 1 by modifying Eq. 4.4 to become

$$\{\Delta\varepsilon\} = [B]\{\Delta q\} - \{\alpha\}<\phi>\{\Delta t\} \qquad (4.11)$$

where $<\phi>$ is the vector of shape functions, $<\Delta t>$ is the temperature increment and $<\alpha>$ contains the thermal expansion coefficients which are assumed not to be affected by orthotropy.

4.4 Special Capabilities

4.4.1 Initial Stresses

In some problems where a self-equilibrating stress distribution exists, it becomes necessary to evaluate the corresponding strain field before the solution proceeds. This option has been implemented in FEPARCS5 in the initialization phase. Thus instead of initializing

the stresses and strains to zero and material properties to the initial state, the program reads the stress state from a file and calculates a corresponding strain field that satisfies equilibrium but may not satisfy compatibility. This process is carried out in steps similar to the flow chart of Fig. 2.16.

4.4.2 Post Tensioning

Post tensioning is a common prestressing method in axisymmetric structures. The method consists of running ducts through the structure before pouring the concrete. When the concrete is poured and has attained sufficient strength, the prestressing tendons are inserted in the ducts, tensioned and anchored to the concrete. During this process the structure deforms but there is no compatibility between the tendons and the concrete. The next step is to grout the ducts to protect the tendons and to establish compatibility of deformation between tendons and concrete under all subsequent loading stages.

Program FEPARCS5 has an option which simulates this process very successfully. For this purpose the program reads a special thermal distribution which is applied only to the prestressing tendons causing an initial strain equal in magnitude to the strain caused by the prestressing excluding elastic losses (approximately). The program then assigns each tendon a level of prestressing corresponding to the initial strain. Nodal loads are then calculated from the prestressing elements alone using Eqs. 3.57 and 3.58 of Section 3.4.3.

Since at that stage there is no compatibility between tendons and concrete, the program evaluates the stiffness matrix of the

structure excluding the prestressing elements. The loads calculated from the prestressing elements are then subtracted from the initialized load vector which is then applied to the structure. At the end of this process a self-equilibrating state of stress exists in the structure which simulates a post tensioning procedure.

This process is considered a load step, the end results of which are used as initial conditions for the next load step, except that the displacements and loads are reassigned to the state before prestressing once convergence is obtained.

4.5 Flow of Operations for Program FEPARCS5

From the operational point of view, program FEPARCS5 is divided into two main execution stages, namely the problem preparation stage and the solution stage. The former is performed only once or as many times as it takes to check the data, whereas the latter is performed for each load step.

As outlined in Section 4.2 the problem preparation stage reads and generates the structural and the loading data, calculates and stores the element shape functions and derivatives at all Gaussian integration points, forms the sky line of the structure stiffness matrix and initializes the stresses, strain and material properties at all integration points. Finally, for each load type (dead loads, live concentrated nodal loads, thermal loads, and normal and tangential surface pressure loads) a separate load vector is formed. If requested an initial stiffness matrix is formulated, triangularized and stored to be used in the initial load method.

Program FEPARCS5 does not choose the size of the load step automatically. This is done by the user. At the beginning of every load step, the user specifies the number of subincrements and whether the tangential stiffness method is to be used or the initial load method. If the former, the user specifies the number of iterates after which the stiffness matrix is to be reevaluated. Also required are the tolerances on convergence, the relaxation factor and finally load factors to specify the load combination for this load step.

Having read the user load step specification and having formed the load increment accordingly, the program proceeds as follows.

1. The program formulates and triangularizes the stiffness matrix in the case of the tangential stiffness method or reads the initial triangularized stiffness matrix from out of core in the case of the initial load method.

2. The program then, solves for an increment of displacement, updates the total displacement vector and updates the total increment of displacement vector.

3. The program updates the stresses and material properties according to the scheme described in Section 4.3.3.

4. If the problem is linear, the program outputs the results. If the problem is nonlinear the program calculates the equilibrating loads using the equations of Section 3.4.3, obtains the unbalanced load vector and checks for convergence as described in Section 4.3.1.

5. If convergence has been obtained the results are output and the load step is considered ended. If convergence has not been

obtained, and the number of iterates has not exceeded the specified maximum, the program uses the unbalanced load vector to obtain a further increment of displacement. For this purpose the program branches back to either step 1, if re-evaluation of the stiffness matrix is required or step 2 if this is not required.

If numerical problems, such as an ill conditioned stiffness matrix, oscillatory convergence, or exceeding the maximum number of iterates, occur, the program automatically stops and prints out the current state of stress and displacement for the user's consideration.

Fig. 4.2 and 4.3 show the flow charts of the operations for the two stages described above.

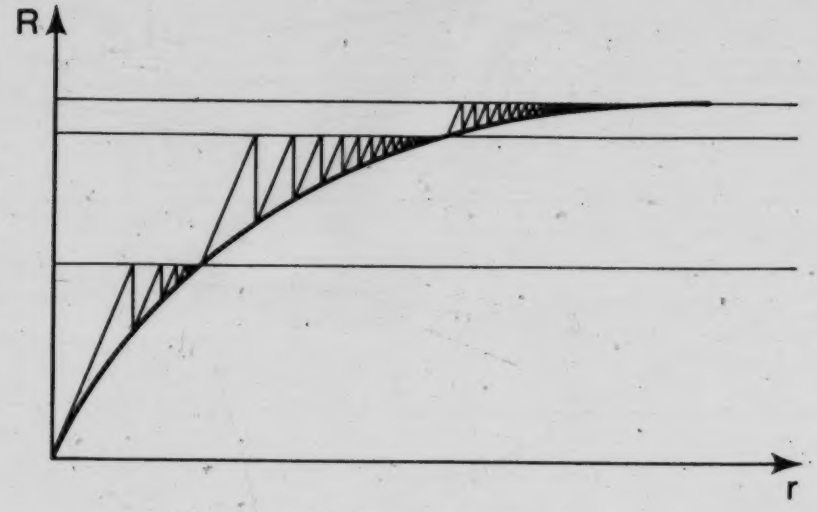

(a) Initial Load Method

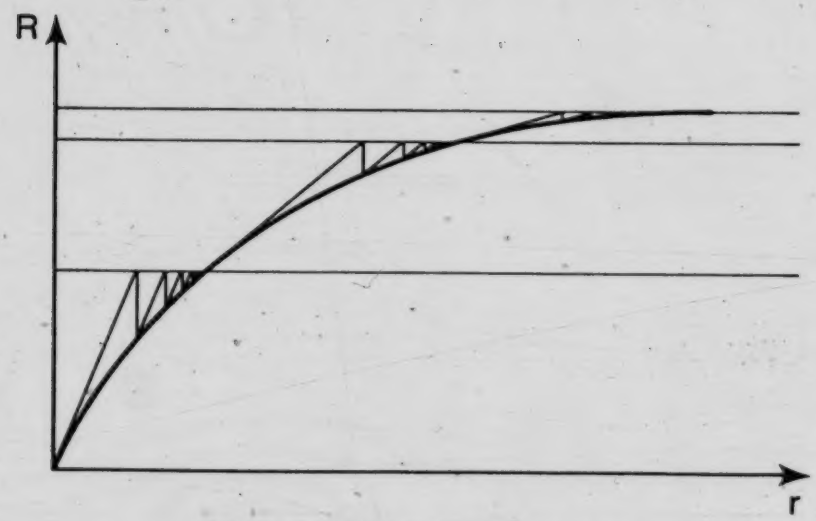

(b) Tangential Stiffness Method

Fig. 4.1 Iterative Schemes

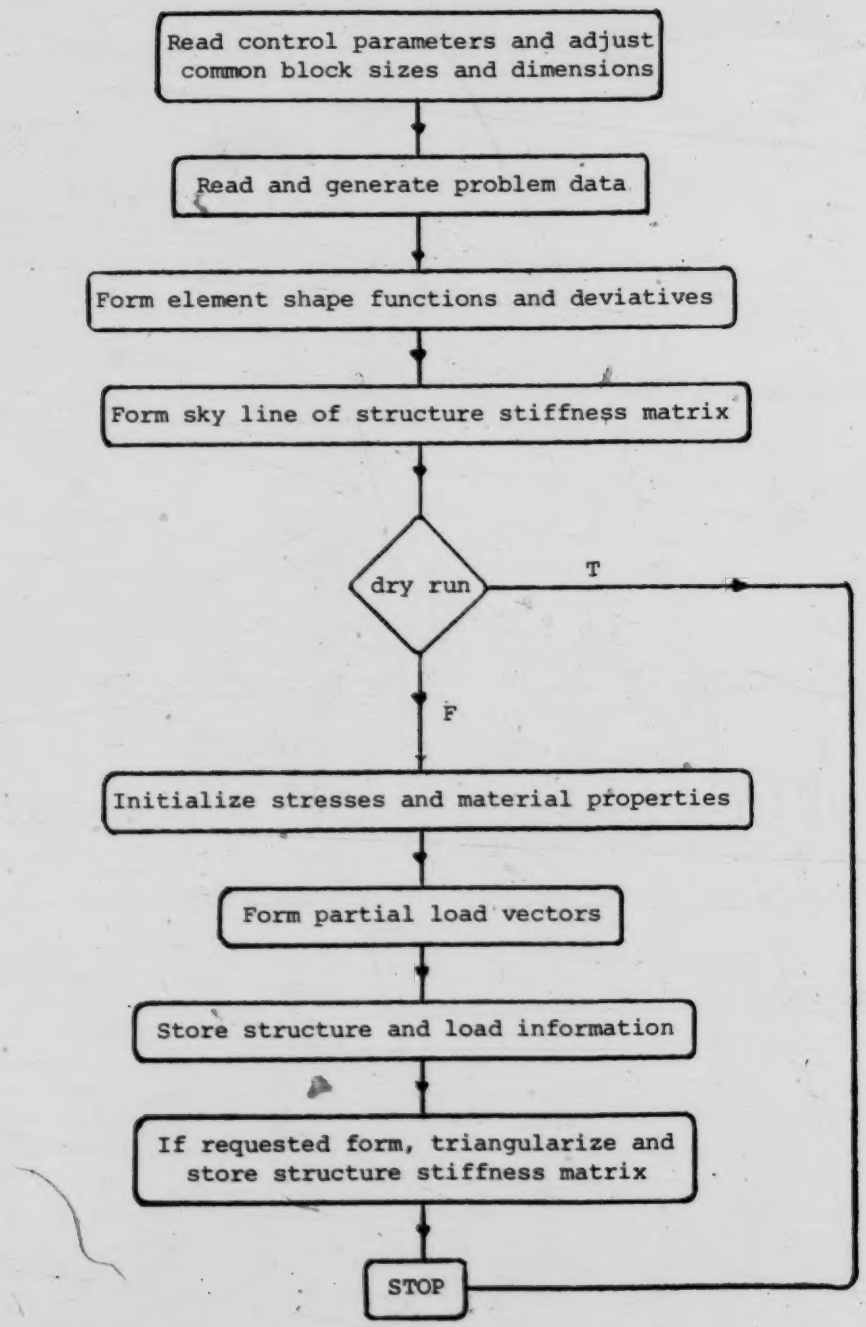
Read control parameters and adjust common block sizes and dimensions
Read and generate problem data
Form element shape functions and deviatives
Form sky line of structure stiffness matrix
dry run
T
F
Initialize stresses and material properties
Form partial load vectors
Store structure and load information
If requested form, triangularize and store structure stiffness matrix
STOP

Fig. 4.2 Flow Chart of Problem Preparation Stage of FEPARCS5

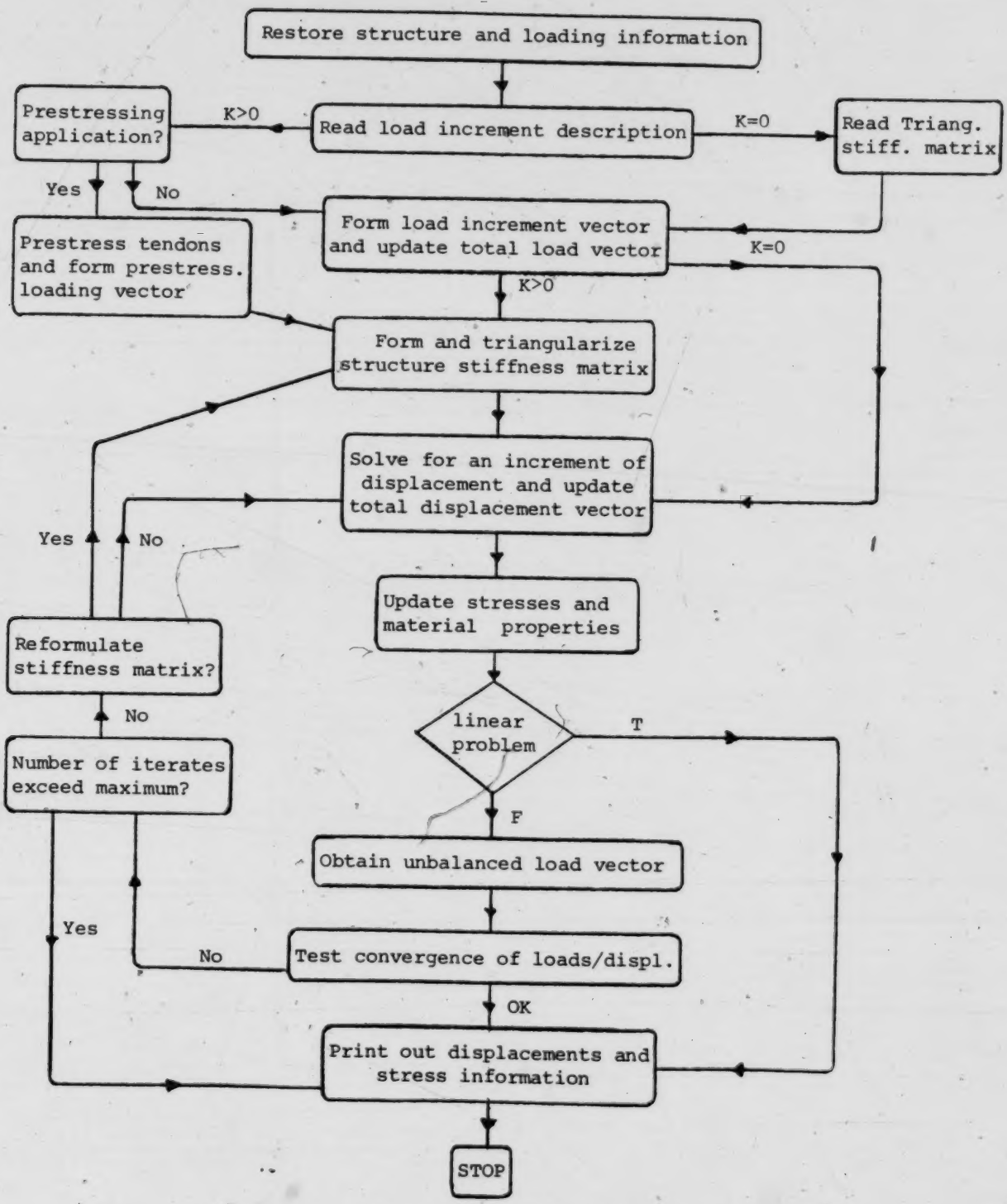

Fig. 4.3 Flow Chart of Solution Stage of FEPARCS5

CHAPTER FIVE

PRELIMINARY INVESTIGATION

5.1 Introduction

A constitutive relation for three dimensional (axisymmetric) behavior of concrete has been proposed in Chapter Two. In Chapter Three a finite element model for incremental analysis of axisymmetric reinforced and/or prestressed concrete structures has been formulated. Chapter Four describes program FEPARCS5 in which the features proposed and formulated in Chapters Two and Three have been implemented. In this Chapter a preliminary investigation of the capabilities of program FEPARCS5 and its ability to characterize the axisymmetric behavior of concrete is conducted.

A series of tests on prestressed concrete wall segments were carried out at the I.F. Morrison Laboratory, University of Alberta by Dr. J.G. MacGregor, Dr. S. Simmonds, Dr. D.W. Murray and Dr. S. Rizkallah during the year 1978 (Chitnuyanondh, et al., 1979). These experiments formed a part of the research program into the effects of overpressure on secondary containment structures mentioned in Section I.1 In this Chapter a simulation of some of these tests is carried out using program FEPARCS5. The results are compared with the experimental results and with the results of an elastic plastic analysis (Chitnuyanondh, et al., 1979). Only two segments out of fourteen will be compared. These are segments no. 1 and no. 3. Segments no. 1 and no. 3 are identical in details but have been tested under different load paths.

5.2 Wall Segment Test Description

The wall segment specimens were 31.5 x 31.5 inches and 10.0 inches thick. The reinforcing consisted of two #3 @3 inches meshes placed one half inch from each face. The prestressing tendons consisted of four 7 wire tendons in one direction and three 6 wire tendons in the other direction. The tendons were placed in ducts 1.07 inches O.D., tensioned and anchored at the ends. Load cells were placed between the anchor heads and the bearing plates. Figures 5.1 to 5.3 show the details of the wall segments.

The primary instrumentation consisted of electric strain gages, placed on the concrete on each face parallel to the main directions of prestressing. A number of Demec points were also installed on both faces.

Loading was applied through two independent perpendicular systems attached to both the steel reinforcing and the prestressing tendons. Segment 1 was tested under biaxial tension with a 2:1 loading ratio. Segment 3 was also tested under biaxial tension but the loading ratio was 1:1 up to 375.0 kips at which point the load in direction 2 was kept constant while the load in direction 1 was increased. Direction 1 was the direction parallel to the 7-wire tendons, while direction 2 was that parallel to the 6-wire tendons. The prestressing level in the tendons in direction 1 was 134.6 psi and in direction 2 it was 124.2 ksi (losses included). The prestressing system was identical in both segments 1 and 3.

5.3 FEPARCS5 Modelling of the Wall Segments

Wall segments no. 1 and no. 3 have been modelled for analysis by program FEPARCS5 as parts of a cylinder 31.5 inches high and 10.5 inches thick having an 110.5 inches internal radius as shown in Fig. 5.4. The finite element model consists of one 12 node cubic element resting on roller boundary conditions as shown in Fig. 5.5. The steel rebars and prestressing tendons are smeared in meridional and circumferential layers as shown in Fig. 5.6.

The material properties are based on data published by Chitnuyanondh, et al., (1979). Table 5.1 contains the material properties required for the proposed constitutive relation. Table 5.2 describes the stress strain curves for the prestressing tendons and the steel rebars.

Surface pressure is applied on the internal face of the cylinder in order to induce tensile stresses in the circumferential direction which, henceforth, is called direction 2. A consistent set of concentrated nodal loads is applied to the top edge in order to induce tensile stresses in the meridional direction which, henceforth, is called direction 1. The prestressing is applied using the post-tensioning option described in Section 4.4.2. The tangent stiffness approach is used throughout the analysis of both segments as a solution strategy.

5.4 Comparison of FEPARCS5 Analysis with the BOSOR5 Theoretical Analysis and with the Experimental Analysis

As mentioned in Section 5.2, segment no. 1 has been loaded with a ratio of 2:1. Fig. 5.7 shows the load-strain response of

this segment. On this figure, the response of FEPARCS5 in direction 1 agrees well with that of BOSOR5 and with the experimental results. In Direction 2 FEPARCS5 and BOSOR5 agree well but both predict higher cracking load and subsequently a response stiffer than that of the experiment.

Segment no. 3 has been loaded with a 1:1 ratio up to 375.0 kips, at which point the loading in direction 2 has been maintained constant, while the loading in direction 1 has been continued. Fig. 5.8 shows the load-strain response of this segment. In this case FEPARCS5 shows a more flexible response in direction 1 compared to both BOSOR5 and the experiment. Direction 2 shows good agreement between all three responses. Table 5.3 contains the loads at which cracking, rebar yield and tendon yield have occurred.

5.5 The Stress Path

The stress path observed for segment no. 3 gives strong evidence supporting the assumption of Section 2.3.8 that in biaxial and triaxial tension cracking in one direction does not precipitate cracking in the perpendicular direction. This stress path is shown in Fig. 5.9. Fig. 5.9 indicates that although direction 2 reaches the maximum tensile strength and starts to descend, direction 1 continues to accept increasing stresses until it assumes the maximum uniaxial tensile strength. At this point cracking normal to direction 2 occurs and the stress in this direction starts to decrease. The stress paths for segment no. 3 obtained from the experiment and BOSOR5 analysis (Chitnuyanondh) are shown on Fig. 5.9 together with

that of FEPARCS5. Agreement between all three paths is fair as far as values are concerned. The pattern discussed above however is very distinct in all three paths.

Ultimate Strength Surface Parameters		Equivalent Uniaxial Strain Surface Parameters		Elastic Moduli	
f_{cu}*	-5090.0	ε_{cu}	0.002	E_{01}*	4.1×10^6
α_c	1.2	α_c	1.3	E_{02}*	4.1×10^6
α_t	0.034	α_t	0.095	E_{03}*	4.1×10^6
ξ_1	13.75	ξ_1	22.5	G_{012}*	1.7×10^6
ρ_1	0.0	ρ_1	0.0	ν_{01}	0.2
ξ_2	3.75	ξ_2	22.5	ν_{02}	0.2
ρ_2	0.0	ρ_2	0.0	ν_{03}	0.2

(a) Wall Segment No. 1

Ultimate Strength Surface Parameters		Equivalent Uniaxial Strain Surface Parameters		Elastic Moduli	
f_{cu}*	-5690.0	ε_{cu}	0.002	E_{01}	4.3×10^6
α_c	1.2	α	1.3	E_{02}	2.2×10^6
α_t	0.034	α	0.12	E_{03}	2.2×10^6
ξ_1	13.75	ξ_1	22.5	G_{012}	1.2×10^6
ρ_1	0.0	ρ_1	0.0	ν_{01}	0.2
ξ_2	3.75	ξ_2	22.5	ν_{02}	0.2
ρ_2	0.0	ρ_2	0.0	ν_{03}	0.2

(b) Wall Segment No. 3

Table 5.1 Wall Segment Material Parameters (Concrete)

#3 Rebars		Prestressing Tendons	
σ (ksi)	ε (10^{-3})	σ (ksi)	ε (10^{-3})
0	0	0	0
58.20	2.04	205.0	6.97
69.60	40.00	228.0	8.40
---	---	237.0	10.0
		240.0	12.0
		250.0	20.0
		251.2	41.0

Table 5.2 Wall Segment Material Parameters (Steel)

	Wall Segment No. 1			Wall Segment No. 3		
	FEPARCS5	BOSOR5	TEST	FEPARCS5	BOSOR5	TEST
Cracking of Direction 1	310	295	320	300	263	330
Cracking of Direction 2	430	350	359	225	200	207
Vertical Rebar Yield	490	475	465	500	530	530
Horizontal Rebar Yield	---	---	---	350	350	355
Vertical Tendon Yield	510	495	500	500	---	---
Horizontal Tendon Yield	---	---	---	375	425	375

Table 5.3 Limit State Loads (all loads shown are those in direction 1 in kips)

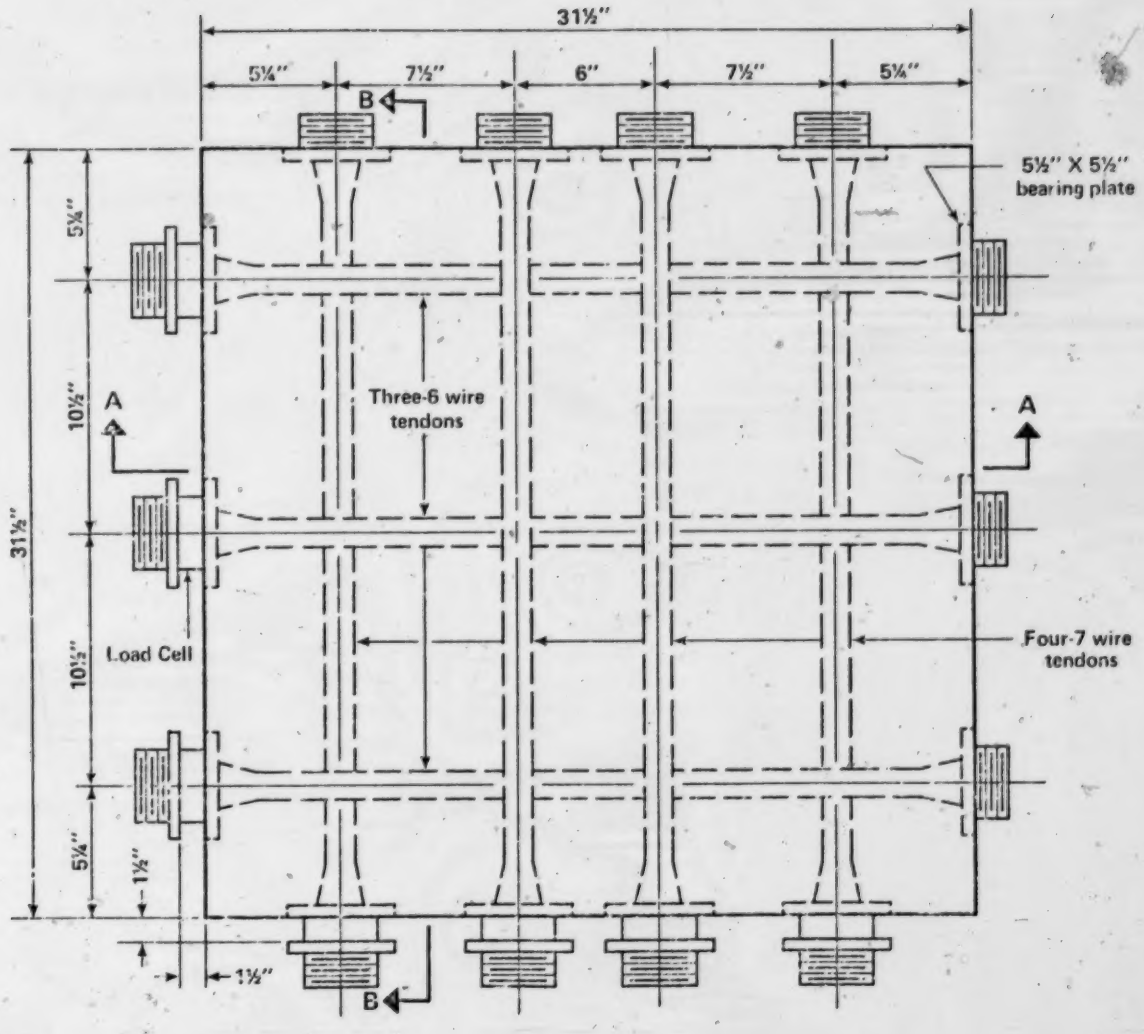

Fig. 5.1 Elevation of Wall Segment Specimen

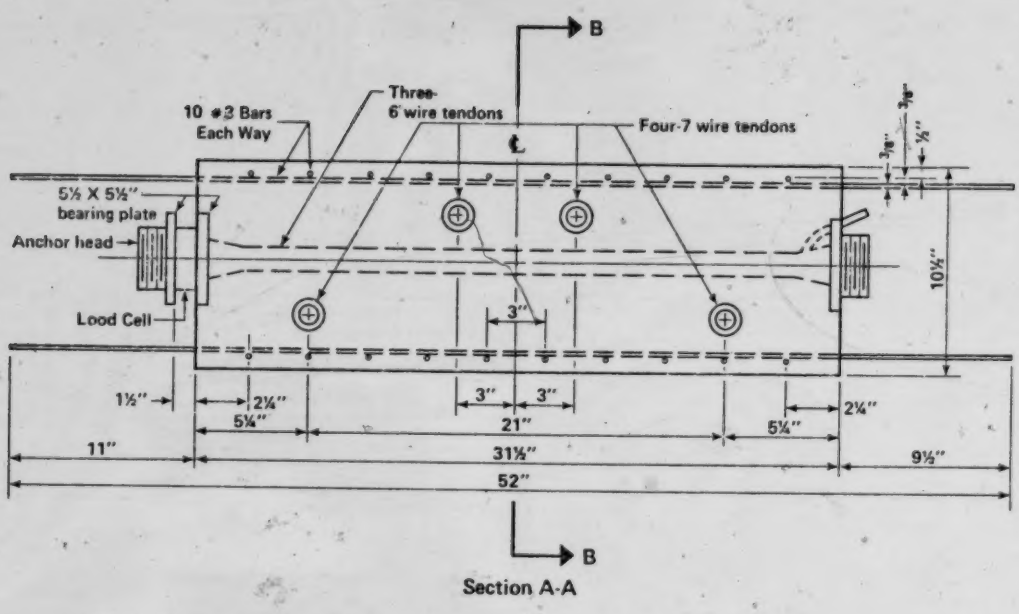

Fig. 5.2 Typical Section A-A Through Wall Segment Specimen

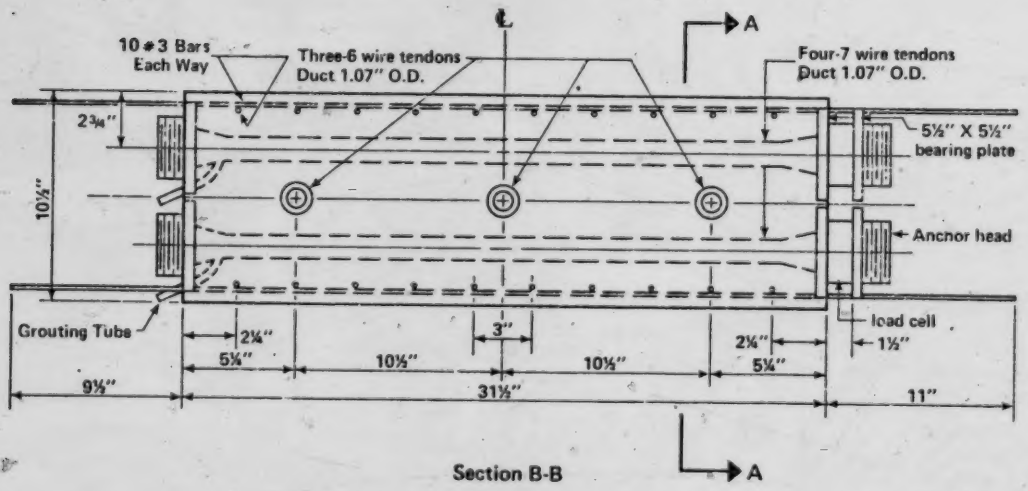

Fig. 5.3 Typical Section B-B Through Wall Segment Specimen

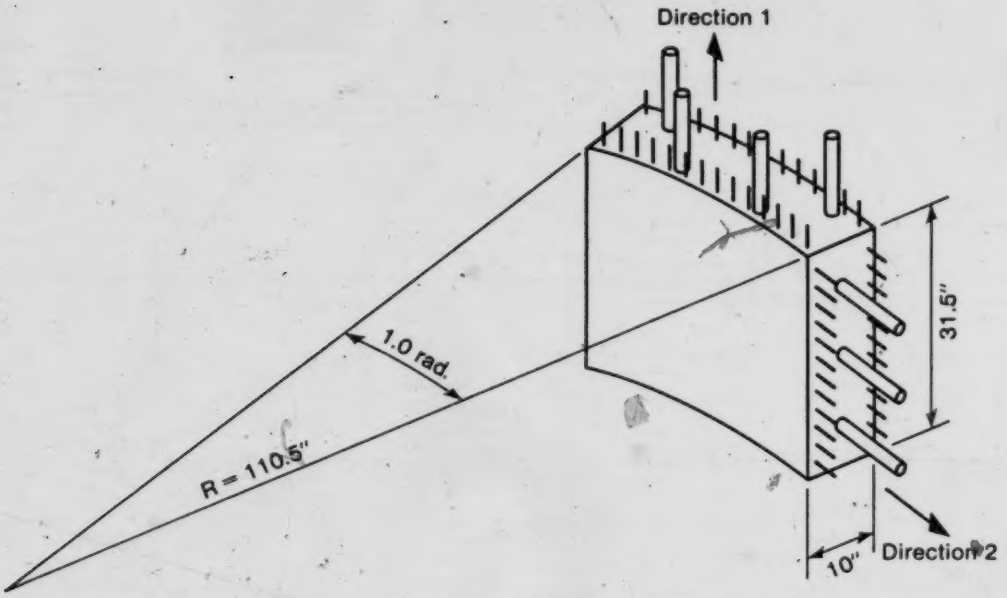

Fig. 5.4 Axisymmetric Modelling of Wall Segment Specimen

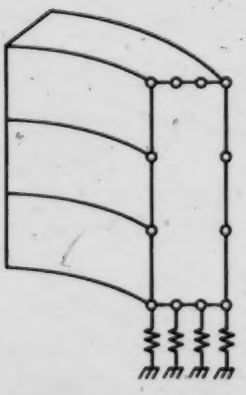

Fig. 5.5 Finite Element Modelling of Wall Segment Specimen

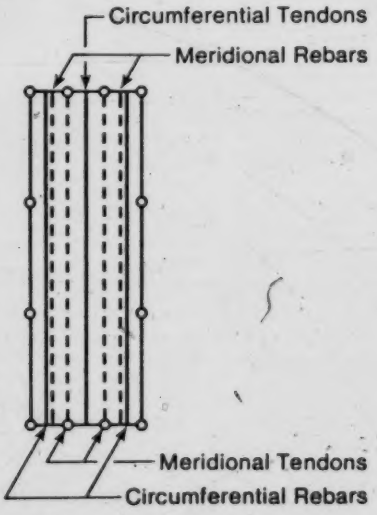

Fig. 5.6 Reinforcing and Prestressing Layers of Wall Segment Finite Element Model

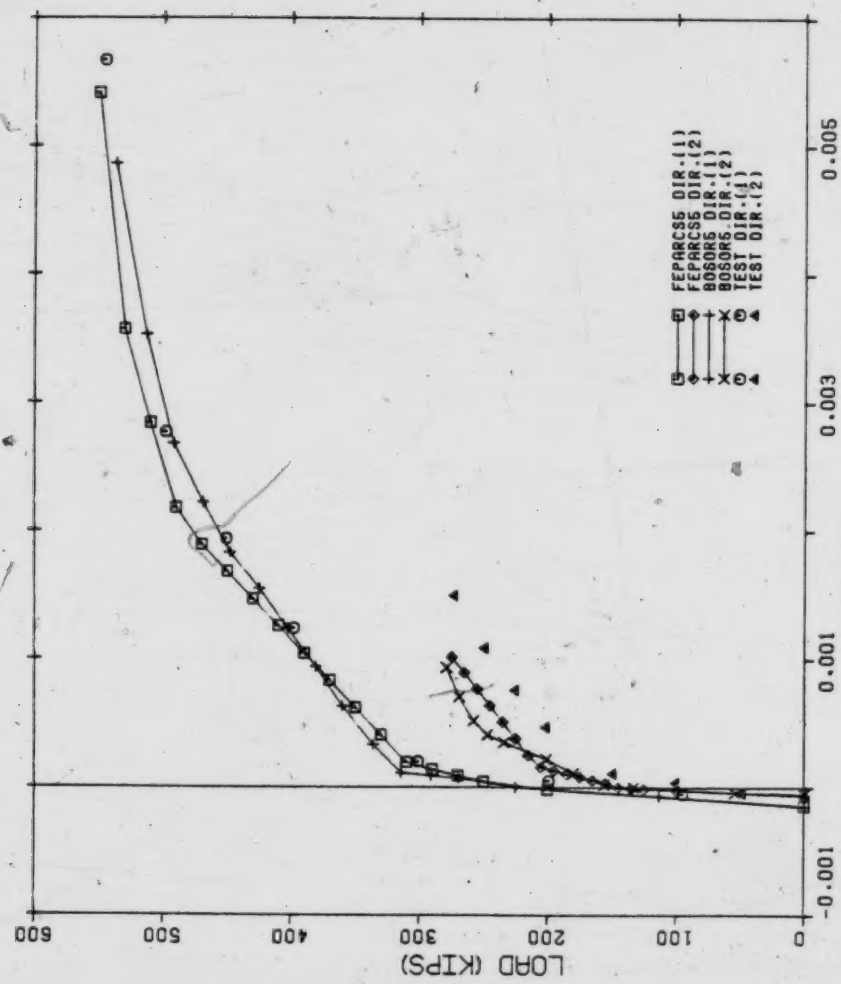

Fig. 5.7 Load Strain Comparison for Segment No. 1

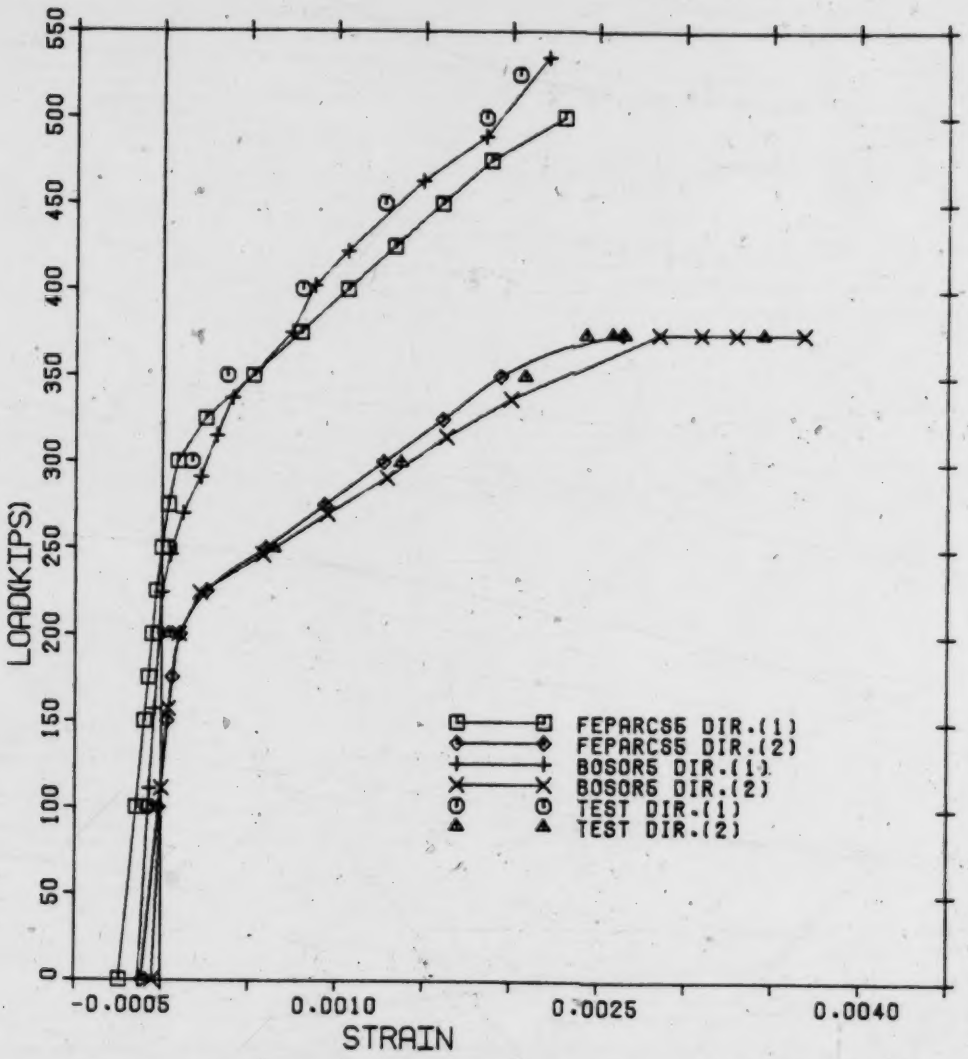

Fig. 5.8 Load Strain Comparison for Segment No. 3

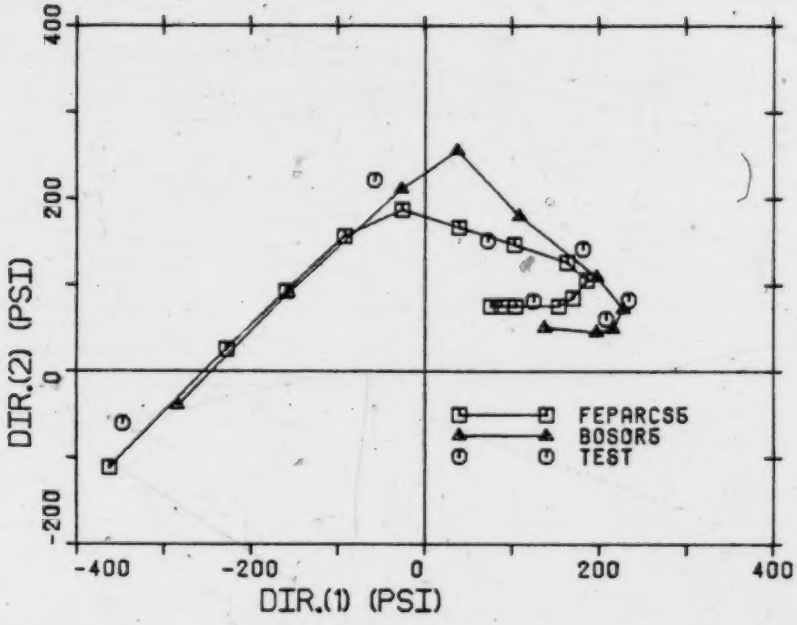

Fig. 5.9 Stress Path Comparison for Segment No. 3

CHAPTER SIX

ANALYSIS OF A CONTAINMENT STRUCTURE

6.1 Introduction

In Chapter Five a preliminary investigation of the capabilities of program FEPARCS5 has been undertaken. The next step is to use the program to analyse a complicated structure which makes more rigorous demands on the different features of the program. In this chapter a finite element model of the test structure mentioned in Section 1.1 is described, an analysis of the model using program FEPARCS5 is presented, and a comparison of the results both with those obtained from the actual test and with those of an elastic plastic theoretical analysis of a similar model carried out by Murray, et al. (1978) using a modified form of program BOSOR5 is discussed.

6.2 Description of Test Structure and Procedure

The test structure, shown in Figures 6.1 to 6.4, was composed of a 3'-6" thick base, a 5" thick - 10' high cylindrical wall which had an internal radius of 4'-10", a ring beam and a 4" thick spherical dome which had an internal radius of 9'-8". A smooth transition between the dome and ring beam was obtained by gradually thickening the dome at the springing line. Four buttresses were placed at 90° intervals around the cylinder to provide anchorage for the circumferential post-tensioning strands. The dome prestressing

tendons were placed on two orthogonal geodetic nets as shown in the upper right hand quadrant of Fig. 6.2. The dome reinforcing was placed on meridional and circumferential lines as shown in the lower right hand quadrant of Fig. 6.2.

The levels of prestressing and the thicknesses have been designed to yield a cracking sequence similar to that expected in the Gentilly-2 containment structure, (Murray et al. 1978). However, the wall has been designed to have lower cracking strength relative to that in the dome than would be expected in the Gentilly-2 structure. In this manner more information can be obtained about the behavior of all components of the test structure before final failure occurred.

Testing of the structure was carried out by water pressure applied through a thin elastic membrane which prevented leakage through the wall of the structure. Five preliminary tests, in which the pressures were kept within 20.0 psi, were carried out to check instrumentation. Subsequently, two actual tests were conducted. In the first test, pressure was raised up to 80.0 psi which was well above cracking pressure. The structure was then unloaded since substantial leaking of water through a damaged membrane made it impossible to maintain pressure. A new liner was installed and the final test was carried out up to failure at 159.9 psi.

First visible cracks were observed at 40.0 psi in the cylinder wall along meridional and circumferential lines. At 140.0 psi splitting cracks at the anchorage of a circumferential tendon appeared on the southwest buttress. At 158.0 psi failure occurred at this location with concrete spalling off. At 159.0 psi three

horizontal tendons in the wall either fractured or lost their anchorage and the adjacent rebars fractured. The liner then ruptured releasing all pressure and ending the test.

Electronic readings were taken at intervals of internal pressure of 5.0 psi. There were 207 electric strain gages placed on the steel reinforcing and 38 electric strain gages placed on concrete face. In addition 74 Demec gages were located along and across a meridional line midway between the northeast and northwest buttresses.

The information on the test contained in this section and the next sections have been obtained from progress reports to the Atomic Energy Control Board of Canada, since final reports have not been published up to the time of writing.

6.3 Finite Element Model of Test Structure

6.3.1 General Description

The finite element mesh for the structure is controlled by the locations of the prestressing strands, the shape of the ring beam and the anticipated stress gradients at the junction of the ring beam and the cylinder wall. Quadratic displacement element are used exclusively to construct the mesh. These elements have been found to give greater flexibility in modelling the geometry of the structure than do linear elements. At the same time the problem size is kept reasonable. Two elements are used through the thickness of the dome and the cylinder wall to enable accurate positioning of the prestressing tendons in the dome and to resolve the problem of intersection of vertical and dome prestressing tendons inside the

ring beam. Figures 6.5 to 6.8 show the mesh and the prestressing and reinforcing layers superimposed on the solid elements.

It has been found by Murray et al. (1978), that the base provides complete fixity at the bottom of the cylinder wall. Therefore, the base has been eliminated from the finite element model and in its place a set of boundary elements have been used as shown in Figures 6.6b and 6.6c. Since only one half of the vertical cross section is modelled, the end of the dome on the axis of symmetry has been provided with a set of horizontal boundary elements as shown in Fig. 6.6a in order to prevent the vertical line from rotating or translating in the horizontal direction.

The connectivity of the elements has been defined so that the local μ-ξ coordinates be as shown in Fig. 6.9. The order of the Gaussian integration rule is 2 x 2 for all solid elements. A two point rule is used for each reinforcing or prestressing layer within a solid element. Altogether, the problem has 226 nodes, 14 boundary elements and 55 solid elements on which a total of 63 longitudinal reinforcing layers, 57 hoop reinforcing layers, 29 longitudinal prestressing layers and 28 circumferential prestressing layers are imposed.

6.3.2 Modelling of Dome Prestressing

In program FEPARCS5 prestressing layers have to be described as meridional or circumferential layers. Therefore, it has been necessary to transform the dome prestressing layers from the actual orthogonal geodetic nets into equivalent meridional and circumferential layers. This has been accomplished by deriving weighting

functions for the contribution of each tendon to the meridional and circumferential directions at the points of intersection of the tendons. The weighting functions have been plotted against the radii of the points of intersection for meridional contributions and circumferential contributions. These plots have been used to obtain the average contribution of meridional tendons per unit width and circumferential tendons per unit length. This process is described in detail in Appendix C.

6.3.3 Materials

The stress strain curves for the different kinds of steel rebars are shown in Figs. 6.10a and 6.10b (Murray, et al, 1978). The maximum strain allowed in rebars is 4%. The stress strain curves for the prestressing tendons are shown in Figs. 6.11a and 6.11b (Murray, et al., 1978). The maximum strain allowed in the dome tendons (0.62"ϕ) is 8%, while the wall prestressing tendons (0.5"ϕ) are allowed only 5% strain.

Two different types of concrete are used in the body of the model. Normal cast in place concrete is used for the cylinder wall up to an elevation of 5.0 ft., and in the ring beam and the dome. Gunite concrete is used in the cylinder wall from elevation of 5.0 ft. to 10.0 ft. The properties of those materials are shown in Table 6.1.

No thermal analysis of this model is required, hence concrete and all rebars are assigned zero thermal properties. However, since the prestressing strains in the tendons are assigned through a thermal field, the tendons are assigned thermal properties corresponding to the required levels of prestressing. There are essentially

three levels of prestressing: 137.7 ksi for the circumferential prestressing in the wall and the ring beam, 90.0 ksi for the vertical prestressing in the wall and 113.1 ksi for the dome prestressing (losses included). The first two levels are induced in 0.5"ϕ tendons. Therefore, two different material types are defined to simulate the 0.5"ϕ tendons with two different thermal expansion coefficients. The dome prestressing is composed of 0.62"ϕ tendons and these are defined to have a different thermal expansion coefficient.

6.3.4 Loads

This model is subjected to a variety of loads; gravity loads, tangential friction losses in the dome, hydrostatic pressure, prestressing loads and the internal pressure. Gravity loads are simulated as described in Section 3.4.1. Friction losses in the dome are simulated by meridional tangential tractions on the middle line of the dome. Hydrostatic pressures are simulated by a normal pressure distribution on the inside face of the model. These three load vectors are added to one dead load vector. Prestressing simulation has been carried out using the procedure outlined in Section 4.4.2. A normal internal pressure of 1.0 psi is used to form an equivalent internal pressure load vector which is incremented in the subsequent pressurization of the structure.

6.4 Analysis of Test Structure

The analysis of the finite element model described in Section 6.3 is performed in several stages. In the problem preparation stage data is read and generated, element shape functions and derivatives

are evaluated, column heights and the addressing array of the stiffness matrix are formed, stresses, strains and material properties are initialized at all integration points, and all basic load vectors are formed. In the second stage the tendons are tensioned, equivalent prestressing loads are evaluated and applied to the structure excluding the tendons. In the third stage dead loads composed of gravity, friction and hydrostatic loads are applied to the structure as one load increment. In the subsequent stages, increments of internal pressure are added to the structure simulating the pressurization of the test structure which ultimately leads to failure. Failure in this analysis is characterized by the inability of the program to obtain convergence on both loads and displacements.

Table 6.2 contains a breakdown of all runs on the Amdahl 470/V7 computer unit at the University of Alberta, Edmonton. The number of iterates required for each load step and the CPU time consumed are shown. Table 6.2 also shows the tolerances on the displacements and the loads, λ_r and λ_p respectively. The number of subincrements (NS) vary between 5 and 10. The maximum number of iterates allowed per load step is 31 up to 125.0 psi, after which the limit is increased to 70 iterates. In the initial stages and up to 40.0 psi the stiffness matrix is evaluated at the beginning of each load step and re-evaluated after each third iterate. In subsequent stages, the material properties available at 20.0 psi are used to formulate, triangularize and store a constant stiffness matrix which is used for all load increments above 40.0 psi. It has been found that this stiffness matrix gives better convergence than the initial stiffness matrix.

6.5 Comparison of Results with the Experimental Results and the BOSOR5 Theoretical Analysis

Program FEPARCS5 outputs nodal displacements, stresses at the Gaussian points for solid elements, and stresses and strains at the Gaussian points for the rebar and prestressing layers. At the time of writing, the experimental results and the BOSOR5 results available consist of displacement profiles and surface strains obtained from Demec readings. Comparisons, therefore, will be restricted to displacement history and profiles, and surface strains. In addition, cracking patterns are discussed.

6.5.1 Displacements

Deflection patterns determined from the FEPARCS5 analysis are reasonably similar to those of BOSOR5 and the test. Fig. 6.12 shows a deflection profile at 120.0 psi. It can be seen that the results of FEPARCS5 on the cylinder wall represent a stiffer behaviour than for the other two sets of results. On the dome, however, FEPARCS5 and BOSOR5 match reasonably up to a point two feet away from the crown. At this point FEPARCS5 maintains the displacement gradient an extra short distance, thereby approaching the test results, while BOSOR5 results level off more rapidly. On this figure it is observed that the displacement gradient of the test structure at 120.0 psi is higher than either that of BOSOR5 or FEPARCS5.

Fig. 6.13 shows the deflection-pressure curves at two points near the top of the dome and the middle of the cylinder. These are the points of maximum deflection. On this figure, BOSOR5 and FEPARCS5 agree well up to 80.0 psi at the top of the dome and

up to 110.0 psi at the middle of the cylinder. After 80.0 psi FEPARCS5 deflection response at the top of the dome approaches the test results while BOSOR5 predicts a somewhat stiffer response. This agrees well with the deflection profiles shown in Fig. 6.12. FEPARCS5 deflection response at the middle of the wall after 110.0 psi predicts more carrying capacity than that shown by BOSOR5. The reason must be that BOSOR5 uses a better descending branch representation of the tensile stress strain curve of concrete. The difference, however, is within 2.5%.

6.5.2 Surface Strains

As mentioned before the strains plotted from the test results are measured from Demec readings, i.e. are measured from displacements over a finite length. Hence, at points, where there is a relatively high displacement gradient, a discrepancy must show between those results and the strain predicted by FEPARCS5. The latter, as mentioned in Chapter Three, are calculated assuming infinitesmal strain and negligible rotations. This is particularly noticeable in the cylinder wall near the base where there is a point of inflection and rotations are not negligible.

Figs. 6.14 to 6.19 show a series of strain histories against internal pressure at a variety of points on the outside surface of the structure. Fig. 6.14 shows the meridional strains at a point 28" above the base of the cylinder. The response of FEPARCS5 agrees reasonably with that of BOSOR5 and the test results up to 105 psi. At this point the response of FEPARCS5 shows considerable stiffening as shown by the curve denoted by ε_1. This discrepancy is to be

expected since this curve is derived from an infinitesmal strain field and the point under consideration lies very near the point of inflection as can be seen in Fig. 6.12. The curve denoted ε_f shows finite (Green's) strains computed from the displacement field of FEPARCS5. This curve reflects the influence of rotations on the strain at this point.

Fig. 6.15 shows the circumferential strains at the same point. Agreement here is reasonable between all three sets of results, although the stiff behavior predicted by FEPARCS5 in the cylinder wall can be observed.

Figs. 6.16 and 6.17 show respectively the meridional and circumferential strains at a point 65" above the base on the outer surface of the cylinder. In the neighborhood of this point, the displacement gradient is very small (see Fig. 6.12) and FEPARCS5 predicts a meridional strain response in good agreement with BOSOR5. The test results, however, are much stiffer. Confirmation of the test results may be obtained once the electric strain gage results are published. In the circumferential direction agreement is good between all three sets of results, although the slightly stiffer wall response of FEPARCS5 is again observed.

Fig. 6.18 shows the meridional strains at a point approximately 8.5" away from the crown on the outer surface of the dome. FEPARCS5 response indicated by ε_i exhibits the stiff behavior characterizing points of high displacement gradient. The curve indicated ε_f is obtained including the rotation from the displacement field of FEPARCS5. The improvement in response is noticeable. Fig. 6.19 shows the circumferential strain at the same point.

FEPARCS5 response agrees well with that of BOSOR5 and the test results.

6.5.3 Cracking Sequence

Program FEPARCS5 outputs cracking information at the Gaussian points. The term "cracking" means that the point has reached its ultimate strength and is forced to deform beyond the corresponding strain. The term 'vertical crack' is used to describe cracks occurring due to circumferential strains, while the term 'horizontal crack' is used to describe those cracks occurring due to meridional strains.

Fig. 6.20 show the progress of vertical cracks as predicted by FEPARCS5. Vertical cracks occur as early as 40.0 psi at the crown of the dome and spread slowly outward on the outer surface of the dome. Extensive vertical cracks appear on the entire length of the cylinder with the exception of the upper and lower two feet at 60.0 psi. As pressure increases vertical cracks spread up and down on the cylinder but never reach the ring beam nor the base. Throughout the analysis the ring beam and the springing line of the dome remain free of vertical cracks. BOSOR5 predicts extensive vertical through cracks in the cylinder wall at 62.0 psi (Murray, et al., 1978). Vertical cracks in the dome start appearing at 67.0 psi and spread slowly in the BOSOR5 analysis. However, at 120.0 psi the pattern of vertical dome cracks predicted by BOSOR5 is similar to that of FEPARCS5. Again the ring beam and the springing region of the dome remain free of vertical cracks throughout the analysis (Murray, et al., 1978). In the test the first visible signs of vertical cracks were observed at 40.0 psi in the wall. At 80.0 psi these

cracks became as extensive as has been predicted by both BOSOR5 and FEPARCS5. The ring beam and the springing of the dome remained free of vertical cracks to the end of the test.

Fig. 6.21 shows the progress of horizontal cracking. The onset of horizontal cracks is predicted by FEPARCS5 at 50.0 psi on the inside surface of the ring beam and the springing of the dome. At 60.0 psi FEPARCS5 predicts horizontal cracks at upper surface of the dome at and near the crown and on the outside surface of the wall two feet below the ring beam. The cracked region on the inside surface of the ring beam continued to spread up and down slowly penetrating the ring beam. At 70.0 psi extensive horizontal cracks are predicted in the dome and the wall. However, the upper surface of the ring beam and the springing of the dome remain crack free. At 120.0 psi horizontal cracks appear everywhere in the structure except in the upper surface of the springing of the dome the outer portion of the ring beam and the outside surface of the wall near the base. BOSOR5 predicts the first horizontal cracks at 30.0 psi on the inside surface of the ring beam. The outside surface of the dome near the crown and the outside surface of the wall under the ring beam are predicted to crack horizontally at 62 psi. After that BOSOR5 shows a pattern of horizontal crack progress which is very similar to that predicted by FEPARCS5. Test results indicate similar behavior on the outside surface. On the inside surface, no information is available since it was inaccessible.

6.6 Limit States for Containment Structures

The objective of the application of the technology developed in this work is to simulate the response of a containment structure to internal over pressure. Internal pressure in nuclear containment structures may occur due to failure of the primary or secondary cooling systems within the structure. Under such hypothetical situations a series of limit states can be defined to indicate the degree of damage (Murray and Epstein, 1976). Damage to such structures may result in a deterioration of the containment function and/or danger to the systems inside the structure. The limit states which may lead to such problems have been identified by Murray and Epstein (1976) as

1. The pressure which causes cracking over a significant portion of the internal surface.
2. The pressure which causes yielding of the reinforcing steel.
3. The pressure at which cracks may penetrate the structure.
4. The pressure at which the prestressing tendons may yield, thus seriously damaging the ability of the structure to reseal itself upon relief of pressure.
5. The pressure at which spalling of concrete may lead to debris inside the structure.
6. The pressure causing rupture of the reinforcing steel or prestressing tendons.
7. The pressure which may initiate a structural mechanism.
8. The pressure at which relative displacements may damage the systems inside the structure.

These limit states may or may not occur in the order they are listed. In Table 6.3 some of these limit states are identified. Ultimate failure of this type of structure may be characterized by rupture of the prestressing tendons. This stage has not been reached in FEPARCS5 analysis. It is possible however to predict rupture of the prestressing tendons by studying the strain profiles and the rate at which strain increases with respect to pressure in the late stages of the analysis. The strain profiles at 140.0 psi for the meridional and circumferential prestressing tendons are shown in Figs. 6.22 and 6.23 respectively. Fig. 6.22 indicates that rupture of the meridional prestressing tendons may occur at the top of the dome. Assuming that the maximum strain of the dome tendons is .05, the based on the strain increment between 137.5 psi and 140.0 psi of internal pressure, rupture may be expected at 181.4 psi. Fig. 6.23 shows two possible points at which rupture of the circumferential tendons may occur; the top of the dome and the middle of the cylinder. The latter, however, possesses higher strain rate loading to failure at 183.5 psi. A discussion with Dr. S. Simmonds has revealed that actual failure of the test structure took place in the form of slippage of two nonadjacent circumferential tendons leading to a partial transfer of load to the middle tendon which then ruptured ending the experiment at 159.9 psi. This is consistent with the findings of FEPARCS5, but it shows the need to establish slippage criteria in programs used for analysis of prestressed concrete structures.

Ultimate Strength Surface Parameters		Equivalent Uniaxial Strain Surface Para.		Initial Elastic Moduli	
f_{cu}	-5680.0	ε_{cu}	-0.00217	E_{01}	$3.1 * 10^7$
α_c	1.2	α_c	1.3	E_{02}	$3.1 * 10^7$
α_t	0.032	α_t	.055	E_{03}	$3.1 * 10^7$
ξ_1	13.75	ξ_1	22.5	G_{012}	$1.3 * 10^7$
ρ_1	0.0	ρ_1	0.0	ν_{01}	0.2
ξ_2	3.75	ξ_2	22.5	ν_{02}	0.2
ρ_2	0.0	ρ_2	0.0	ν_{03}	0.2

(a) Material No. 1 (Normal Concrete)

Ultimate Strength Surface		Equivalent Uniaxial Strain Surface		Initial Elastic Moduli	
f_{cu}	-3540.0	ε_{cu}	-0.00238	E_{01}	$1.8 * 10^7$
α_c	1.2	α_c	1.3	E_{02}	$1.8 * 10^7$
α_t	.048	α_t	0.05	E_{03}	$1.8 * 10^7$
ξ_1	13.75	ξ_1	27.5	G_{012}	$0.75 * 10^7$
ρ_1	0.0	ρ_1	0.0	ν_{01}	0.2
ξ_2	3.75	ξ_2	22.5	ν_{02}	0.2
ρ_2	0.0	ρ_2	0.0	ν_{03}	0.2

(b) Material No. 2 (Gunite)

Table 6.1 Concrete Material Properties of Test Structure

Load Step	Description	CPU (Sec)	No. of Iterates	λ_r	λ_p	URF**	NS*
0	Problem Preparation	2.05	---	--	--	--	--
1	Prestressing	37.60	6	0.001	0.005	0.5	10
2	(G + F + H)***	60.88	10	0.001	0.003	0.5	10
3	20.0 psi	48.00	8	0.001	0.003	0.5	10
4	40.0 psi	46.65	8	0.001	0.001	0.5	10
5	50.0 psi	73.08	17	0.001	0.001	0.5	10
6	60.0 psi	65.34	17	0.001	0.003	1.0	10
7	70.0 psi	88.05	23	0.001	0.005	1.0	10
8	75.0 psi	50.79	21	0.001	0.005	1.0	5
9	80.0 psi	48.34	20	0.001	0.007	1.0	5
10	85.0 psi	49.37	21	0.001	0.007	1.0	5
11	90.0 psi	47.65	20	0.001	0.008	1.0	5
12	95.0 psi	43.52	18	0.001	0.008	1.0	5
13	100.0 psi	46.12	19	0.001	0.008	1.0	5
14	105.0 psi	42.98	18	0.001	0.008	1.0	5
15	110.0 psi	47.47	20	0.001	0.008	1.0	5
16	115.0 psi	59.61	26	0.001	0.008	1.0	5
17	117.3 psi	55.04	24	0.001	0.008	1.0	5
18	120.0 psi	56.98	25	0.001	0.009	1.0	5
19	122.5 psi	79.14	33	0.001	0.010	1.0	5
20	125.0 psi	71.16	30	0.001	0.010	1.0	5
21	127.5 psi	79.24	33	0.001	0.011	1.0	5
22	130.0 psi	91.20	39	0.001	0.012	1.0	5
23	132.5 psi	107.90	48	0.001	0.013	1.0	5
24	135.0 psi	110.09	49	0.001	0.015	1.0	5
25	137.5 psi	86.06	38	0.001	0.017	1.0	5
26	140.0 psi	144.29	64	0.001	0.019	1.0	5

Table 6.2 Load Steps of FEPARCS5 Analysis of Finite Element Model of Test Structure

*** G : gravity load
F : friction losses
H : hydrostatic pressure
** URF: under-relaxation factor
* NS: number of subincrements

Limit State Description	Pressure	Location
extensive vertical cracks	60.0	cylinder wall
extensive horizontal cracks	70.0	cylinder and dome
ring beam cracks	50.0	horizontal cracks on inside surface
yielding of dome circumferential 6 mm rebars (72.5 ksi)	90.0	top of dome
yielding of wall circumferential 3 mm rebars (48.0 ksi)	117.5	from 2' to 8.5' above base
yielding of dome meridional 6 mm rebars (72.5 ksi)	90.0	top of dome
yielding of wall meridional 6 mm rebars (48.0 ksi)	110.0	inside surface immediately below ring beam
yielding of wall circumferential prestressing tendons (240.0 ksi)	130.0	from 3' to 7.0' above base
yielding of dome circumferential prestressing tendons (220.0 ksi)	110.0	top of dome
yielding of wall meridional prestressing tendons (240.0 ksi)	--	----------
yielding of dome meridional prestressing tendons (220.0 ksi)	120.0	top of dome
spalling*of concrete	115.0	inside surface of dome near ring beam

Table 6.3 Pressures Corresponding to Limit States of the Finite Element Model

* spalling is defined as cracking parallel to the surface and may cause concrete to separate from the structure

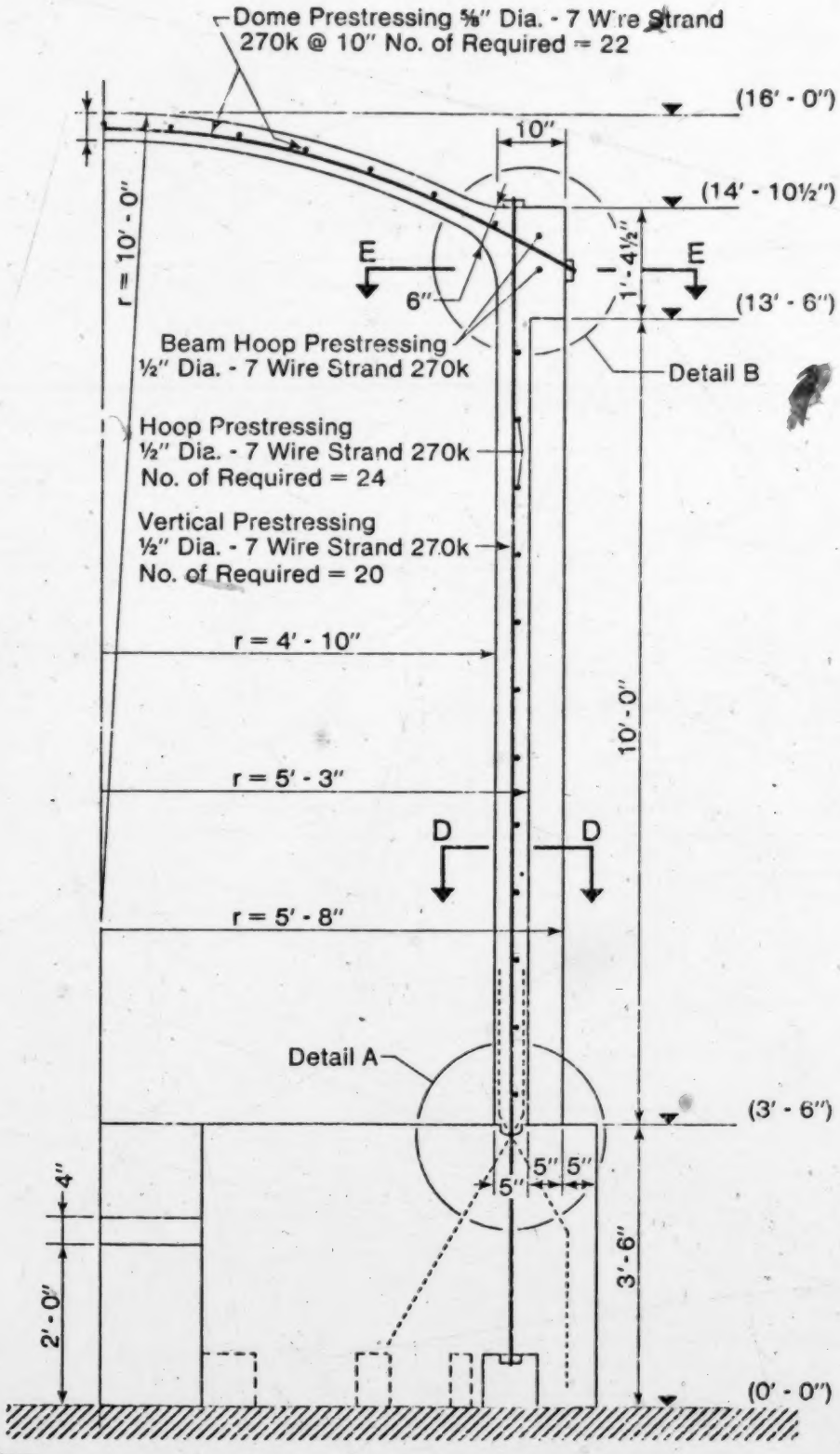

Fig. 6.1 Elevation of Test Structure

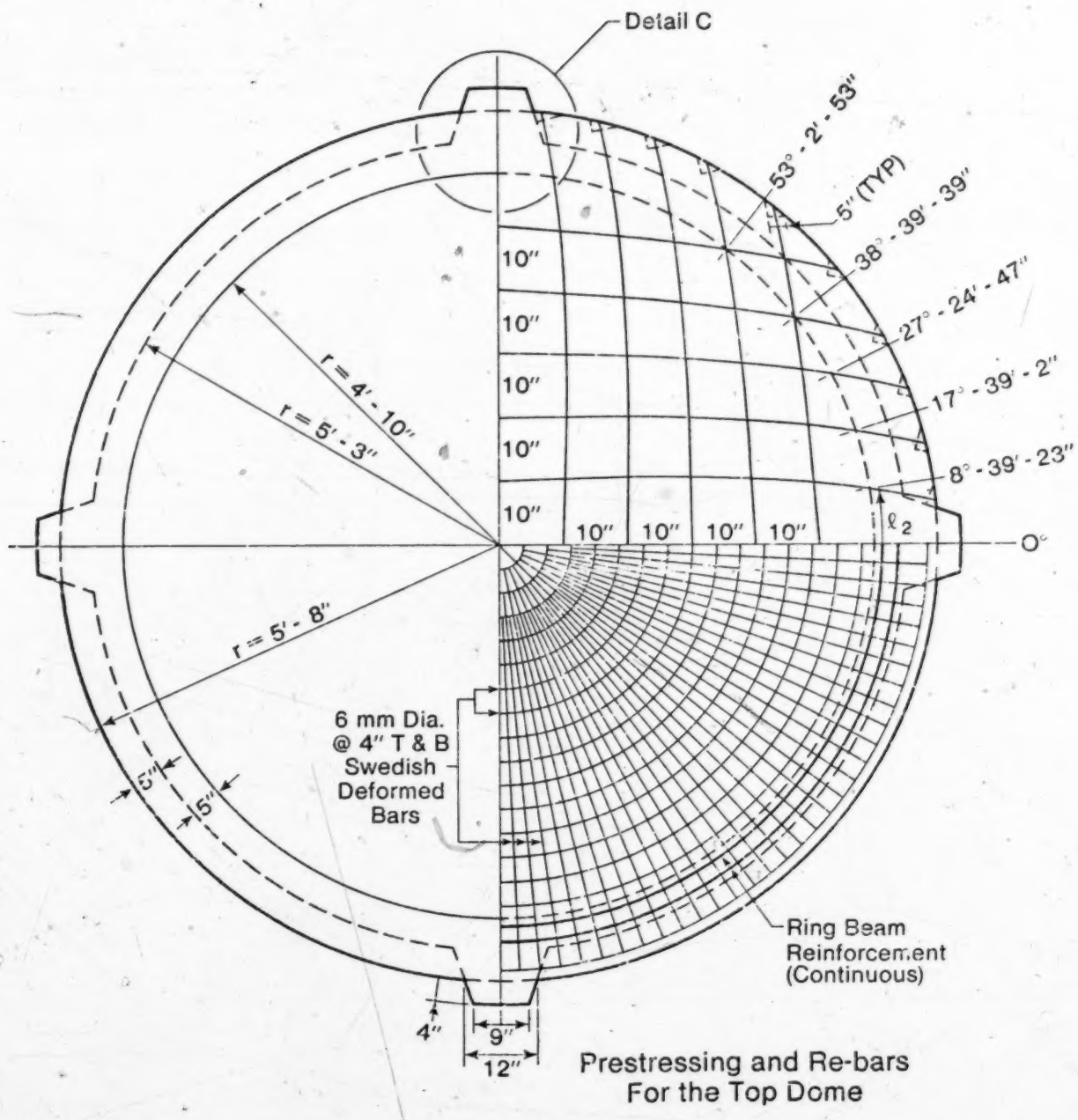

Fig. 6.2 Prestressing and Rebars for the Dome of the Test Structure

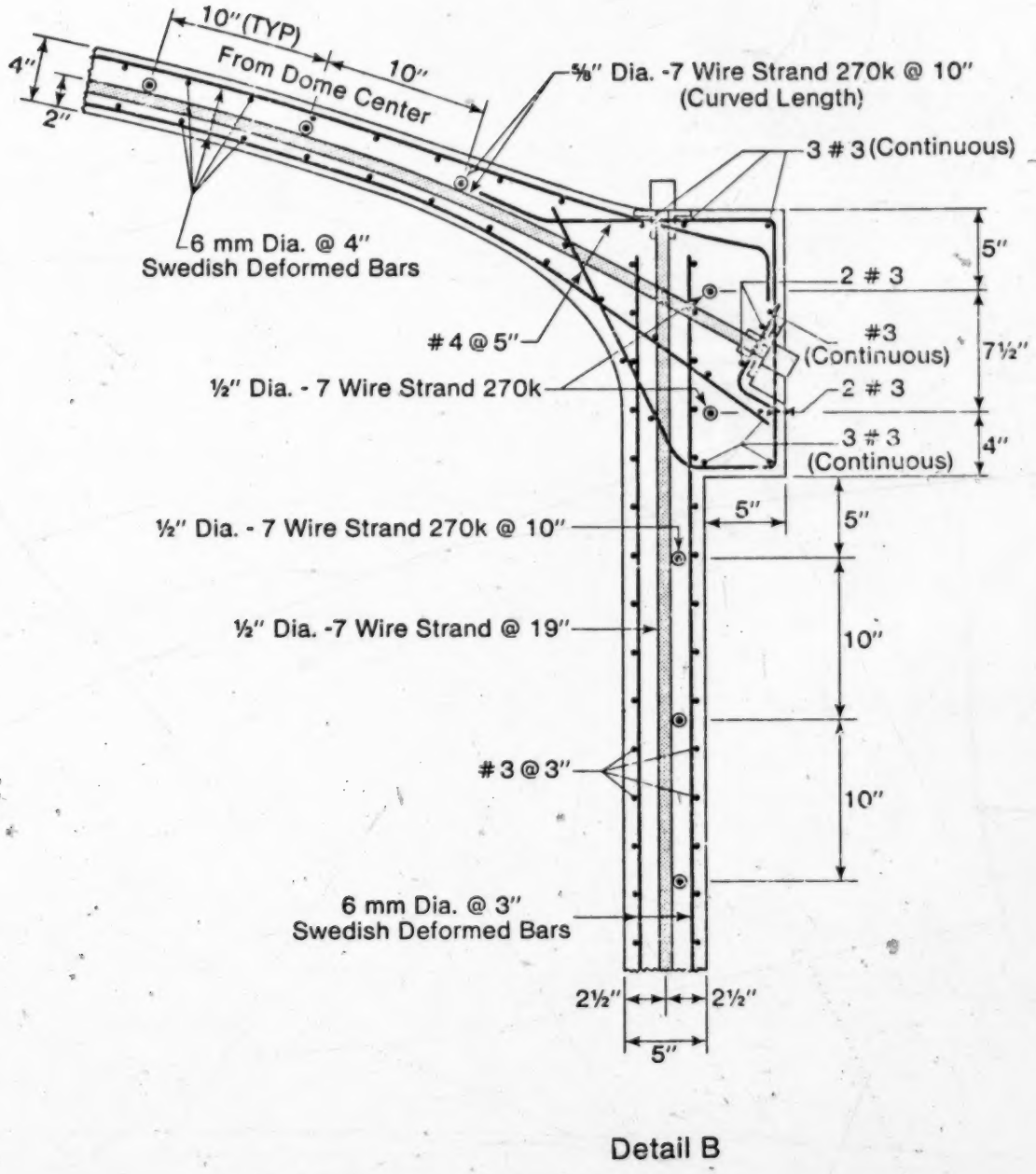

Detail B

Fig. 6.3 Detail of Ring Beam of Test Structure

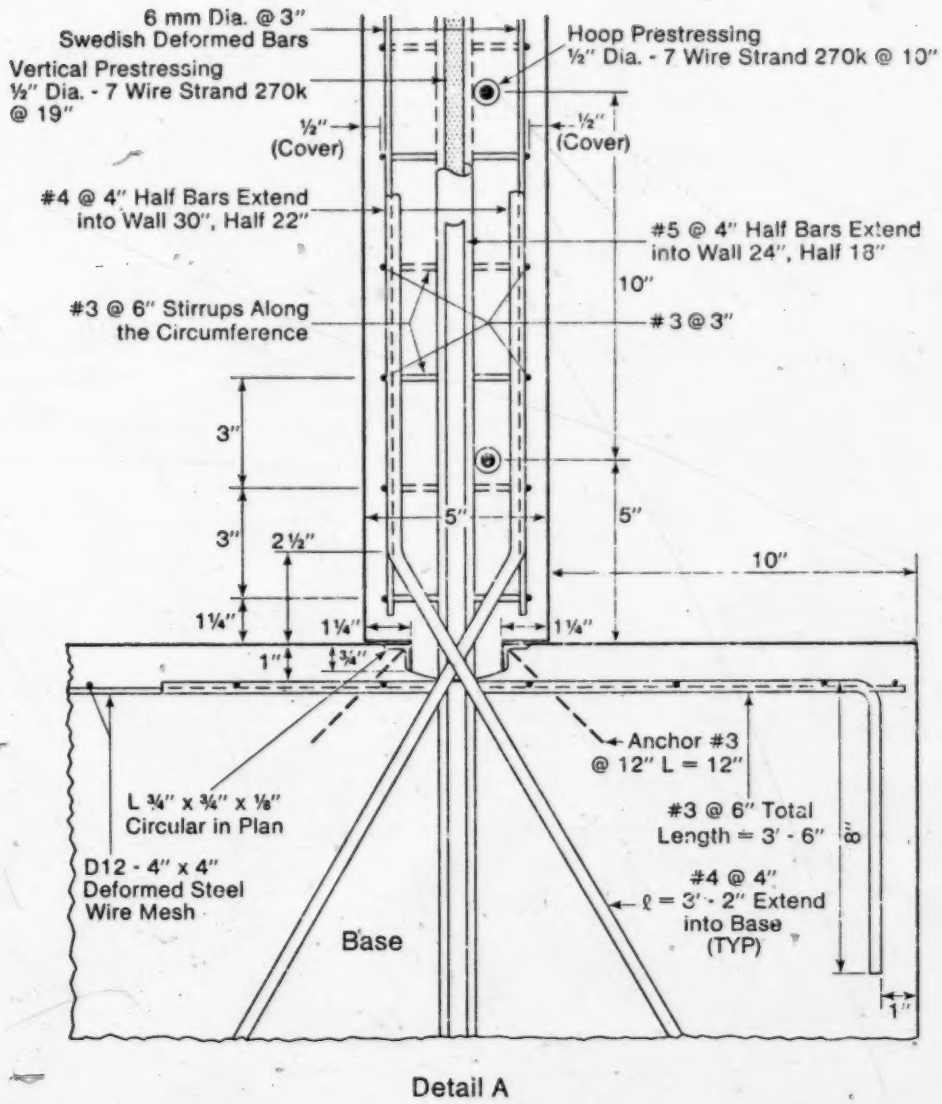

Detail A

Fig. 6.4 Detail of Cylinder Wall Base Connection of Test Structure

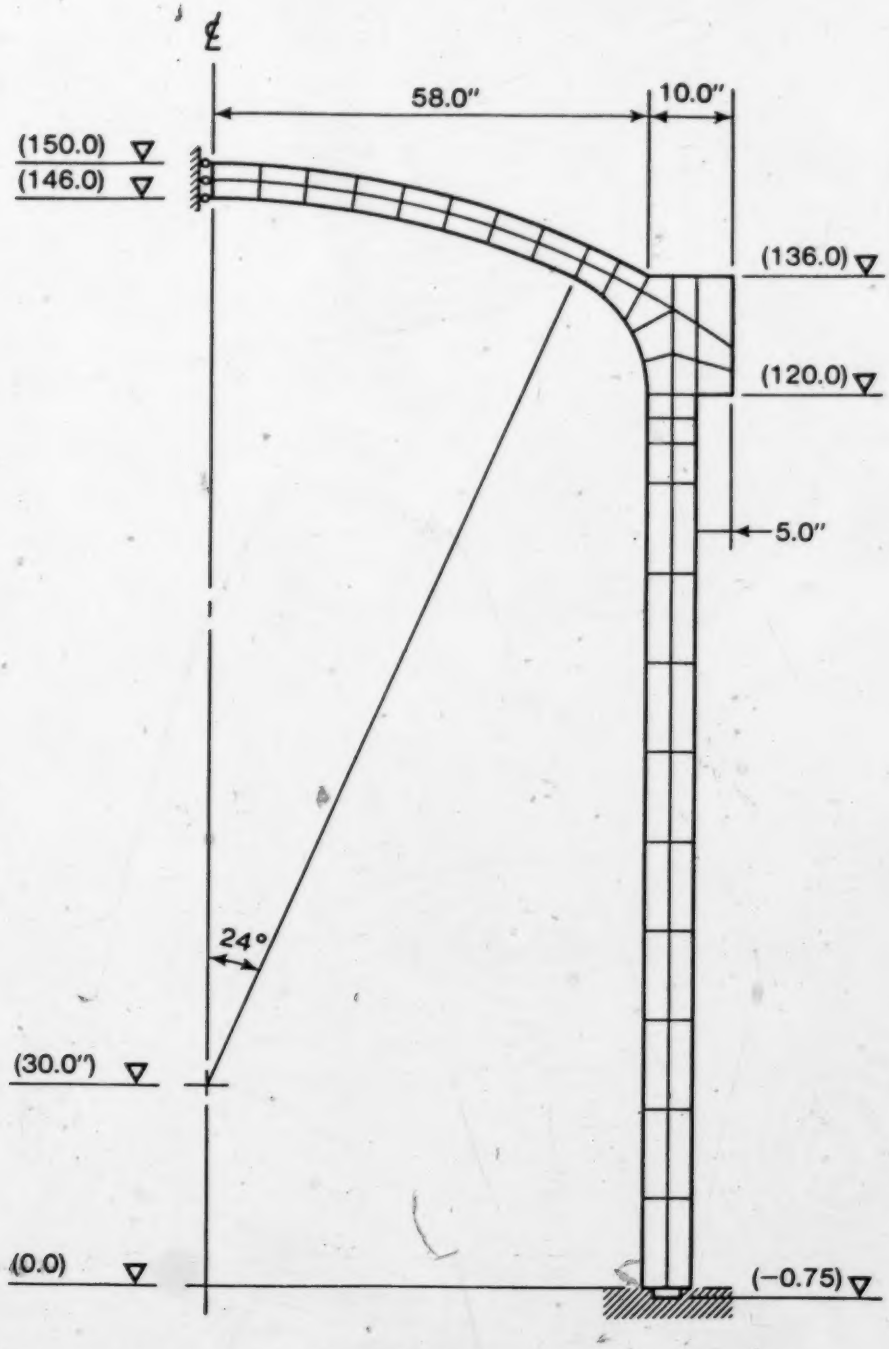

Fig. 6.5 Finite Element Mesh of Test Structure

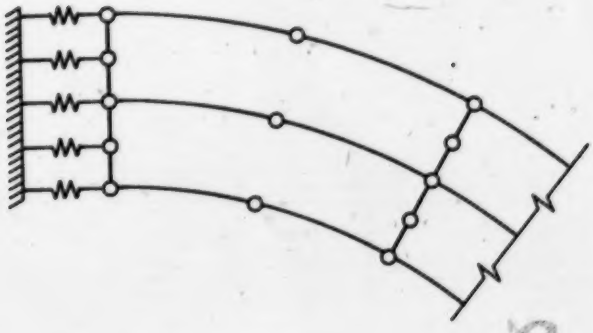

(a) Top of Dome

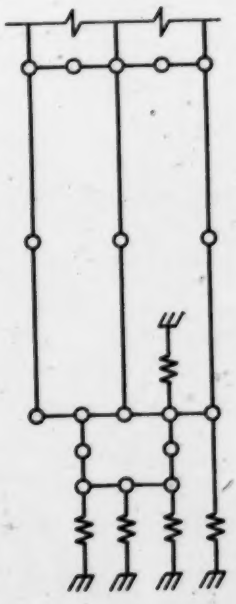

(b) Cylinder Base

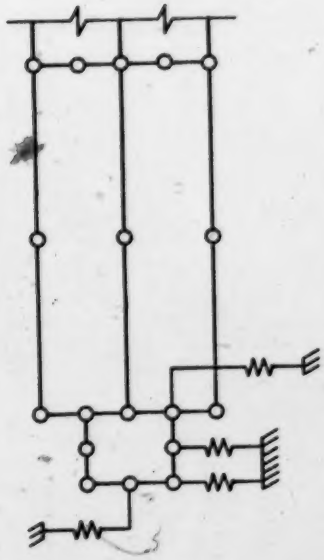

(c) Cylinder Base

Fig. 6.6 Boundary Condition Simulation for Finite Element Model of Test Structure

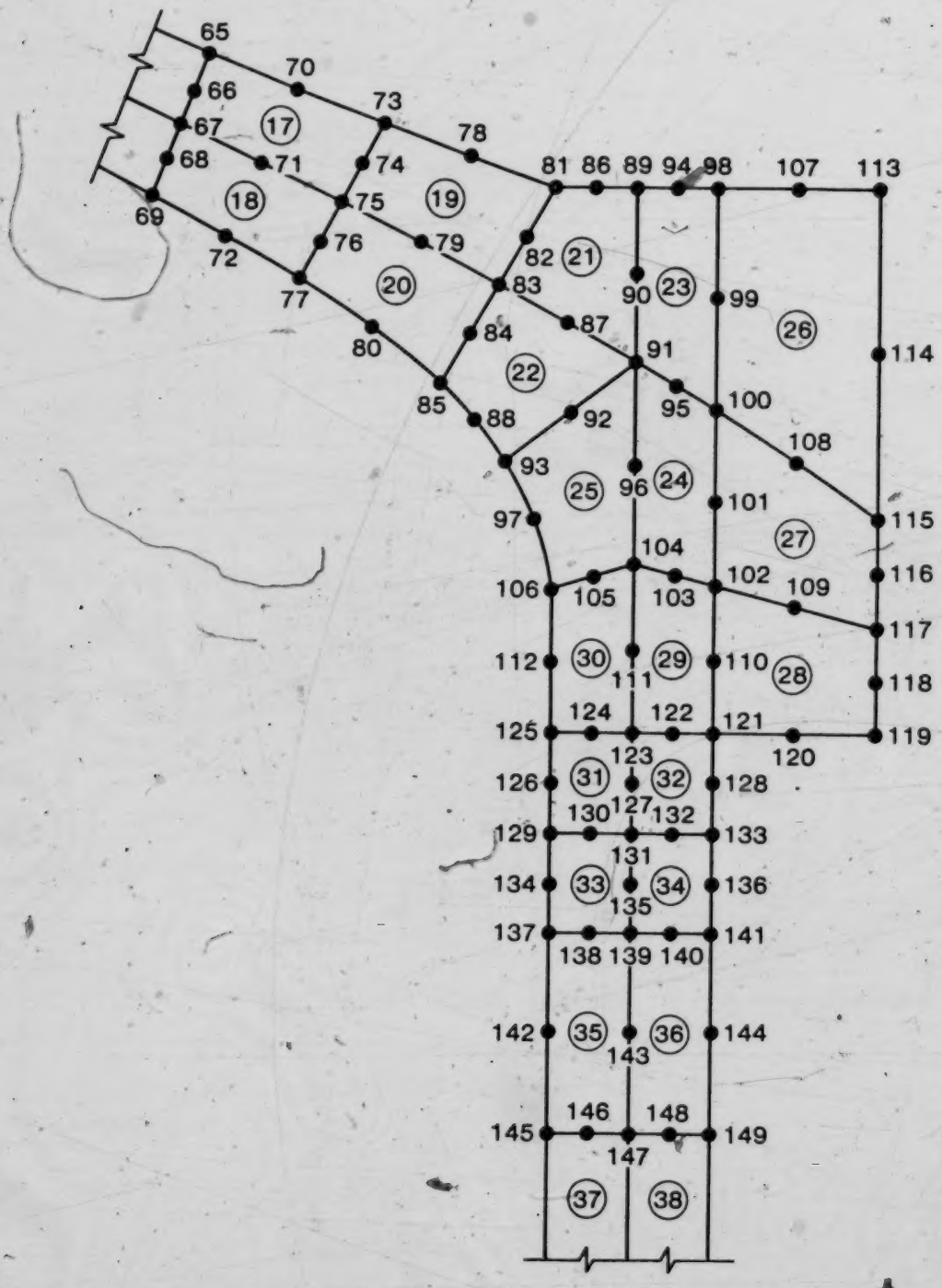

Fig. 6.7 Detail of Finite Element Model of Ring Beam Area

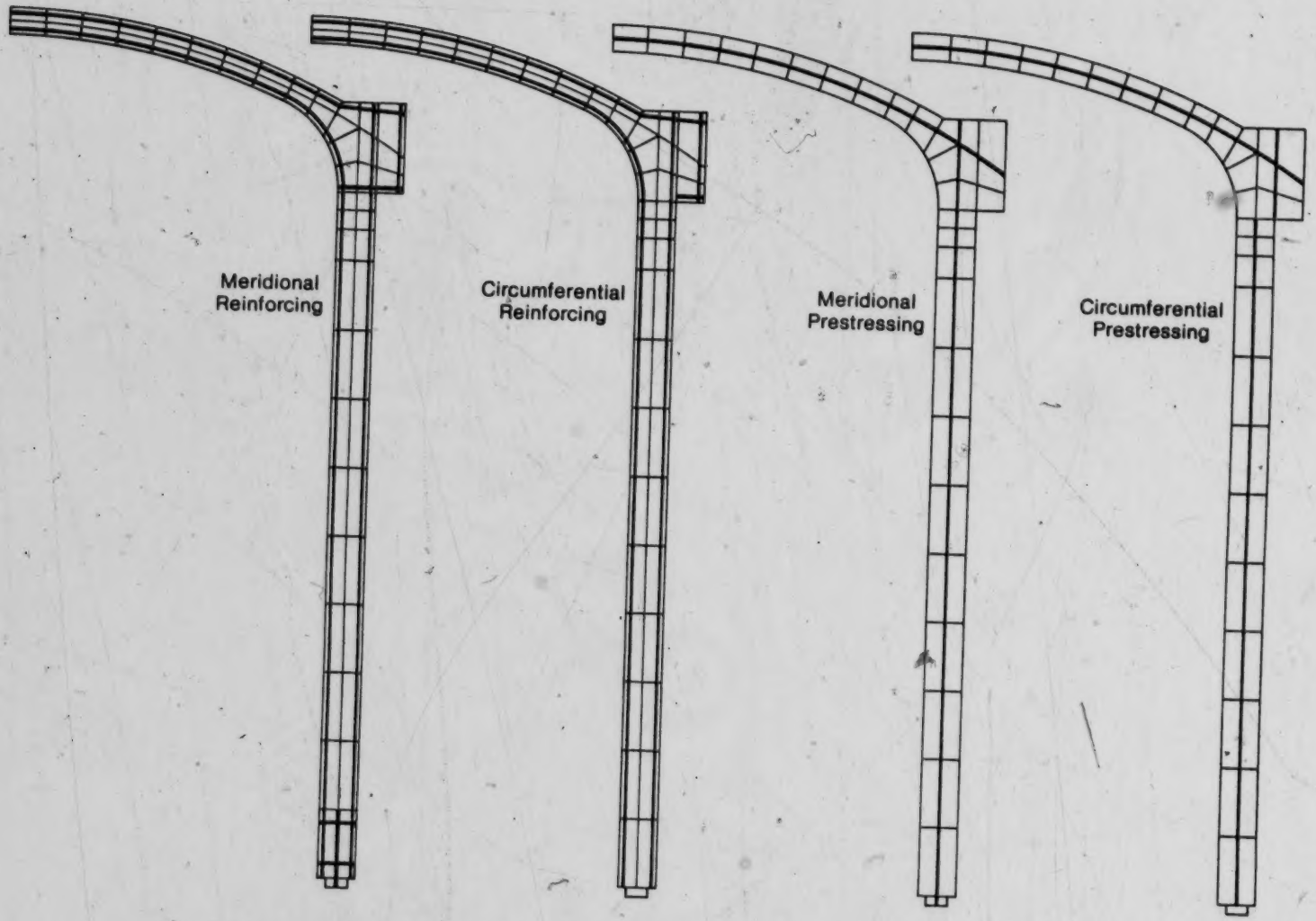

Fig. 6.8 Reinforcing and Prestressing Layers of Finite Element Model of Test Structure

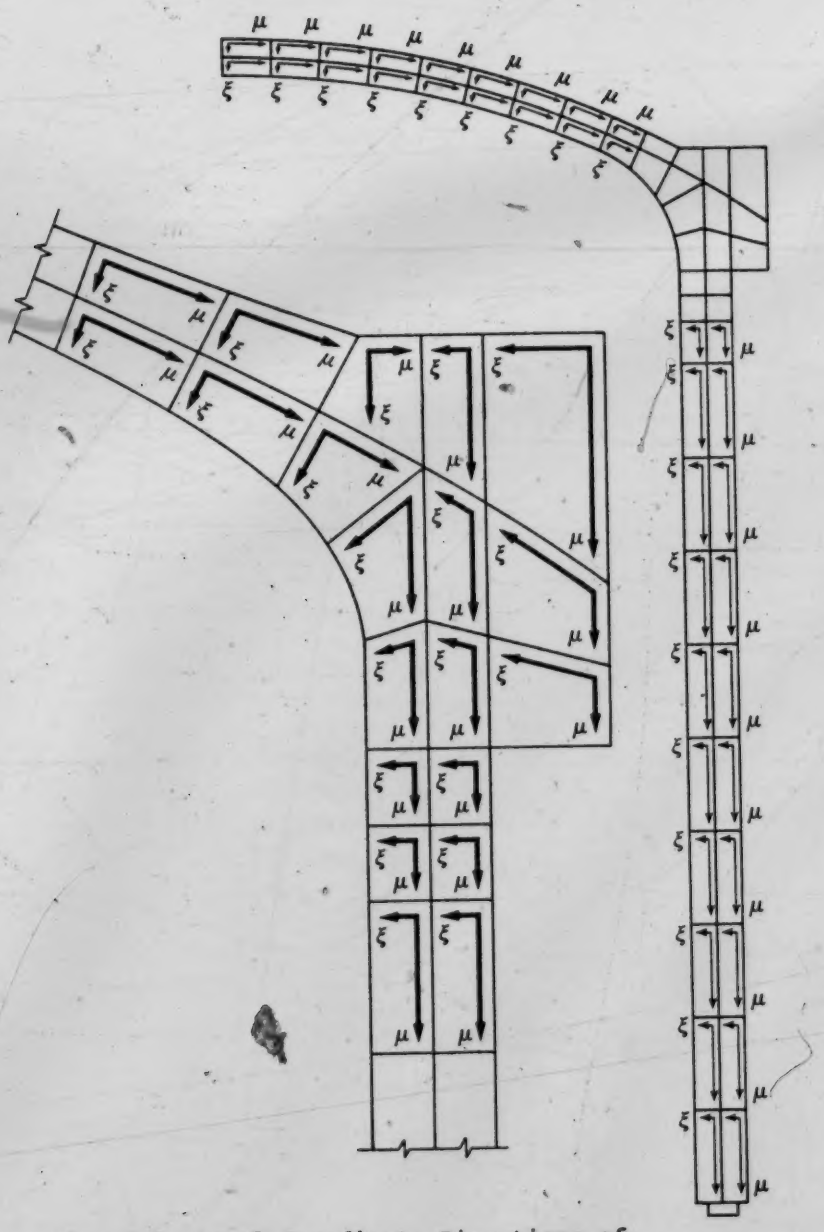

Fig. 6.9 Local Coordinate Directions of Finite Element Mesh

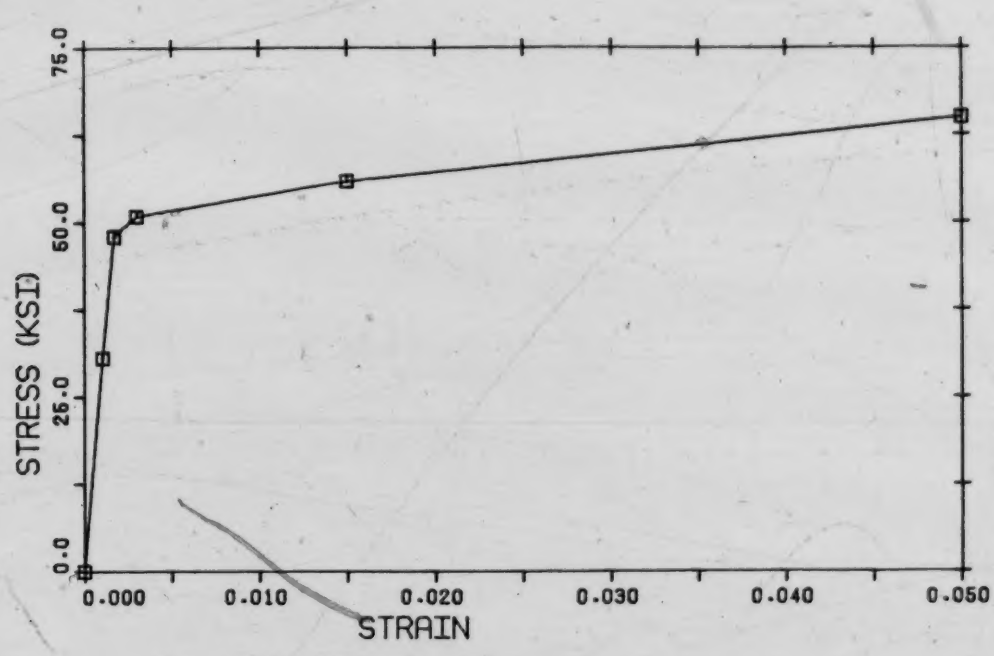

(a) #3 Bars

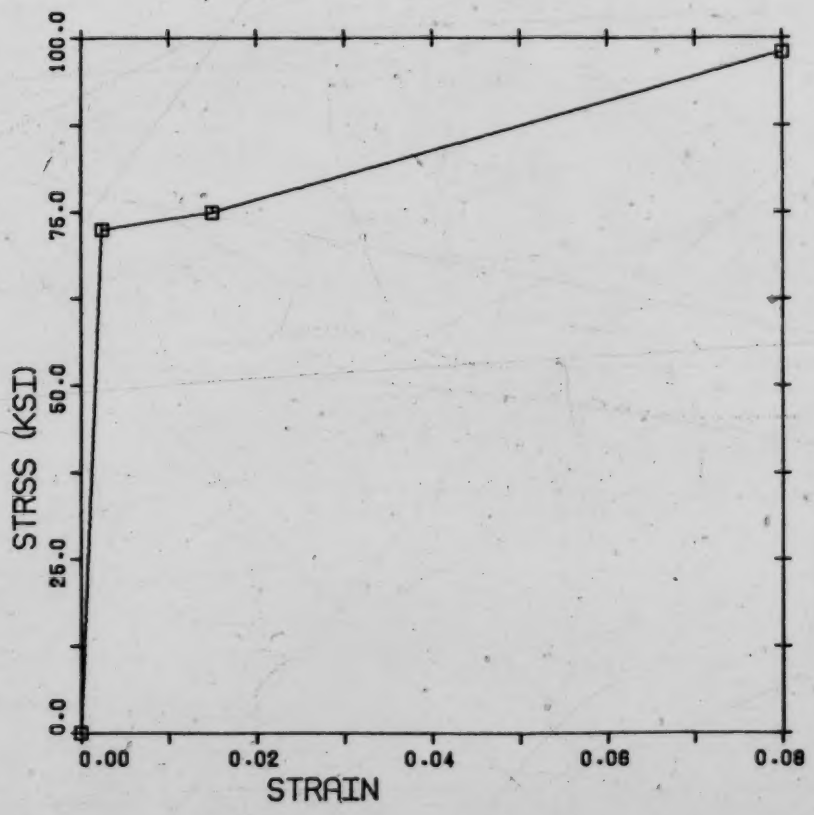

(b) 6 mm Bars

Fig. 6.10 Stress Strain Curves for Prestressing Bars

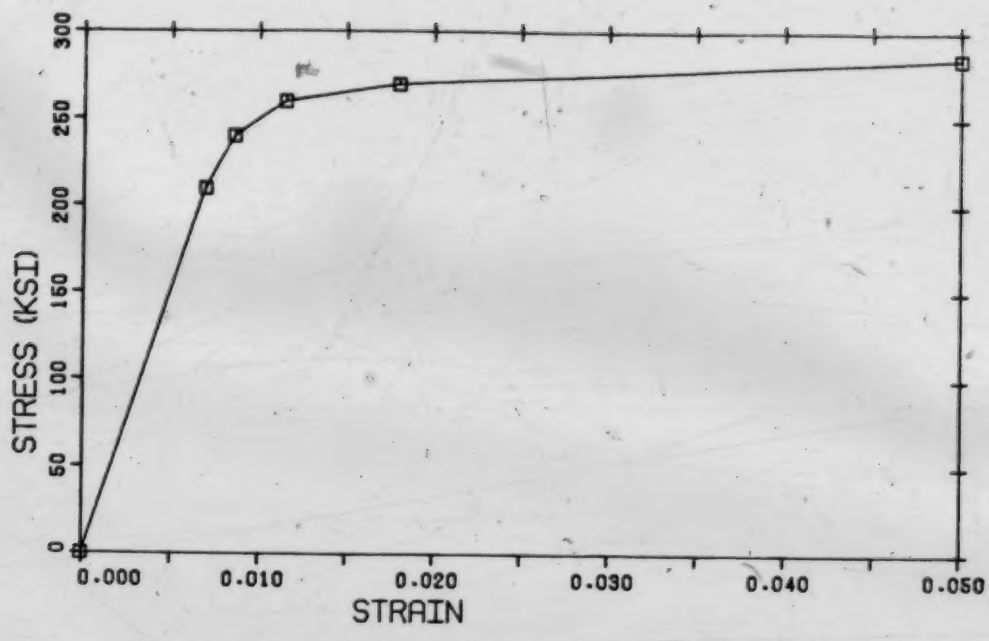

(a) 0.5" ϕ Strand

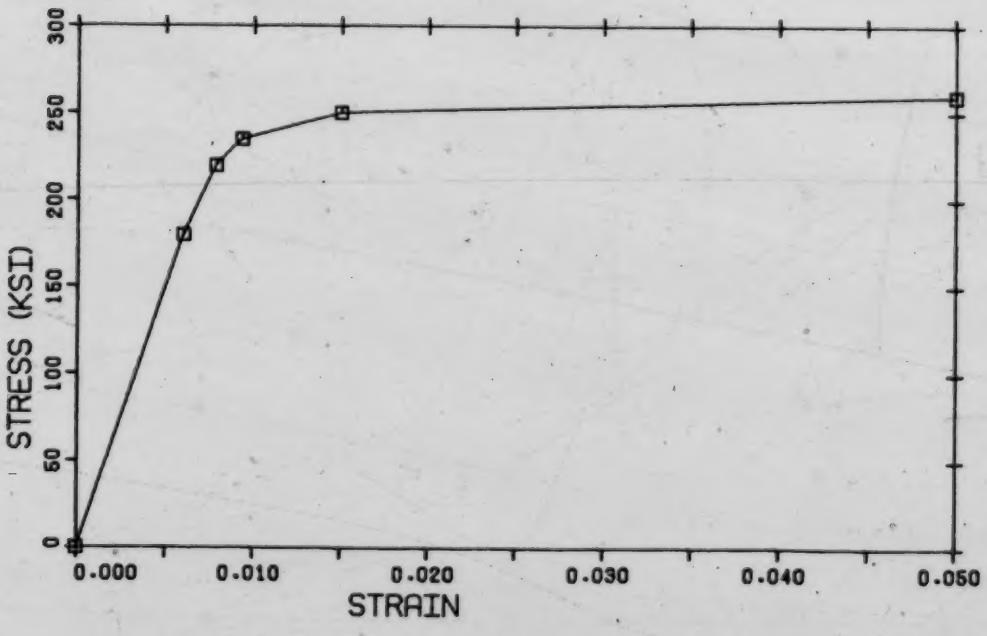

(b) 0.62" ϕ Strand

Fig. 6.11 Stress Strain Curves for Prestressing Tendons

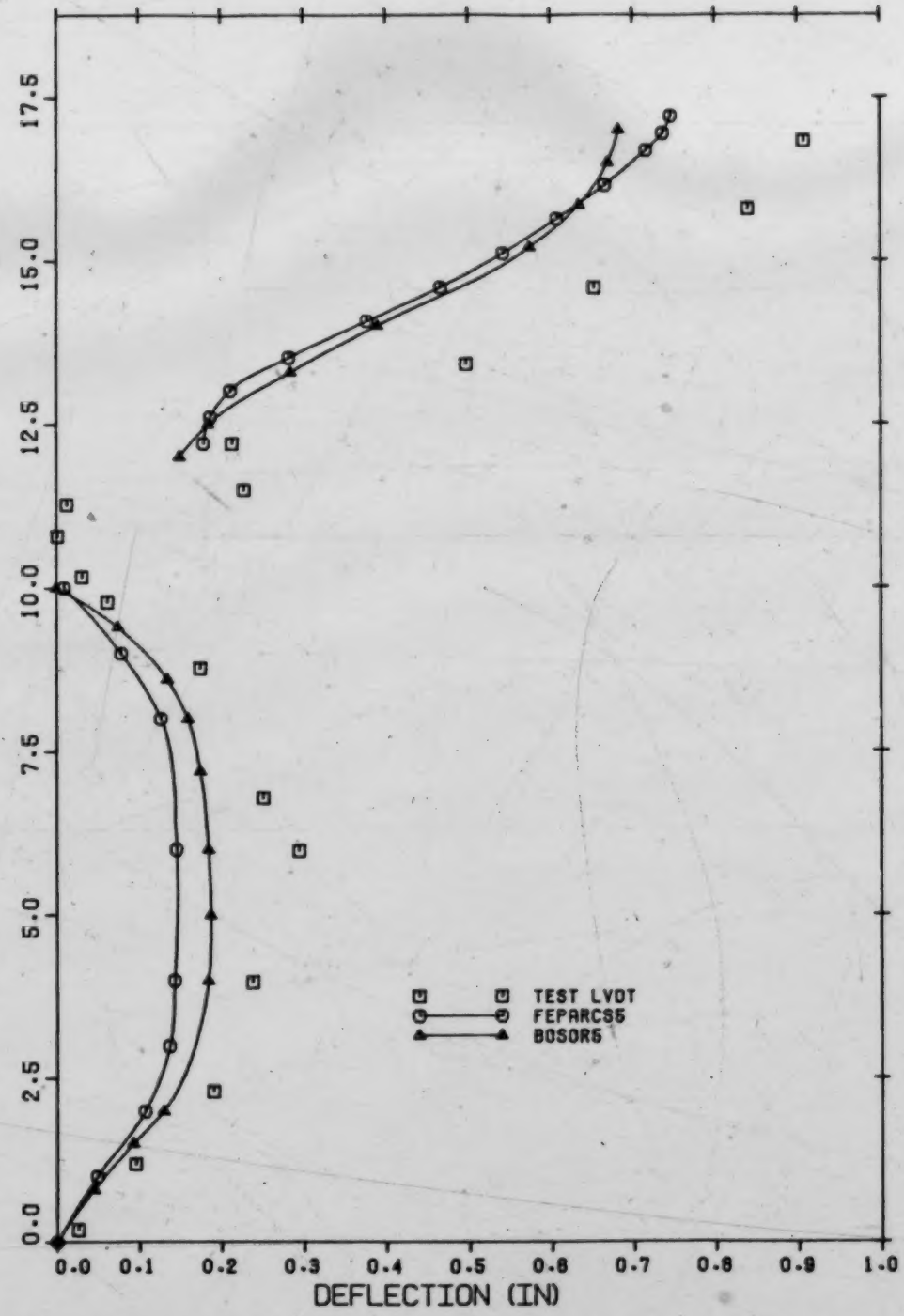

Fig. 6.12 Comparison of Deflection Profiles at 120.0 psi

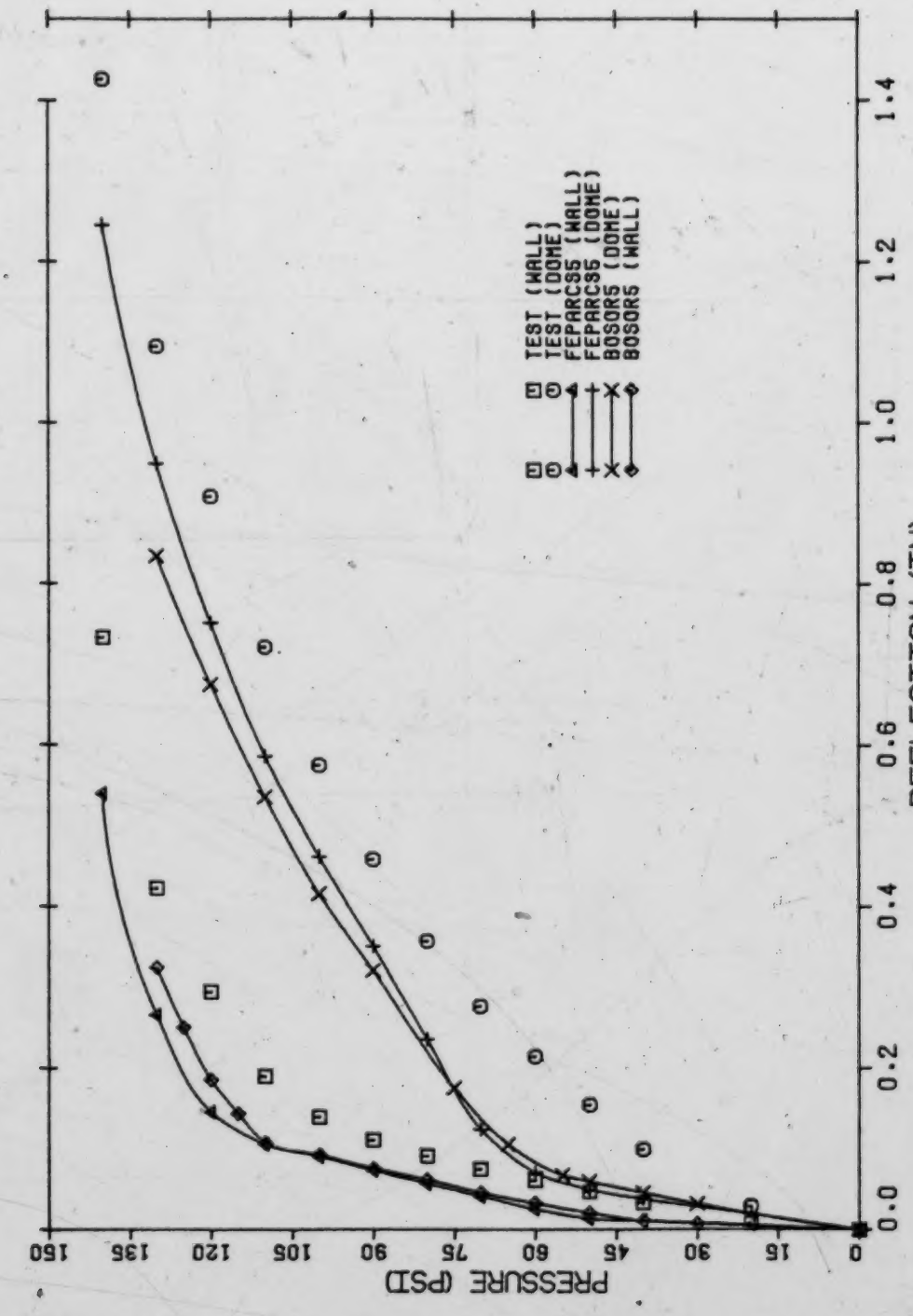

Fig. 6.13 Comparison of Internal Pressure versus Maximum Deflection of Wall and Dome

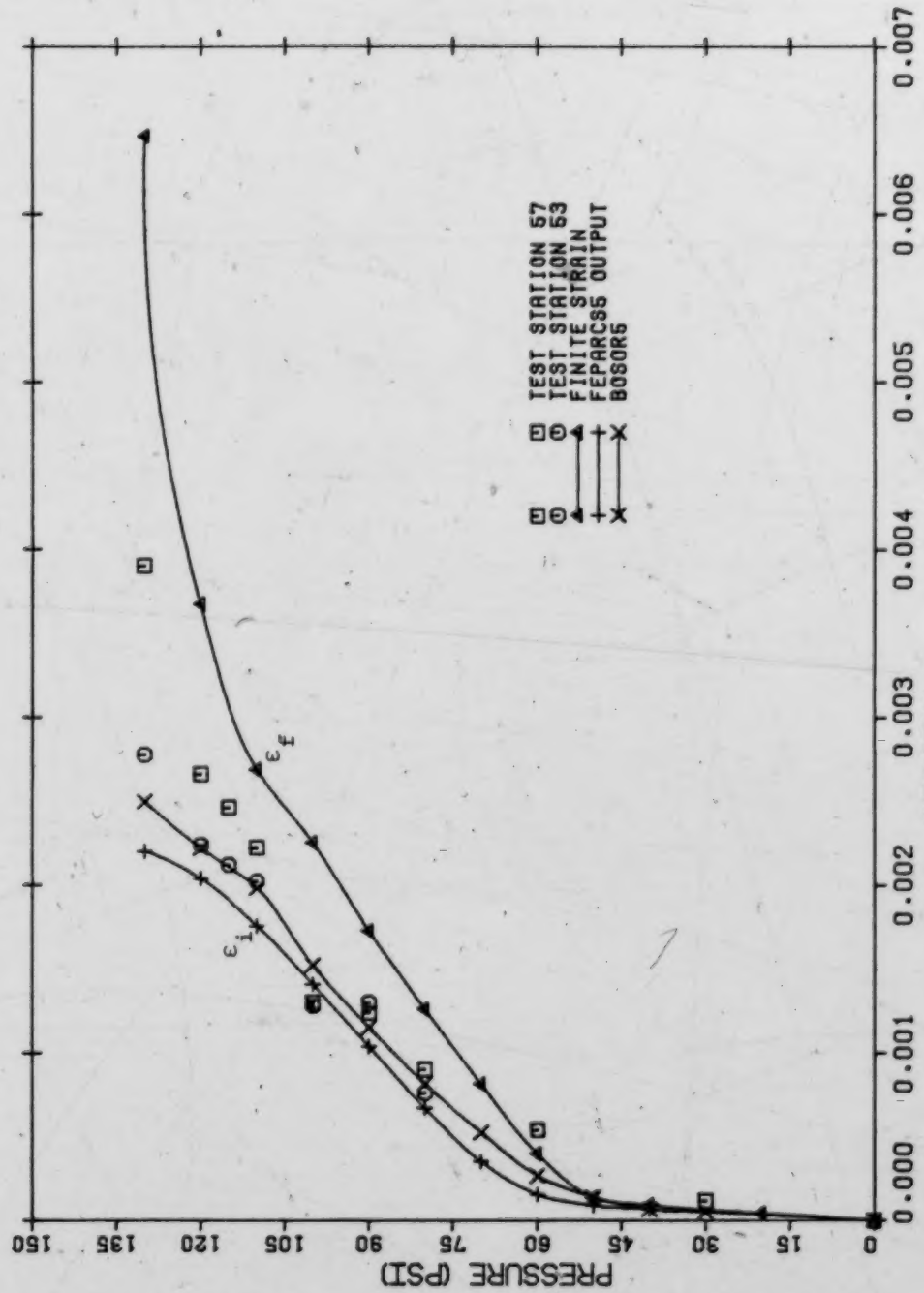

Fig. 6.14 Comparison of Meridional Strains in Wall at 28.0 inches above Base

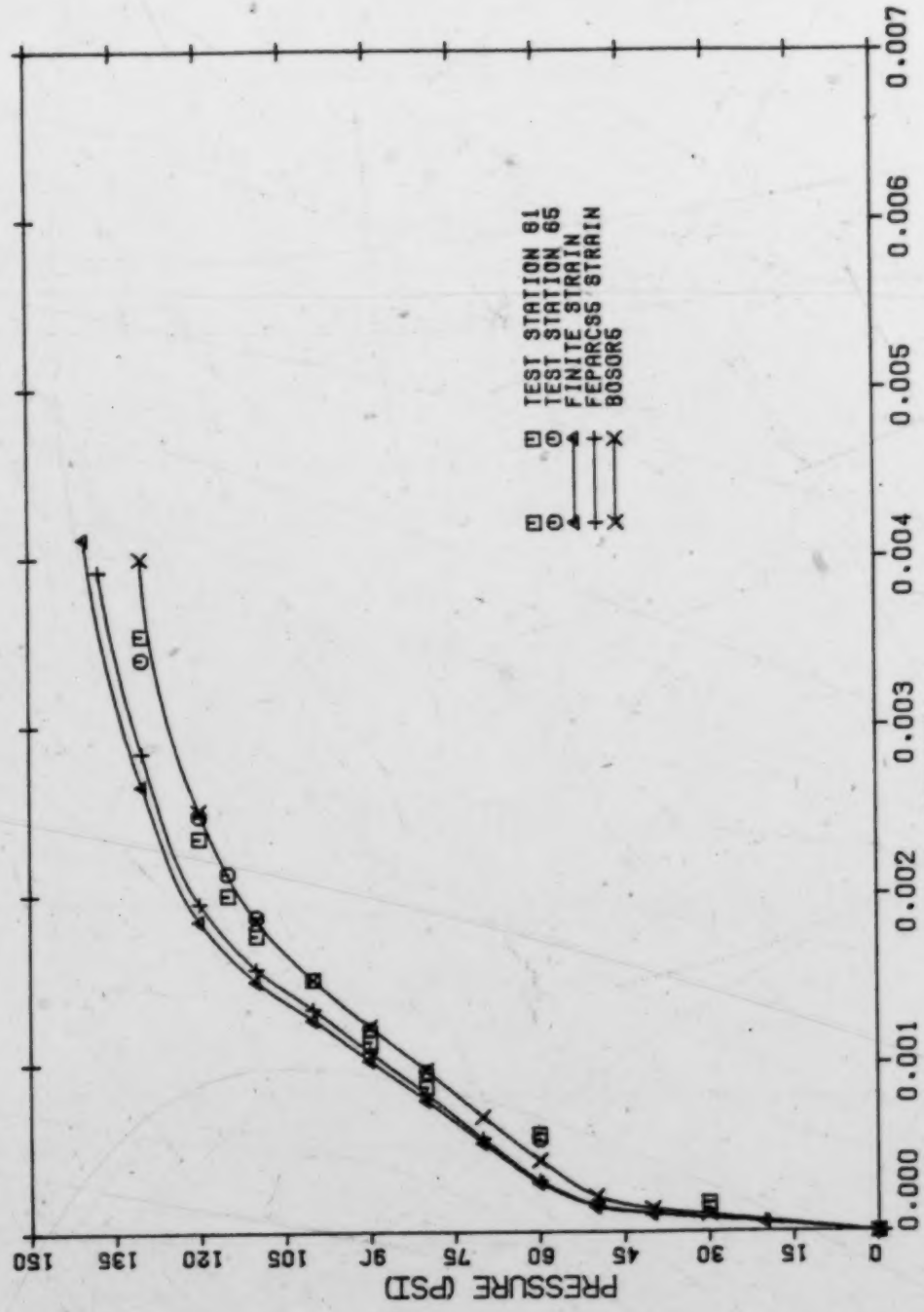

Fig. 6.15 Comparison of Circumferential Strains in Wall at 28.0 inches above Base

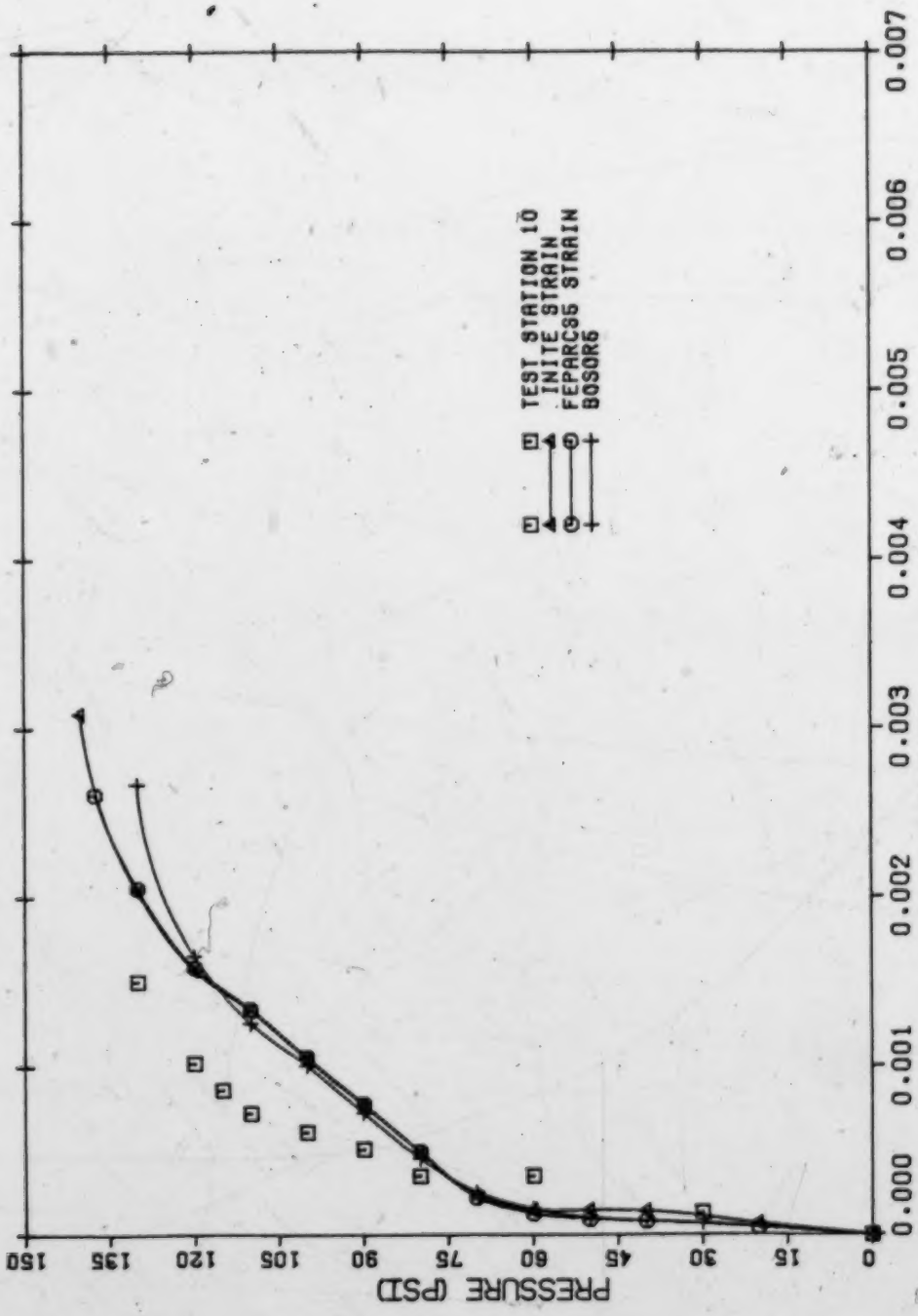

Fig. 6.16 Comparison of Meridional Strains in Wall at 65.0 inches above Base

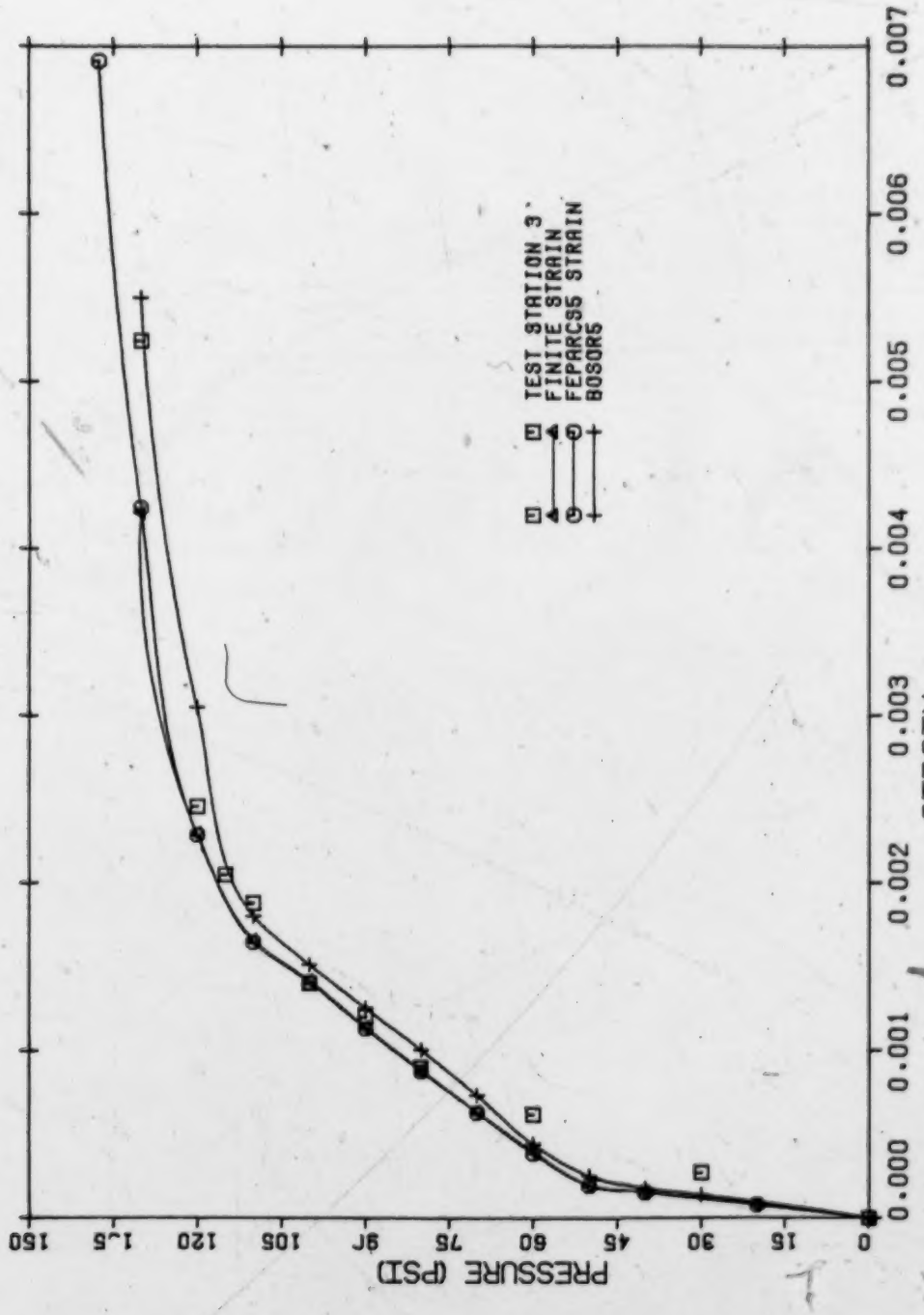

Fig. 6.17 Comparison of Circumferential Strains in Wall at 65.0 inches above Base

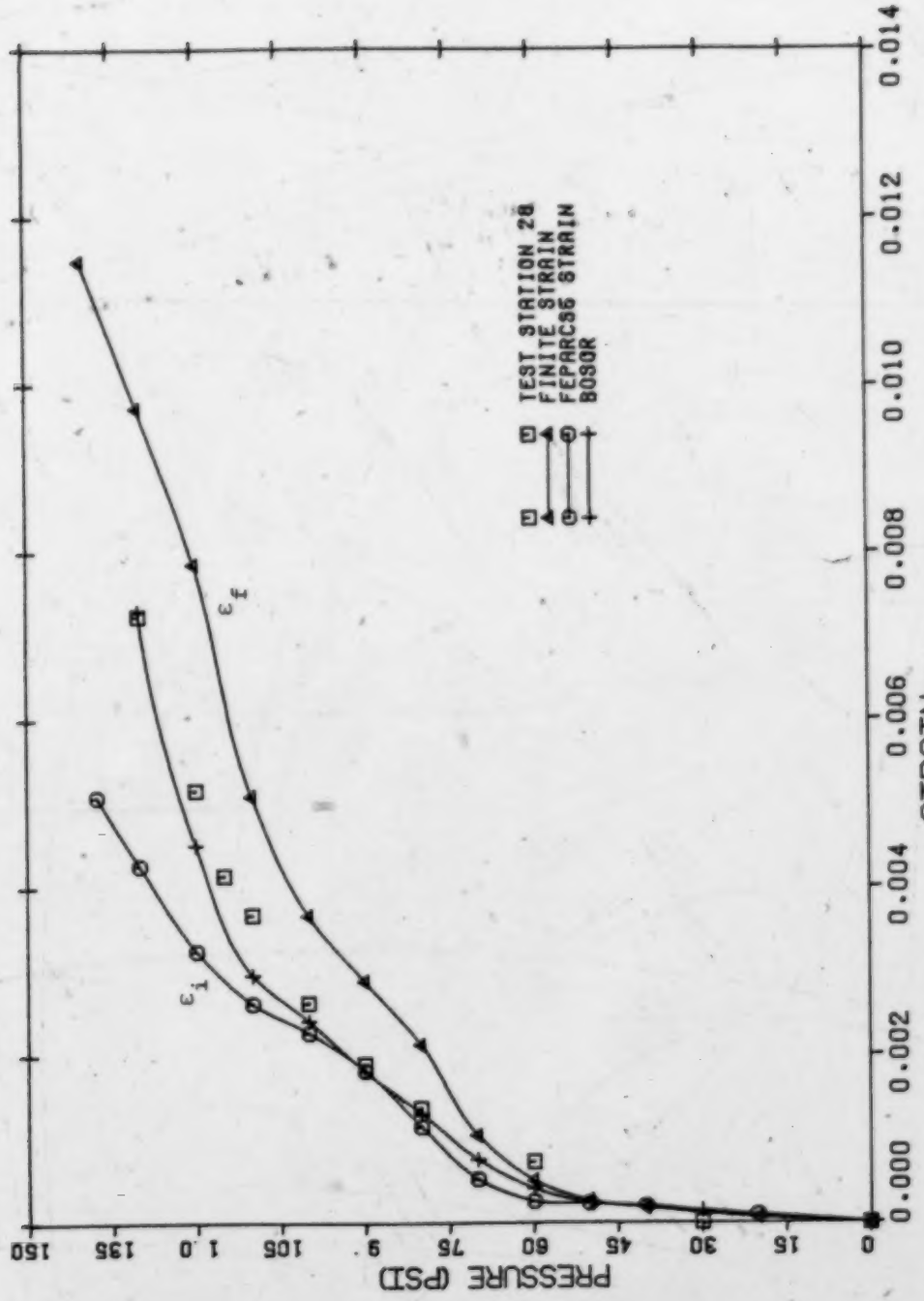

Fig. 6.18 Comparison of Meridional Strains Near Top of Dome

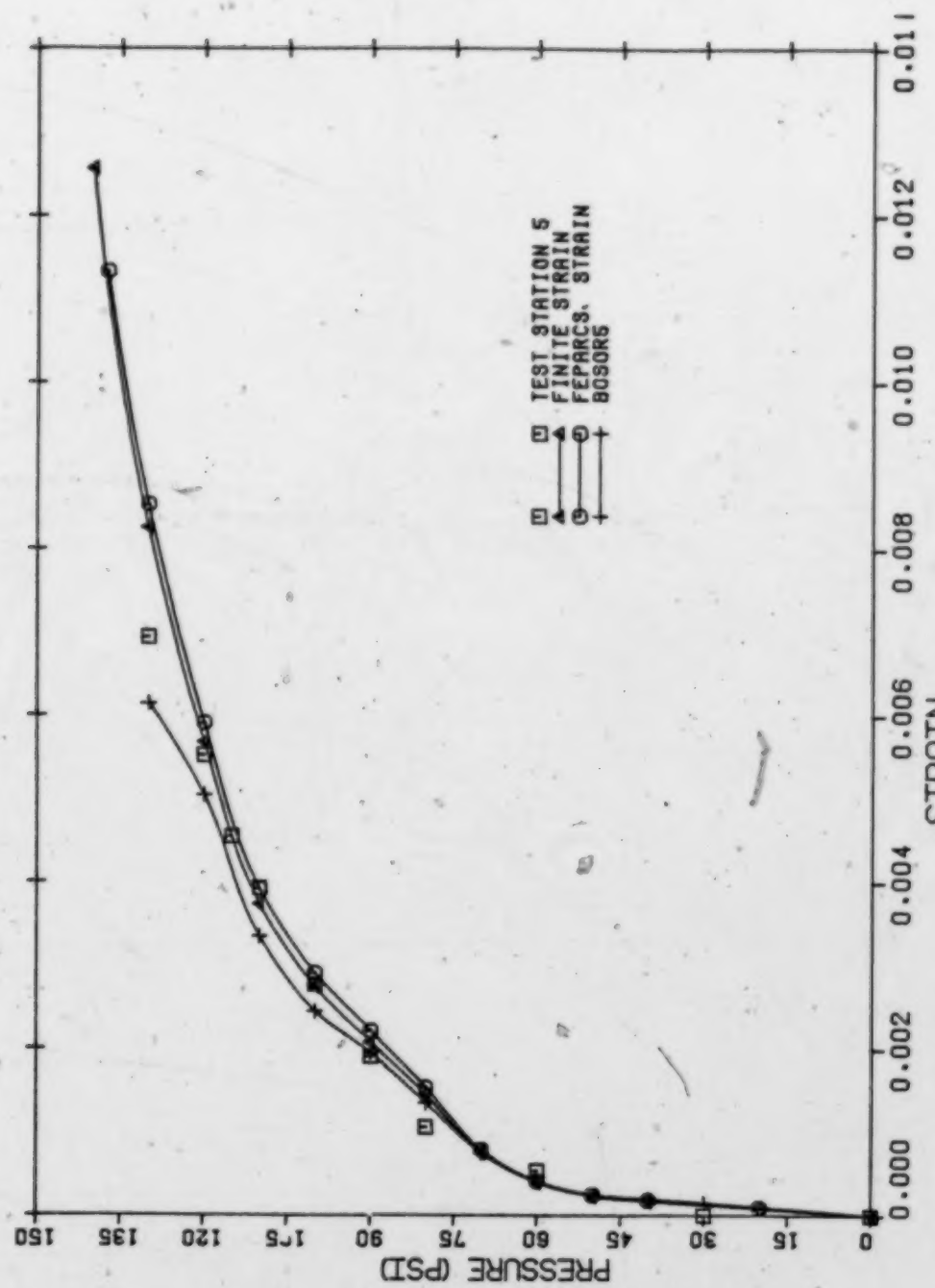

Fig. 6.19 Comparison of Circumferential Strains Near Top of Dome

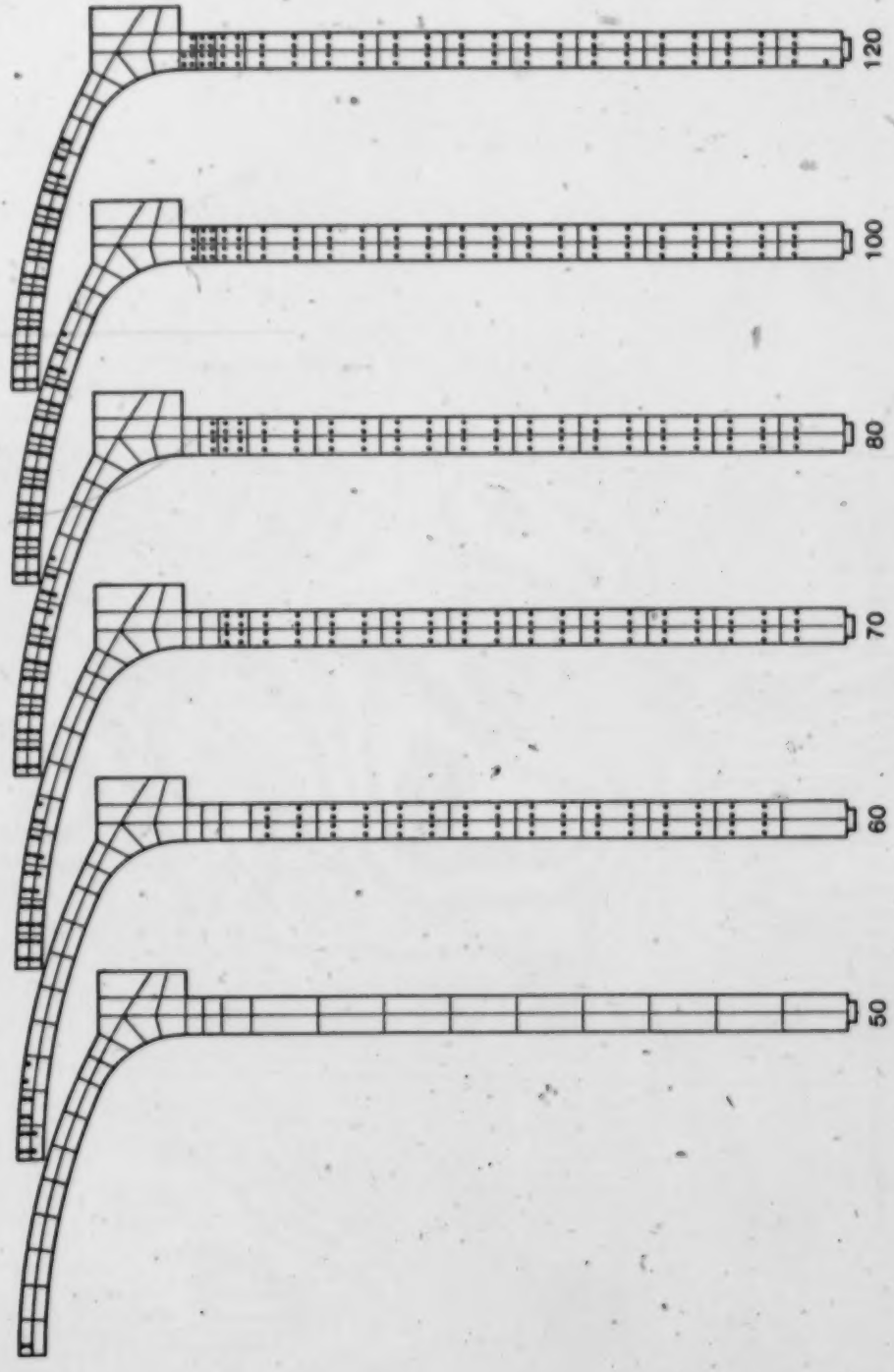

Fig. 6.20 Progress of Vertical Cracking

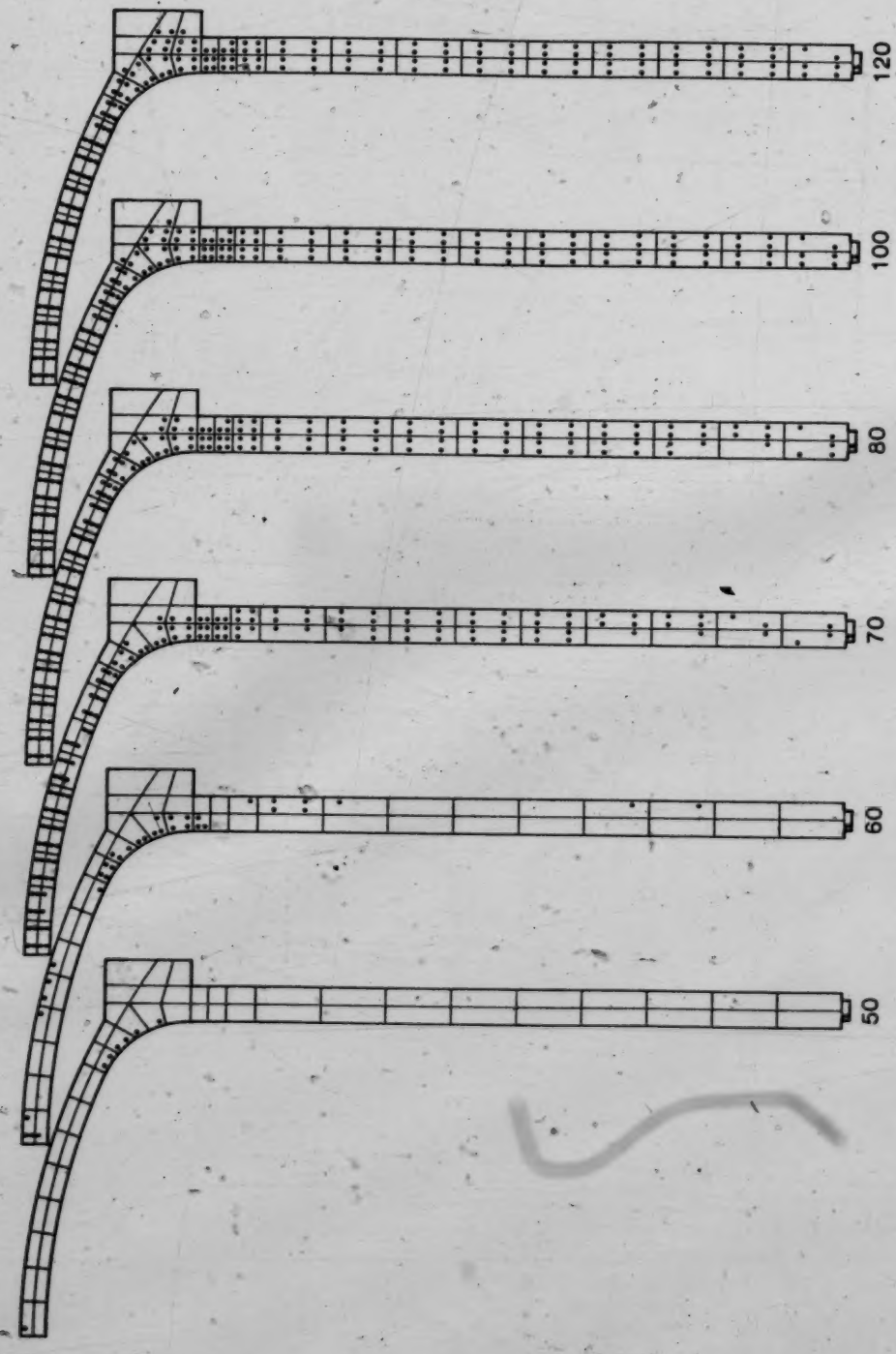

Fig. 6.21 Progress of Horizontal Cracking

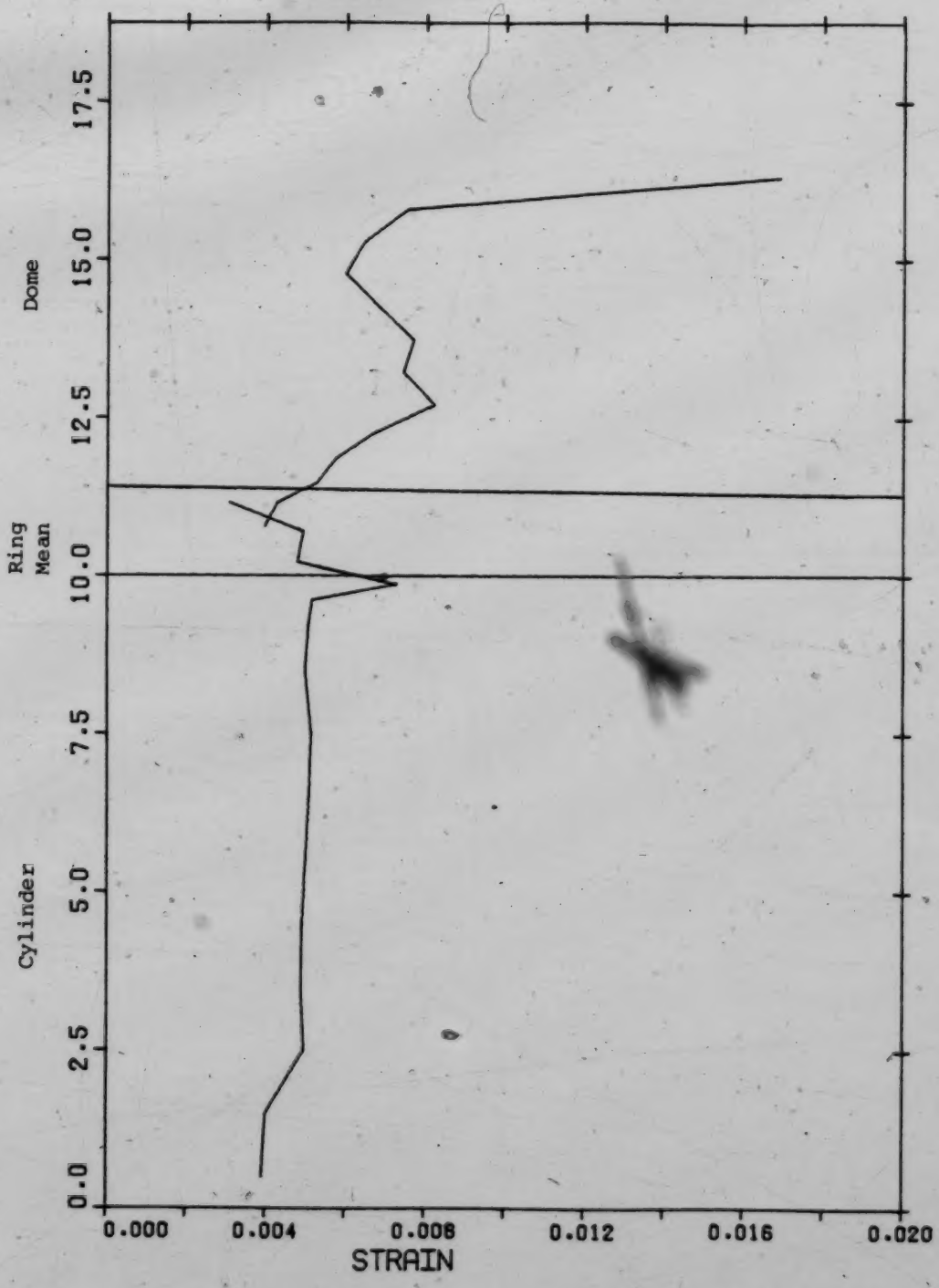

Fig. 6.22 Profile of Strain in Meridional Prestressing Tendons at 140.0 psi

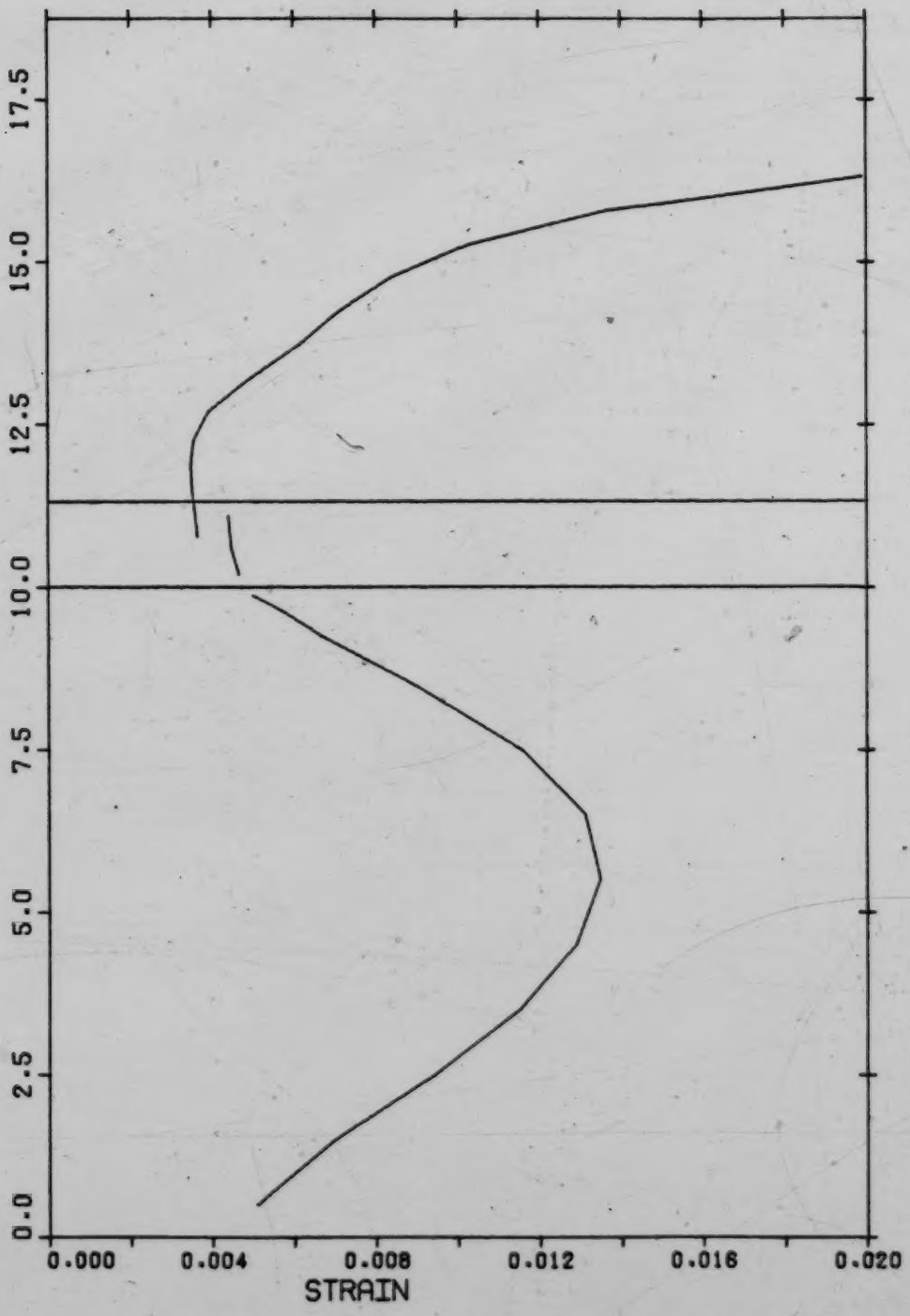

Fig. 6.23 Profile of Strain in Circumferential Prestressing Tendons at 140.0 psi

CHAPTER SEVEN

SUMMARY AND CONCLUSIONS

A nonlinear elastic (hypoelastic) constitutive relation has been proposed for analysis of plane and axisymmetric reinforced and/or prestressed concrete structures. This constitutive relation is based on the equivalent uniaxial strain concept which has been introduced by Darwin and Pecknold (1974, 1977a and 1977b). A new characterization of Poisson's ratio has been introduced and post failure conditions have been imposed on the failure surface such that the determination of the stress-equivalent uniaxial strain relation parameters may be more realistic.

Special isoparametric finite elements have been developed for representation of reinforcing bars and prestressing tendons in the meridional and circumferential directions. These elements together with the well known isoparametric axisymmetric serendipity finite element family (Zienkiewicz, 1971) have been incorporated in a finite element program (FEPARCS5) for nonlinear analysis of plane or axisymmetric reinforced and/or prestressed concrete structures. The proposed constitutive relation has been incorporated in program FEPARCS5 as well as a number of features such as a post-tensioning simulation procedure.

Program FEPARCS5 has been used to analyse two prestressed wall segments under biaxial tension (Chitnuyanondh, et al., 1979) with results comparing favorably with the test results and with BOSOR5 results. In analysing these segments the numerical instability of the

original constitutive relation (Elwi and Murray, 1979) has been eliminated by the addition of controls on the post failure behavior. Convergence has been good up to the yielding of the prestressing tendons. In these analyses the tangential stiffness method has been used as an iteration scheme with re-evaluation of the stiffness matrix every three iterations.

Finally, program FEPARCS5 has been used to analyse a finite element model of the test structure erected and tested under internal pressure at the I.F. Morrison Laboratory in 1978 by J.G. MacGregor, S. Simmonds, D.W. Murray and S. Rizkalla. The results of the FEPARCS5 analysis have been compared with the test results and with the results of an elastic plastic analysis of BOSOR5 (Murray, et al., 1978). The comparisons have been based on progress reports since the final reports on the test and the BOSOR5 analysis commissioned by the Atomic Energy Control Board of Canada have not been published at the time of writing.

The constitutive relationship developed herein appears to be adequate for the nonlinear analysis of prestressed concrete structures of the type under consideration. On a material level the relationship has shown reasonable agreement with the two-dimensional test results of Kupfer, Hilsdorf, and Rüsch (1969), as indicated in Figs. 2.9 to 2.11, and with the three-dimensional test results of Shickert and Winkler (1977), as indicated in Figs. 2.13 to 2.15. When combined with the strain softening characteristics in tension, shown in Fig. 2.2, it allows a reasonable simulation of the nonlinear response of cracked concrete under biaxial stress conditions, as indicated by the comparisons in Figs. 5.7 to 5.9.

However, a number of problems with the constitutive model require further investigation. More (numerical) testing is required to see if the softening branch is significantly affected by the reinforcing ratio. The tendency of a multiaxial stress state to degenerate to a uniaxial state under iteration, which has been curbed herein by adopting the failure mode constraints described in Sect. 2.3.8 require further study. The model should also be compared against material tests in which the principal stress directions do not remain constant.

The FEPARCS5 program, which has been developed in association with this work, has been shown to be capable of reasonably simulating the nonlinear behavior of a prestressed concrete secondary containment structure and hence to be suitable for the analysis of thin-walled structures of this type. Prestressing effects and nonlinear (time-independent) response are treated without major problems. The primary difficulties are the determination of convergence criteria and the deterioration of the convergence characteristics when a substantial portion of the concrete in the structure has reached the strain-softening range. The latter difficulty has been dealt with by using the tangent stiffness matrix at 20 psi as the matrix for iteration of unbalanced forces at higher pressures. However, the entire area of convergence criteria and solution procedures for structures containing strain-softening materials is one which appears to require further study.

REFERENCES

1. Almroth, B.O., Stren, P. and Brogan, F.A., 'Future Trends in Nonlinear Structural Analysis', Computers and structures, Vol. 10, 1979, pp. 368-374.

2. Argyris, J.H., Faust, G., Szimat, J., Warnke, E.P., and Willam, K.J., 'Recent Developments in the Finite Element Analysis of Prestressed Concrete Reactor Vessels', Nuclear Engineering and Design, 28, 1974, pp. 42-75.

3. Argyris, J.H., Krempl, E., Willam, K.J., and Menton, D., 'Constitutive Models and Finite Element Solution of Inelastic Behavior', U.S.-German Symposium on "Formulations and Computational Algorithms in Finite Element Analysis", M.I.T., Boston, Mass., August 9-13, 1976.

4. Bashur, F.K., and Darwin, D., 'Nonlinear Model for Reinforced Concrete Slabs', CKINC Report-SL-76-03, The University of Kansas Center for Research, University of Kansas, Lawrence, Kansas, December, 1976.

5. Bathe, K.J. and Wilson, E.L., 'Numerical Methods in Finite Element Analysis', Prentice-Hall Inc., Engelwood Cliffs, N.J., 1976.

6. Bazant, Z.P., and Bhat, P., 'Endochronic Theory of Inelasticity and Failure of Concrete', Journal of the Engineering Mechanics Division, ASCE, Vol. 102, No. EM4, 1976, pp. 701-722.

7. Bazant, Z.P., 'Some Questions of Material Inelasticity and Failure in the Design of Concrete Structures for Nuclear Reactors', The 3rd International Conference on Structural Mechanics in Reactor Technology, London, U.K., September 1975, Transactions paper H1/1.

8. Bushnell, D., 'Large Deflection Elastic Plastic Creep Analysis of Axisymmetric Shells', ASME, J. AMD-Vol. 6, November, 1973, pp. 103-138.

9. Cedolin, L. Crutzen, Y.E.J. and Poli, S.D., 'Triaxial Stress Strain Relationship for Concrete', Journal of the Engineering Mechanics Division, ASCE, Vol. 103, No. EM3, June 1977, pp. 423-439.

10. Cedolin, L., Crutzen, Y.R.J. and Poli, S.D., 'Stress Strain Relationship and Ultimate Strength of Concrete under Triaxial Loading Conditions', Construzioni in Cemento Armato, Research Center for Reinforced and Prestressed Concrete Structures, Vol. 14, Politechnico di Milano, 1976.

11. Chen, A.G.T., and Chen, W.F., 'Constitutive Relations for Concrete', Journal of the Engineering Mechanics Division, ASCE, Vol. 101, No. EM4, August 1975, pp. 465-481.

12. Chitnuyanondh, L., Rizkalla, S., Murray, D.W., and MacGregor, J.G., 'An Effective Uniaxial Tensile Stress Strain Relationship for Prestressed Concrete', Structural Engineering Report No. 74, Department of Civil Engineering, University of Alberta, Edmonton, Alberta, February, 1979.

13. Coon, M.D. and Evans, R.J., 'Incremental Constitutive Laws and their Associated Failure Criteria with Application to Plain Concrete', International Journal of Solids and Structures, Vol. 8, 1972, pp. 1169-1183.

14. Darwin, D. and Pecknold, D.A., 'Analysis of Cyclic Loading for Plane R/C Structures', Computers and Structures, Vol. 7, 1977, pp. 137-147.

15. Darwin, D. and Pecknold, D.A., 'Nonlinear Biaxial Stress Strain Law for Concrete', Journal of the Engineering Mechanics Division, ASCE, Vol. 103, No. EM2, April, 1977, pp. 229-241.

16. Darwin, D. and Pecknold, D.A., 'Inelastic Model for Cyclic Biaxial Loading of Reinforced Concrete', Civil Engineering Studies, Structural Research Series No. 409, University of Illinois, Urbana, Champaign, Urbana, Illinois, July, 1974.

17. Elwi, A.A., and Murray, D.W., 'A 3D Hypoelastic Concrete Constitutive Relationship', Journal of the Engineering Mechanics Division, ASCE, Vol. 105, No. EM4, August 1979, pp. 623-642.

18. Elwi, A.A., and Murray, D.W., 'Substructure Analysis of Plane Frames', Structural Engineering Report No. 64, Department of Civil Engineering, University of Alberta, Edmonton, Alberta, June, 1977.

19. Epstein, M. and Murray, D.W., "A Biaxial Law for Concrete Incorporated in the BOSOR5 Code', Computers and Structures, Vol. 9, No. 1, July 1978, pp. 57-63.

20. Epstein, M. and Murray, D.W., 'An Elastic Stress Analysis of a Gentilly Type Containment Structure: vol. 1', Structural Engineering Report No. 55, Department of Civil Engineering, University of Alberta, Edmonton, Alberta, April, 1976.

21. Evans, R.H., and Marathe, M.S., 'Microcracking and Stress Strain Curves for Concrete in Tension', Materials and Structures, vol. 1, No. 1, January-February, 1968, pp. 61-64.

22. Fellipa, C.A., 'Procedures for Computer Analysis of Large Nonlinear Structural System', Large Engineering Systems, ed. A. Wexler, Pergamon Press, London, U.K., 1976, pp. 60-101.

23. Fellipa, C.A., 'Finite Element Analysis of Three Dimensional Cable Structures', Computational Methods in Nonlinear Mechanics, The Texas Institute for Computational Mechanics, 1974, pp. 311, 324.

24. Geistefeldt, H., 'Material Law for Concrete under Multiaxial Stresses', the 4th International Conference on Structural Mechanics in Reactor Technology, San Francisco, California, August 1977, paper H5/1.

25. Geistefeldt, H., 'Constitutive Equations for Cracked Reinforced Concrete Based on a Refined Model', The 4th International Conference on Structural Mechanics in Reactor Technology, San Francisco, California, August 1977, Transactions paper H5/2.

26. Hsu, T.T.C., Slate, F.O., Sturman, G.H. and Winter, G., 'Micro-cracking of Plain Concrete', Journal of the American Concrete Institute, Proceedings Vol. 60, No. 14, February, 1963, pp. 209.

27. Kotsovos, M.D. and Newman, J.B., 'Behavior of Concrete Under Multiaxial Stresses', Journal of the American Concrete Institute, Proceedings Vol. 74, No. 9, September 1977, pp. 443-446.

28. Kupfer, H.B. and Gerstle, K.H., 'Behavior of Concrete Under Biaxial Stresses', Journal of the Engineering Mechanics Division, ASCE, Vol. 99, No. EM4, August 1973, pp. 853-866.

29. Kupfer, H.B., Hilsdorf, H.K. and Rüsch, H., 'Behavior of Concrete Under Biaxial Stresses', Journal of the American Concrete Institute, Proceedings Vol. 66, No. 8, August 1969, pp. 656-666.

30. Link, J., 'Numerical Analysis Oriented Biaxial Stress Strain Relation and Failure Criterion of Plain Concrete', The 4th International Conference on Structural Mechanics in Reactor Technology, San Francisco, California, August 1977, Transactions paper H1/2.

31. Link, J., 'Eine Formulierung des Zweinxialen Verformungs und Bruchverhaltens von Beton und deren Anvendung auf die Wirklichkeitsnahe Berechnung von Stahlbeton Platten', Deutscher Auschuss für Stahlbeton, Heft 270, Berlin, W.G., 1976.

32. Liu, T.C.F., Nilson, A.H., and Slate, F.O., 'Biaxial Stress Strain Relation for Concrete', Journal of the Structural Division, ASCE, Vol. 100, No. ST5, May, 1974, pp. 901-916.

33. Mroz, Z., 'Mathematical Models of Inelastic Concrete Behavior', Inelasticity and Nonlinearity in Structural Concrete, University of Waterloo Press, 1972.

34. Murray, D.W., 'Octahedral Based Stiffness Matrices', Journal of the Engineering Mechanics Division, ASCE, Vol. 105, No. EH4, August, 1979, pp. 501-514.

35. Murray, D.W., Chitnuyanondh, L., Wong, C. and Rijub-Agha, K., 'Inelastic Analysis of Prestressed Concrete Secondary Containments', Structural Engineering Report No. 67, Department of Civil Engineering, University of Alberta, Edmonton, Alberta, July, 1978.

36. Ottosen, N.S., 'Constitutive Model for Short Time Loading of Concrete', Journal of the Engineering Mechanics Division, ASCE, Vol. 105, No. EM1, February, 1979, pp. 127-141.

37. Ottosen, N.S. and Andersen, S.I., 'Structural Failure of Thick Walled Concrete Elements', The 4th International Conference on Structural Mechanics in Reactor Technology, San Francisco, California, August, 1977, Transactions paper H4/3.

38. Ottosen, N.S., and Andersen, S.I., 'Theoretical and Experimental Studies for Optimization of PCRV Top Closures', The 3rd International Conference on Structural Mechanics in Reactor Technology, London, U.K., September, 1975, Transactions paper H3/6.

39. Pian, T.H.H., 'Variational Principles for Incremental Finite Element Methods', Journal of the Franklin Institute, Vol. 302, No. 5 and 6, November/December, 1976.

40. Romstad, K.M., Taylor, M.A. and Herrmann, L.R., 'Numerical Biaxial Characterization for Concrete', Journal of the Engineering Mechanics Division, ASCE, Vol. 100, No. EM5, October, 1975, pp. 935-948.

41. Saenz, I.P., Discussion of 'Equation for the Stress Strain Curve for Concrete' by Desay: and Krishnan, Journal of the American Concrete Institute, Proceedings Vol. 61, No. 9, September 1964, pp. 1229-1235.

42. Sarne, Y., 'Material Nonlinear Time Dependent Three Dimensional Finite Element Analysis for Reinforced and Prestressed Concrete Structures', Ph.D. Thesis, MIT, Cambridge, Mass., December, 1974.

43. Scanlon, A. and Murray, D.W., 'Time Dependent Reinforced Concrete Slab Deflections', Journal of the Structural Division, ASCE, Vol. 100, No. ST9, September 1974, pp. 1911-1924.

44. Scanlon, A., and Murray, D.W., 'An Analysis to Determine the Effects of Cracking in Reinforced Concrete Slabs', Proceedings of the Specialty Conference on Finite Element Method in Civil Engineering, McGill University, Montreal, Quebec, June 1-2, 1972.

45. Schickert, G. and Winkler, H., 'Results of Test Concerning Strength and Strain of Concrete Subjected to Multiaxial Compressive Stresses', Deutscher Ausschuss für Stahlbeton, Heft 277, Berlin, W.G., 1977.

46. Schnobrich, W.C., 'Behavior of Reinforced Concrete Structures Predicted by the Finite Element Method', Computers and Structures, Vol. 7, 1977, pp. 365-376.

47. Truesdell, C., 'Hypo-elasticity', Journal of Rational Mechanics and Analysis, Vol. 4, 1955, pp. 83-133.

48. Willam, K.J. and Warnke, E.P., 'Constitutive Model for the Triaxial Behavior of Concrete', IABSE Seminar on 'Concrete Structures Subjected to Triaxial Stresses', ISMES, Bergamo, Italy, IABSE Proceedings Vol. 19, 1975.

49. Zienkiewicz, O.C., Irons, B.M., Ergatoudis, J., Ahmad, S. and Scott, F.C.', Isoparametric and Associated Element Families for Two and Three Dimensional Analysis', in 'Finite Element Methods in Stress Analysis' eds. Holand, I. and Bell, K., The Technical University of Norway, Trondheim, Norway, 1970.

50. Zienkiewicz, O.C., 'The Finite Element Method in Engineering Science', McGraw-Hill, 1971.

APPENDIX A

PARAMETERS OF ULTIMATE SURFACES

As mentioned in Section 2.3.7 the values of the coefficients in Eqs. 2.43 are chosen such that the principal radii of the ultimate surface r_1 and r_2 pass through a set of control points. for $\sigma_2 = \sigma_3 \leq \sigma_1$, then $\theta = o°$ (Fig. 2.6b) and the points on the surface trace the variation of r_1 as σ_a varies. This curve must pass through the uniaxial tensile strength point where $\sigma_2 = \sigma_3 = o$ and $\sigma_1 = f_t$ (and hence is called the extension branch). It must also pass through the biaxial compression point where $\sigma_2 = \sigma_3 = f_{cb}$ and $\sigma_1 = o$. The nondimensional values of the tensile and biaxial compression strengths may be defined as

$$\alpha_t = f_t/f_{cu} \tag{A.1a}$$

$$\alpha_c = f_{cb}/f_{cu} \tag{A.1b}$$

One additional point on the extension curve is required to define the parabolic variation of r_1 for Eq. 2.43a. An arbitrary high compression point with $\bar{\sigma}_a = \xi$ may be selected from experimental data to serve this purpose. Let the value of $\bar{\tau}_a$ at this point be ρ_1 as illustrated in Fig. 2.6c.

To define the variation of r_2 ($\theta = 60°$ on Fig. 2.6b) it is required that $\sigma_1 = \sigma_3 \geq \sigma_2$. This curve must pass through the uniaxial compression point $\sigma_1 = \sigma_3 = o$ and $\sigma_2 = -f_{cu}$ (and hence is called the compression branch). It is also required to intersect the hydrostatic axis on the rendulic plane at the same location as the

extension curve ($\bar{\sigma}_a = \xi_o$), and to pass through the experimental point (ξ, ρ_2) where ρ_2 is determined in the same manner as ρ_1.

The values of the coefficients in Eqs. 2.43 can be determined from the 5 control points described above and the additional condition of intersection at ξ_o as follows

$$a_2 = \frac{\sqrt{1.2}\,\xi\,(\alpha_t - \alpha_c) - \sqrt{1.2}\,\alpha_t\alpha_c + \rho_1\,(2\alpha_c + \alpha_t)}{(2\alpha_c + \alpha_t)(3\xi - 2\alpha_c)(3\xi + \alpha_t)} \cdot 9 \tag{A.2}$$

$$a_1 = \frac{1}{3}(2\alpha_c - \alpha_t)\,a_2 + \frac{\sqrt{1.2}\,(\alpha_t - \alpha_c)}{(2\alpha_c + \alpha_t)} \tag{A.3}$$

$$a_o = \frac{2}{3}\alpha_c a_1 - \frac{4}{9}\alpha_c^2\,a_2 + \sqrt{\frac{2}{15}}\;\alpha_c \tag{A.4}$$

$$\xi_o = -(a_1 + \sqrt{a_1^2 - 4a_o a_2})/2a_2 \tag{A.5}$$

$$b_2 = \frac{\rho_2\,(\xi_o + 1/3) - \sqrt{2/15}\,(\xi_o + \xi)}{(\xi + \xi_o)(3\xi - 1)(3\xi_o + 1)} \cdot 9 \tag{A.6}$$

$$b_1 = (\xi + 1/3)b_2 + (\sqrt{1.2} - 3\rho_2)/(3\xi - 1) \tag{A.7}$$

$$b_o = -\xi_o\,b_1 - \xi_o^2\,b_2 \tag{A.8}$$

The ultimate surface for stresses is therefore completely defined and serves to evaluate the σ_{ic}'s required in Eqs. 2.21 to 2.26.

However Eqs. 2.21 to 2.34 also require the evaluation of the equivalent uniaxial strains ε_{ic} associated with the ultimate strength points σ_{ic} as mentioned in Section 2.3.7. This is done through the

definition of an equivalent uniaxial strain surface analogous to the stress ultimate surface. Control points for strain can be defined analogous to those described for stresses and Eqs. A.1 to A.8 can be used directly with the appropriate change of variables. It should be noted, however, that uniaxial strains are available from tests only for control points corresponding to f_t and f_{cu}. Equivalent uniaxial strains at the other three control points are fictitious strains that cannot be observed directly (Elwi and Murray, 1979). These points have been determined, herein, by trial and error until reasonable strain correspondence was obtained.

APPENDIX B

ISOPARAMETRIC SHAPE FUNCTIONS

The shape functions for the linear, quadratic and cubic rectangular isoparametric elements used in program FEPARCS5 are defined in terms of the normalized coordinates μ and ξ as follows (Zienkiewicz, 1971).

(i) Linear Elements:

$$\phi_i = (1+\xi\xi_i)(1+\mu\mu_i)/4 \quad , i=1,2,3,4 \qquad (B.1)$$

(ii) Quadratic Elements:

$$\phi_i = (1+\xi\xi_i)(1+\mu\mu_i)(\xi\xi_i+\mu\mu_i-1)/4 \quad , i=1,3,5,7 \qquad (B.2)$$

$$\phi_i = (1-\xi^2)(1+\mu\mu_i)/2 \quad , i=2,6 \qquad (B.3)$$

$$\phi_i = (1+\xi\xi_i)(1-\mu^2)/2 \quad , i=4,8 \qquad (B.4)$$

(iii) Cubic Elements:

$$\phi_i = (1+\xi\xi_i)(1+\mu\mu_i)[9(\xi^2+\mu^2)-10]/32 \quad , i=1,4,7,10 \qquad (B.5)$$

$$\phi_i = 9(1+\xi\xi_i)(1-\mu^2)(1+9\mu\mu_i)/32 \quad , i=5,6,11,12 \qquad (B.6)$$

$$\phi_i = 9(1+\mu\mu_i)(1-\xi^2)(1+9\xi\xi_i)/32 \quad , i=2,3,8,9 \qquad (B.7)$$

where i refers to the node numbers appearing in Fig. 3.2, and ξ_i and μ_i are the nodal normalized coordinates.

APPENDIX C

MODELLING OF DOME PRESTRESSING TENDONS

The prestressing tendons in the dome of the test structure are arranged in two orthogonal geodetic meshes as shown in Fig. 6.2. In order to model those tendons in terms of stiffness as well as forces and stresses for use in an axisymmetric finite element program, the geodetic meshes must be transformed into an equivalent meridional and circumferential mesh. This task is performed using vector analysis.

Let subscript ξ denote tendons which lie in planes passing through the y axis and let subscript μ denote those tendons which lie in planes passing through the x-axis as shown in Fig. C.1. Let θ_ξ denote the angle plane ξ describes with plane y-z and let θ_μ denote the angle that plane μ describes with plane x-z. The coordinates of the point of intersection of two tendons is written as

$$x = z \tan \theta_\xi \tag{C.1a}$$

$$y = z \tan \theta_\mu \tag{C.1b}$$

$$z = R\alpha \tag{C.1c}$$

where R is the radius of the dome and

$$\alpha = 1.0/(\tan^2 \theta_\xi + \tan^2 \theta_\mu + 1.0)^{1/2} \tag{C.2}$$

Let $\vec{P}$ be the unit vector along the position vector of the point of intersection of two tendons.

$$\vec{P} = \alpha \tan \theta_\xi \vec{i} + \alpha \tan \theta_\mu \vec{j} + \alpha \vec{k} \qquad (C.3)$$

where $\vec{i}$, $\vec{j}$ and $\vec{k}$ are the base vectors of system x-y-z. The unit normals to planes ξ and μ are written respectively as

$$\vec{O}_\xi = - \cos \theta_\xi \vec{i} + \sin \theta_\xi \vec{k} \qquad (C.4a)$$

$$\vec{O}_\mu = - \cos \theta_\mu \vec{j} + \sin \theta_\mu \vec{k} \qquad (C.4b)$$

The vectors tangent to tendons ξ and μ at the point of intersection are written as

$$\vec{Q}_\xi = \vec{O}_\xi \times \vec{P} \qquad (C.5a)$$

$$\vec{Q}_\mu = \vec{O}_\mu \times \vec{P} \qquad (C.5b)$$

where $\times$ a cross product. Using the definitions of Eqs. C.3 and C.4, Eqs. C.5a and C.5b can be written as

$$\vec{Q}_\xi = (\beta_\xi \sin \theta_\xi \tan \theta_\mu) \vec{i} - (\beta_\xi \cos \theta_\xi (\tan^2 \theta_\xi + 1.0))\vec{j} + (\beta_\xi \cos \theta_\xi \tan \theta_\mu) \vec{k} \qquad (C.6a)$$

$$\vec{Q}_\mu = - (\beta_\mu \cos \theta_\mu (\tan^2 \theta_\mu + 1.0)) \vec{i} + (\beta_\mu \sin \theta_\mu \tan \theta_\xi) \vec{j} + (\beta_\mu \cos \beta_\mu \tan \theta_\xi) \vec{k} \qquad (C.6b)$$

where β_ξ and β_μ are defined as

$$\beta_\xi = 1.0/(\tan^2 \theta_\mu + 1.0/\cos^2 \theta_\xi)^{1/2} \qquad (C.7a)$$

$$\beta_\mu = 1.0/(\tan^2 \theta_\xi + 1.0/\cos^2 \theta_\mu)^{1/2} \qquad (C.7b)$$

The unit vector in the circumferential direction at the point of intersection of two tendons is written as

$$\vec{C} = \vec{k} \times \vec{P} \tag{C.8}$$

substituting for $\vec{P}$ from Eq. C.3, Eq. C.8 can be written as

$$\vec{C} = \gamma \tan\theta_\mu \vec{i} - \gamma \tan\theta_\xi \vec{j} \tag{C.9}$$

where,

$$\gamma = 1.0/(\tan^2\theta_\xi + \tan^2\theta_\mu)^{1/2} \tag{C.10}$$

The unit vector $\vec{M}$ lying along the meridian at the point of intersection is written as

$$\vec{M} = \vec{C} \times \vec{P} \tag{C.11}$$

Substituting for $\vec{C}$ and $\vec{P}$ using Eqs. C.3 and C.9, Eq. C.11 is written as

$$\vec{M} = \delta \tan\theta_\xi \vec{i} + \delta \tan\theta_\mu \vec{j} - \delta(\tan^2\theta_\xi + \tan^2\theta_\mu)\vec{k} \tag{C.12}$$

where,

$$\delta = 1.0/(\tan^2\theta_\xi + \tan^2\theta_\mu + (\tan^2\theta_\xi + \tan^2\theta_\mu)^2)^{1/2} \tag{C.13}$$

The contributions of tendons ξ and μ to the circumferential direction can be written respectively as

$$w_{c\xi} = \vec{Q}_\xi \cdot \vec{C} \tag{C.14a}$$

$$w_{c\mu} = \vec{Q}_\mu \cdot \vec{C} \tag{C.14b}$$

The contribution of tendons ξ and μ to meridional direction can be written respectively as

$$w_{m\xi} = \vec{Q}_{\xi} \cdot \vec{M} \qquad \text{(C.15a)}$$

$$w_{m\mu} = \vec{Q}_{\xi} \cdot \vec{M} \qquad \text{(C.15b)}$$

Eqs. C.14a to C.15b can be written as

$$w_{c\xi} = \gamma\beta_{\xi} (\sin \theta_{\xi} \tan^2 \theta_{\mu} + \tan \theta_{\xi} (\cos \theta_{\xi}) \qquad \text{(C.16a)}$$

$$w_{c\mu} = \gamma\beta_{\mu} (\sin \theta_{\mu} \tan^2 \theta_{\xi} + \tan \theta_{\mu} (\cos \theta_{\mu}) \qquad \text{(C.16b)}$$

$$w_{m\xi} = \alpha^2 \delta \beta_{\xi} \tan \theta_{\mu} \cos \theta_{\xi} \qquad \text{(C.16c)}$$

$$w_{m\mu} = \alpha^2 \delta \beta_{\mu} \tan \theta_{\xi} \cos \theta_{\mu} \qquad \text{(C.16d)}$$

Eqs. C.16a to C.16d describe weight functions to be applied at the point of intersection of two tendons. The required form of contribution must be an average per unit width for the meridional direction and an average per unit length for the circumferential direction. For this purpose Eq. C.16d has been plotted for the 6 tendons appearing in Fig. 6.2 for mesh μ as shown in Fig. C.2. The average meridional contribution was then obtained using the formula

$$w_{ma} = (w_{m1} + 2 (\Sigma w_{m2} + \ldots + w_{m6}))/(\pi R/2) \qquad \text{(C.17)}$$

This average was then plotted on the same figure. Since both stiffness and prestressing force as described in Sections 3.3.2 and 4.4.2 are directly related to the area of a meridional tendon, the average weight function obtained by Eq. C.17 can be applied directly to a tendon area.

To obtain the contribution to the circumferential direction Eq. C.16b has been plotted for the 6 tendons appearing in Fig. 6.2 for mesh μ as shown in Fig. C.3. The average meridional contribution was then obtained for each ten inch arc length using the formula

$$w_{ca} = (1.0 + \Sigma(w_{c2} + \cdots w_{cn}))/n \qquad (C.18)$$

where n is the number of tendons appearing in the band described by a particular 10 inch arc length. These contributions were then plotted on the same figure. As with the meridional contributions, the circumferential weight functions can be applied directly to the area of a tendon to simulate both stiffness and prestressing force formulated in Sections 3.3.3 and 4.4.2 respectively.

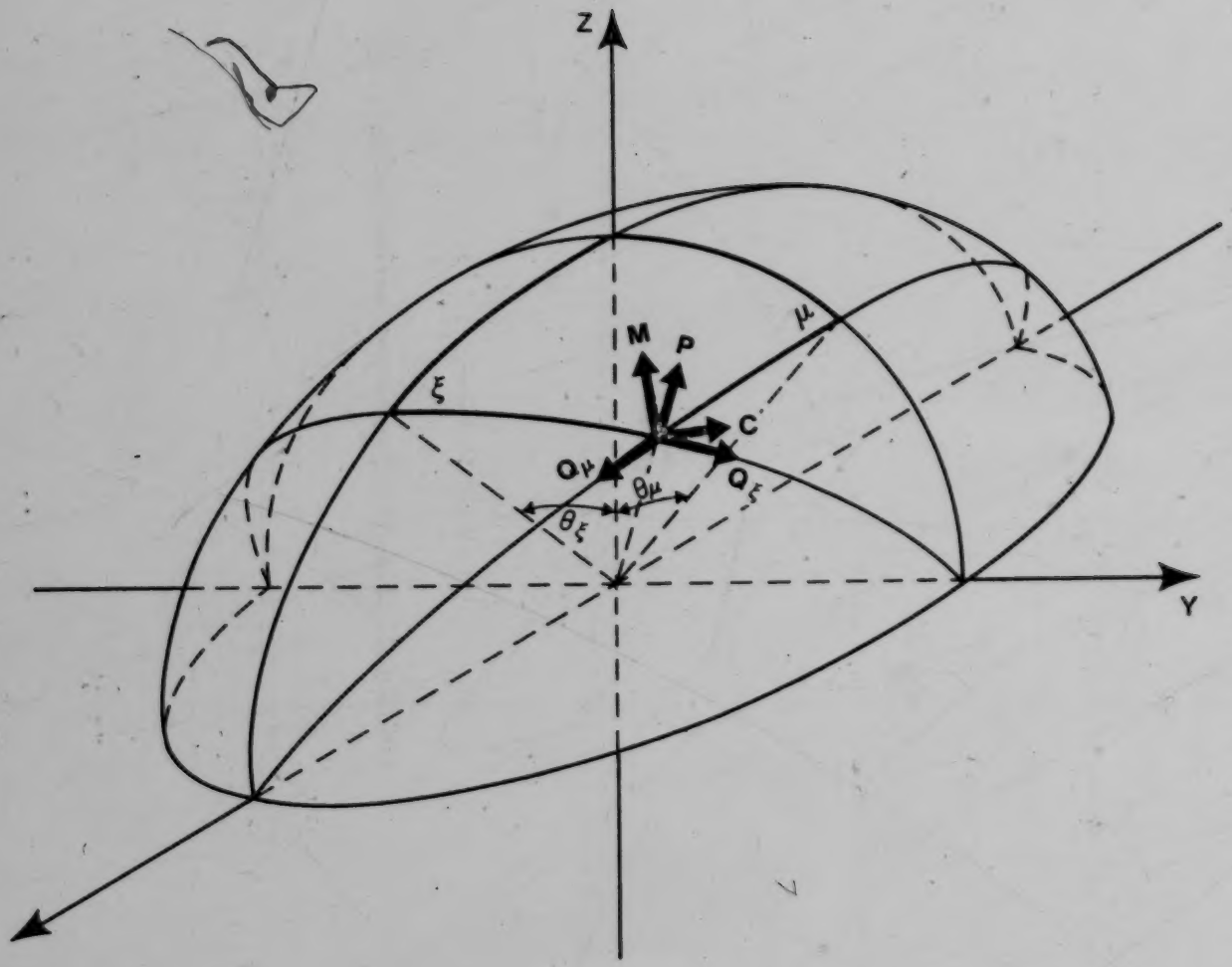

Fig. C.1 Vector Representation of the Dome Prestressing Mesh

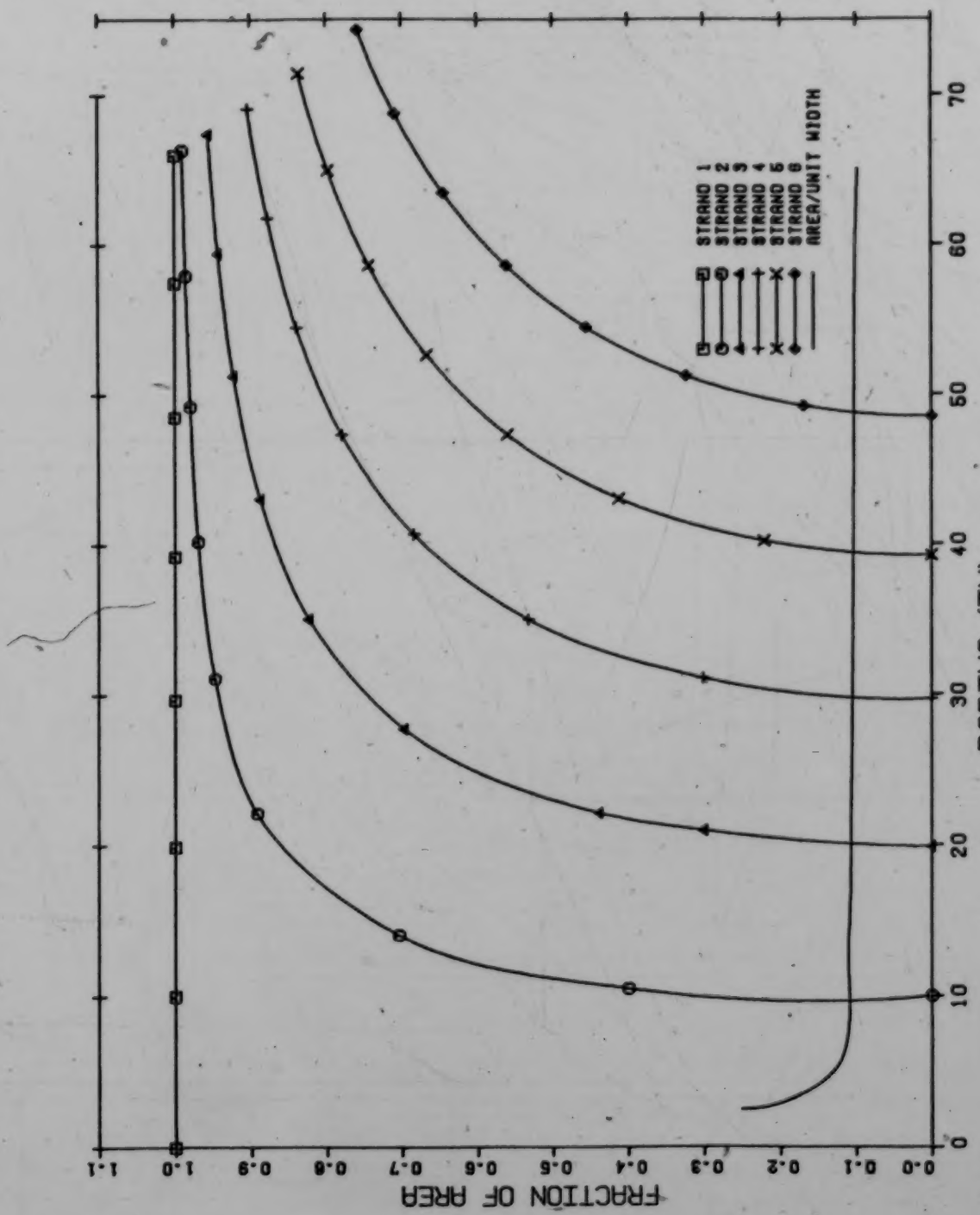

Fig. C.2 Meridional Contribution of the Dome Prestressing Mesh

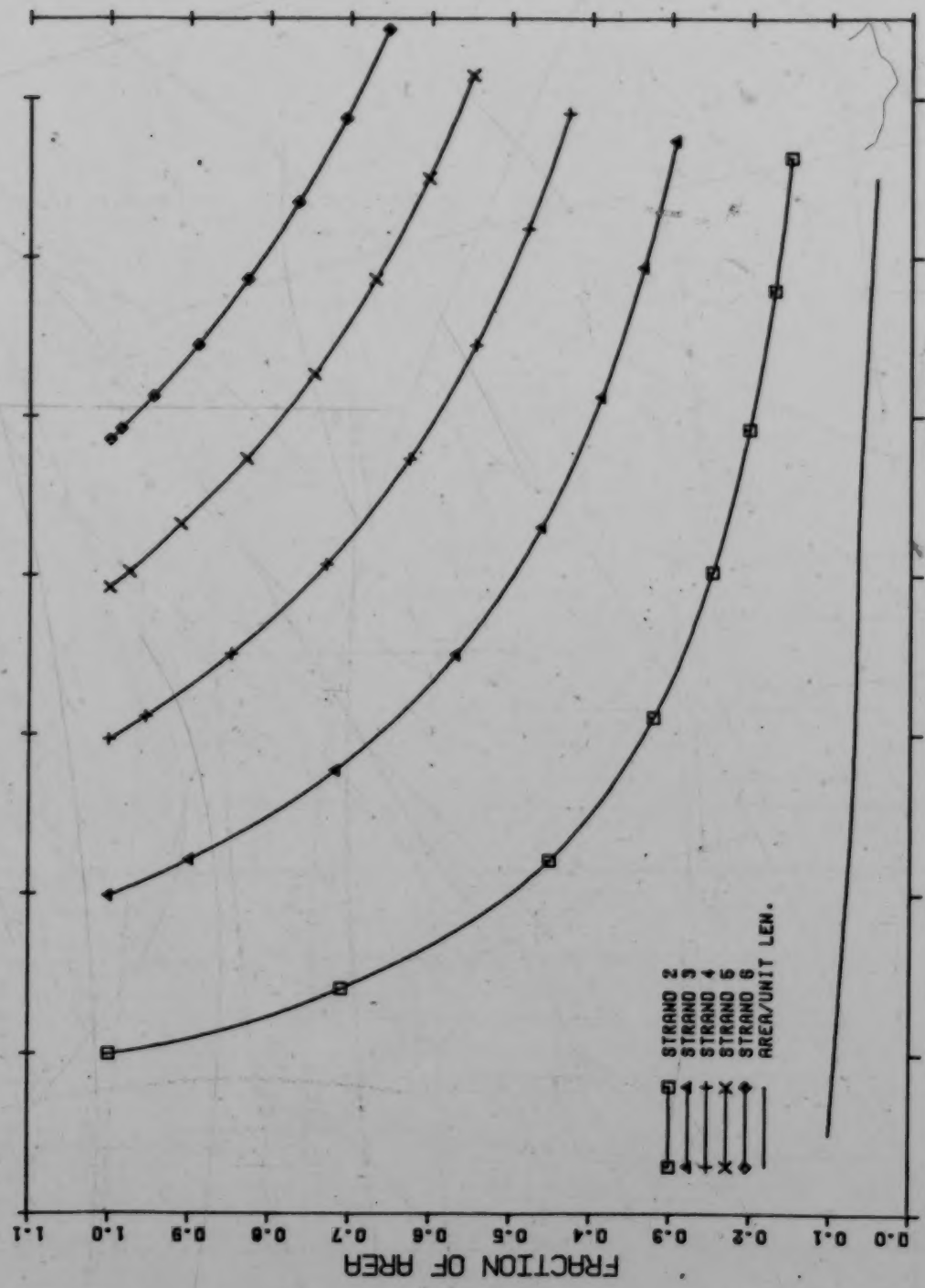

Fig. C.3 Circumferential Contribution of the Dome Prestressing Mesh